THESIS FOR THE DEGREE OF DOCTOR OF PHILOSOPHY

Quantum Electro- and Acoustodynamics in Waveguides

ANDREAS ASK

Department of Microtechnology and Nanoscience (MC2)

Applied Quantum Physics Laboratory

CHALMERS UNIVERSITY OF TECHNOLOGY

Göteborg, Sweden 2021

Quantum Electro- and Acoustodynamics in Waveguides
ANDREAS ASK
ISBN: 978-91-7905-462-5

Doktorsavhandlingar vid Chalmers tekniska högskola
Ny serie Nr 4929
ISSN 0346-718X

Applied Quantum Physics Laboratory
Department of Microtechnology and Nanoscience (MC2)
Chalmers University of Technology
SE-412 96 Göteborg
Sweden
Telephone: +46 (0)31-772 1000

Cover
Sketch of an atom in front of a mirror and its representation as a time-bin tensor network.

Printed by Chalmers Reproservice
Göteborg, Sweden 2021

Quantum Electro- and Acoustodynamics in Waveguides
ANDREAS ASK
Department of Microtechnology and Nanoscience (MC2)
Applied Quantum Physics Laboratory
Chalmers University of Technology

Abstract

The study of light-matter interaction in superconducting quantum circuits has seen remarkable progress over the last 20 years. By engineering artificial atoms, novel quantum phenomena have been demonstrated, and old ideas have come into a new light. Beyond their application to basic science, the prospect of implementing large-scale quantum information processing with superconducting circuits has fueled a rapid development of surrounding technologies, with ever-increasing control over their behavior as a result. The field's success stems primarily from the flexible design and strong non-linearity of the artificial atom, whose coherent interaction with both electrical and mechanical degrees of freedom has opened many doors for science.

This thesis deals with the interaction between artificial atoms and quantum fields in one-dimensional waveguides. The waveguide represents a one-dimensional environment for the atom, which we use to study the properties of open quantum systems. All quantum systems are, in fact, open, and interactions between the system and its environment lead inevitably to a loss of energy and quantum coherence. A continuous loss of information into the environment is called a Markovian process. The work contained in this thesis indicates that deviations from a Markovian process can be detected in the steady state of driven systems. This could simplify the detection of non-Markovianity in open quantum systems, as no information about the system's transient dynamics would be necessary.

Specifically, this thesis considers both electromagnetic fields in microwave transmission lines and acoustic fields in the form of surface acoustic waves (SAWs) traveling on the surface of solids. The recent realization of artificial atoms interacting with acoustic waves has opened up a new research field called quantum acoustics. We have built a model of the interaction between atoms and SAWs that predicts the existence of a new regime where the atom forms its own cavity. Additionally, we have considered synthesizing electromagnetically induced transparency, a quantum optics phenomena in opaque media where the absorption of photons is canceled, in waveguides using multiple closely spaced two-level systems.

Some of the work in this thesis represents experimental work done in collaboration. In the first experiment, we studied the routing of acoustic waves at the

quantum level. In the other experiment, we demonstrated electromagnetically induced transparency by creating an effective Λ system using a giant artificial atom. This thesis reviews the numerical techniques used to model these experiments.

Keywords: quantum optics with artificial atoms, waveguide QED, circuit QED, quantum acoustics

Acknowledgements

First and foremost, I would like to thank my supervisor, Göran Johansson, for giving me the opportunity to do research. I am especially grateful for your ability to keep the spirit lifted; your reassurance that everything will be alright in the end has been a great help at times. I also want to thank my assistant supervisor, Anton Frisk Kockum, for allowing me to work on several exciting projects. I have learned a lot from working with you.

I want to thank Maria Ekström and Thomas Aref for teaching me about acoustic waves. And thanks to all the other members of QT for answering my, often very naive, questions about experiments. Your laughs when I tried to point out the circulator in the cryostat also reassured me I made the right choice of becoming a theoretician.

I would like to thank Arne Grimsmo and Alexander Blais for their hospitality during my visit to Université de Sherbrooke; especially to Arne for teaching me about tensor networks.

A special thank you goes out to all the past and present members of AQP. It has been fantastic to be surrounded by so many creative and inspiring people during these five years. Our long coffee breaks probably delayed my Ph.D. by one order of magnitude, but it was all worth it.

I want to thank Emely Wiegand for her feedback during the preparation of this thesis.

Finally, I want to thank my friends and family for their tireless support.

List of publications

This thesis is based on the work contained in the following papers:

[I] A. Ask, M. Ekström, P. Delsing, and G. Johansson, "Cavity-free vacuum-Rabi splitting in circuit quantum acoustodynamics", Phys. Rev. A **99**, 013840 (2019).

[II] M. K. Ekström, T Aref, A Ask, G Andersson, B Suri, H Sanada, G Johansson, and P Delsing, "Towards phonon routing: controlling propagating acoustic waves in the quantum regime", New Journal of Physics **21**, 123013 (2019).

[III] A. M. Vadiraj, A. Ask, T. G. McConkey, I. Nsanzineza, C. W. S. Chang, A. F. Kockum, and C. M. Wilson, "Engineering the level structure of a giant artificial atom in waveguide quantum electrodynamics", Phys. Rev. A **103**, 023710 (2021).

[IV] A. Ask, Y.-L. L. Fang, and A. F. Kockum, "Synthesizing electromagnetically induced transparency without a control field in waveguide QED using small and giant atoms", (2020), arXiv:2011.15077.

[V] A. Ask and G. Johansson, "Non-Markovian steady states of a driven two-level system", (2021), arXiv:2102.11140.

We always refer to these publications as paper I-V.

Other papers that are outside the scope of this thesis:

[VI] N. Wall Wennerdal, A. Ask, P. Holmvall, T. Löfwander, M. Fogelström, "Breaking time-reversal and translational symmetry at edges of d-wave superconductors: Microscopic theory and comparison with quasiclassical theory", Phys. Rev. Research **2**, 043198 (2020)

List of figures

Contents

1 Introduction

Quantum computations rely on the ability to control individual quantum degrees of freedom. Ultimately, the goal is to perform specific computational tasks, and quantum simulations beyond the reach of modern supercomputers [1, 2]. These are ambitious goals that require coherent control of dynamical quantum systems and precise measurement techniques to extract the information encoded in the quantum bits, the "qubits". A large-scale fault-tolerant quantum computer, where the inevitable errors of individual qubits are corrected, is still a long way to go [3]. However, considerable efforts in that direction are currently pursued [4, 5]. Noisy intermediate-scale quantum (NISQ) computers based on ($\sim 50-100$) non-corrected qubits are, on the other hand, already here [6–8]. There is a number of potentially useful applications for NISQ computers [9], e.g., to quantum chemistry [10–12], classical optimization [13, 14], and quantum many-body simulations [15, 16]. However, whether the quantum gates are too noisy for near-term devices to outperform algorithms run on classical computers remains to be seen.

One of the most promising implementations of large-scale quantum computing is based on qubits made from low-loss superconducting circuits, fabricated on-chip using standard lithographic techniques, and operating in the microwave regime [17–21]. Beyond their practical application in quantum computing, there is another aspect of these qubits of a more fundamental nature that makes them remarkable objects; they behave like artificially made atoms. In fact, they are foremost *artificial atoms*, and only in specific parameter regimes do they approximately behave like two-level systems and can be used as qubits. Since the properties of artificial atoms are chosen by the engineer, unlike natural atoms with properties chosen by nature, they have given science a chance to study light-matter interaction with better control and explore new regimes [22, 23]. Some of these new regimes are studied or utilized in all of the papers appended to this thesis.

Before artificial atoms could be reliably engineered and manipulated, natural atoms interacting with photons in microwave cavities [24–27], and single trapped ions probed by laser light [28–32], had been studied by Serge Haroche and David Wineland in pioneering work in the field of quantum optics. Work for which they were awarded the Nobel Prize in Physics in the year 2012. By interchanging the natural atoms with superconducting artificial atoms, and the cavities with superconducting resonators, quantum optics could be realized on-chip, a field that was named circuit quantum electrodynamics (circuit QED) [33, 34] in analogy to

its atomic counterpart: cavity quantum electrodynamics (cavity QED). The recent success and rapid development of artificial atoms over the last two decades do not mean that artificial atoms have replaced natural atoms and ions by any means; each system has its own favorable properties. Trapped ions have, e.g., exquisite coherence times with single-qubit memory times of up to an hour [35, 36] (which is long compared to the superconducting qubits' coherence time of $\sim 100\mu$s [37]), but might be more challenging to scale-up than devices fabricated on-chip [38].

Artificial atoms made from superconducting circuits can also interact with the electromagnetic field in one-dimensional (1D) co-planar waveguides. In that case, the atom interacts with traveling microwave photons instead of the stationary photons in a cavity. The confinement of the electromagnetic field to 1D enhances many effects seen in similar quantum optical experiments in 3D space. An early demonstration of this was the nearly perfect extinction of the electromagnetic field in the forward direction when a low-power coherent beam was scattered against an artificial atom. More than 99% of the power in the incoming field was reflected using an artificial atom [39], compared to the 12% extinction observed with trapped ions and molecules [40, 41]. The study of such experiments, where one or several atoms interact with a 1D radiation channel, is referred to as waveguide QED. The theoretical studies in paper III, IV, and V are all performed with implementations of waveguide QED using superconducting atoms in mind. Still, they could, in principle, be realized in other waveguide QED systems. As we experimentally demonstrate in paper II and theoretically study in paper I, artificial atoms can also interact with phonons in acoustic waveguides, forming a hybrid electro-acoustic system that can be referred to as waveguide quantum acoustodynamics (waveguide QAD), but is more commonly referred to as circuit QAD. Essential concepts of all the appended papers are introduced below, and their main results are summarized in the end.

Before we proceed, let us summarize and clear up some terminology introduced so far, primarily because we might use these terms interchangeably throughout the thesis. Quantum optics is a broad field that studies the interaction between light and matter. Quantum electrodynamics (QED) is the theory that accounts for the quantum nature of both the atom and the electromagnetic field and is thus often used to explain quantum optical phenomena where a fully quantum treatment is necessary. When a cavity modifies the electromagnetic field, it is referred to as cavity QED, and if the system is built from superconducting circuits, it is referred to as circuit QED. In waveguide QED, which can be implemented in circuit QED, the interaction between light and matter is essentially one-dimensional compared to the three-dimensional interaction between optical light and natural atoms. It is not always necessary to use a full quantum treatment of the electromagnetic field; this is then called a semi-classical analysis, even though the system might operate in the field of circuit/cavity/waveguide QED and behave fully quantum. Also, waveguide QED might instead be referred to as quantum optics with artificial

atoms – purely for historical reasons.

1.1 The superconducting artificial atom and waveguide QED

The quantum behavior of superconducting circuits is an example of macroscopic quantum mechanics, where collective degrees of freedom in the circuits behave quantum mechanically. The quantum behavior of these circuits was discussed by Legget almost 40 years ago [42], in which he suggested that macroscopic tunneling and energy quantization could potentially be observed in SQUID-based circuits. Shortly after, macroscopic tunneling was indeed observed in a Josephson junction [43, 44]. The quantum "particle" was the phase difference of the superconducting order parameter across the junction, and the quantization of its energy-levels was soon measured as well [45]. The first coherent control of a macroscopic quantum state in a superconducting circuit was performed by Nakamura *et al.* in 1999 [46], using a predecessor of the type of artificial atom used in the experiments in paper II and III, called the transmon, introduced in 2007 by Koch *et al.* [47]. The transmon was much less sensitive to charge noise than earlier versions which increased the coherence times significantly. A few milestones in the early development of circuit QED that highlights its rapid development are: coherent coupling between a qubit and a single photon [33], resolving and generating photonic Fock states [48, 49], coherent state transferring and storage [50], single atom lasing [51], and demonstration of two-qubit gates for quantum information processing [52].

Resonance fluorescence is one of the fundamental phenomena in quantum optics. It describes the resonant absorption and re-emission of electromagnetic waves by an atom. In 2010 this was demonstrated using a superconducting artificial atom in a microwave transmission line for the first time by Astafiev *at al.* [53] and constitutes the beginning of waveguide QED with superconducting circuits. Although the reflection of a low-power coherent field against an artificial atom, as in the resonance fluorescence experiment, has a classical counterpart, *bunching* and *anti-bunching* of light do not. In bunched light, photons are emitted by the atom in pairs, whereas in anti-bunched light, they are emitted one and one. These are pure quantum effects that do not have a classical analogy and were demonstrated in a transmon in Ref. [54]. In both these two experiments, the lowest transition of the atom, the $|0\rangle - |1\rangle$ transition, was weakly driven. In another experiment, the $|1\rangle - |2\rangle$ transition was driven strongly, giving rise to an Autler-Townes doublet due to the Stark effect [55], that could be measured by probing the $|0\rangle - |1\rangle$ transition [39].

Another essential concept in waveguide QED has to do with collective effects when multiple emitters are placed close to each other. By exchanging both real and virtual photons, atoms couple via the waveguide and can have their collective

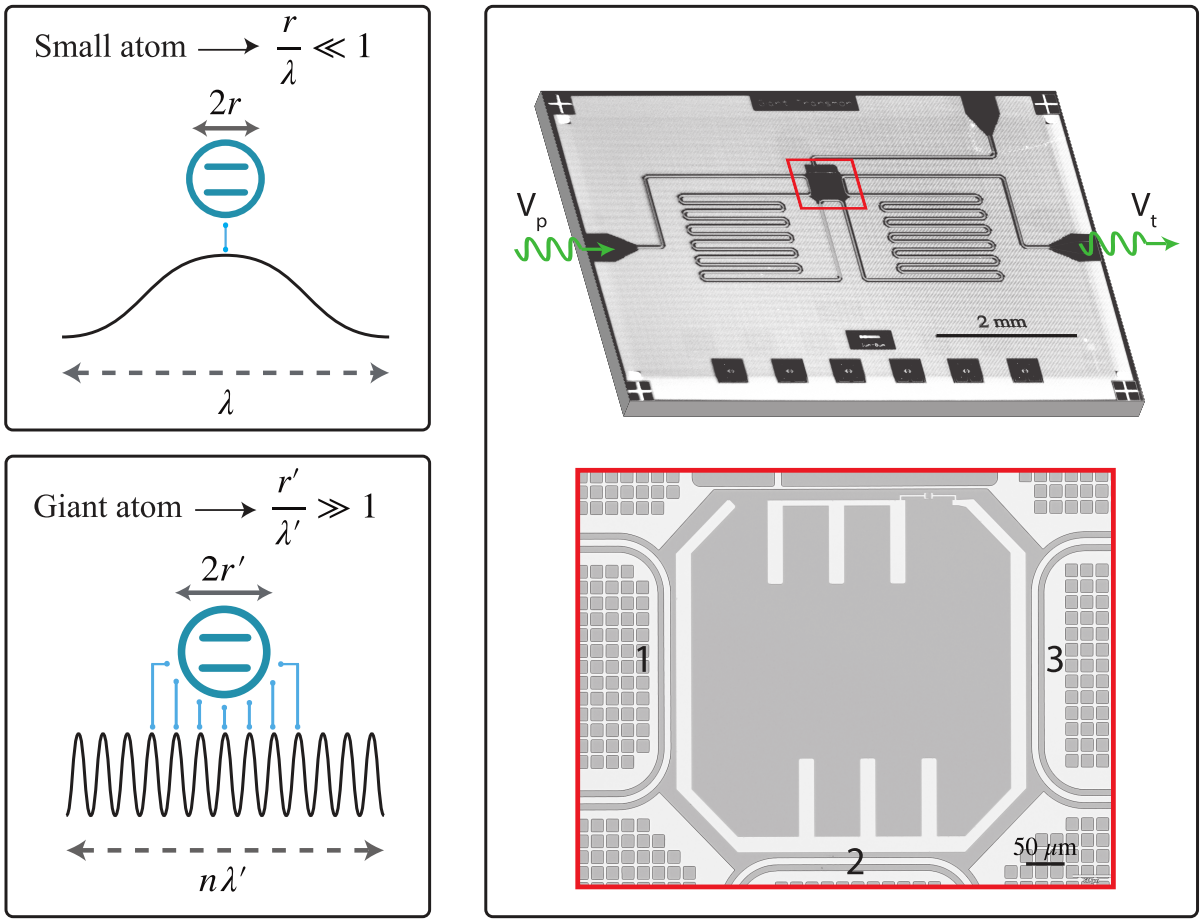

Figure 1.1: *A giant artificial atom in waveguide QED. The giant atom is formed by a transmon atom coupled to a meandering transmission line at multiple points, wavelengths apart. The atom is then not point-like from the perspective of the electromagnetic field, as it usually is in quantum optical experiments. The right panel is an optical micrograph of the giant atom in paper III with* 3 *coupling points.*

decay suppressed or enhanced, which is called sub- and superradiance and was studied by Dicke already in 1954 [56]. These phenomena were demonstrated with two transmons in a transmission line, and clear signatures of a distance-dependent coupling were shown [57]. We study multiple atoms in a waveguide in paper IV to investigate another classic quantum optics effect called electromagnetically induced transparency [Sec. 1.4]; waveguide mediated coupling plays a crucial role there as well.

1.2 Giant atoms

A giant atom is coupled to a waveguide at multiple points, wavelengths apart. This is a new regime of quantum optics, where the atom is no longer seen as point-like from the perspective of the electromagnetic field. Such an atom has

several exciting features, as was first pointed out by Kockum *et al.* [58], e.g., the decay rate of individual transitions of the atom becomes frequency-dependent. Interestingly, while some transitions can be enhanced, others can be suppressed. This effect was demonstrated experimentally in paper IV, where a giant atom was realized by coupling a transmon atom to a meandering transmission line, see Fig. 1.1. Moreover, in Ref. [59], several giant atoms with overlapping coupling points were used to create a so-called decoherence-free subspace [60], in which the atoms can switch from a radiative and non-radiative state while still maintaining their waveguide mediated coupling. This regime cannot be realized with regular atoms with a single coupling point.

Another regime of giant atoms is when the coupling points are separated by a distance such that the propagation time-delay of emitted radiation between the points is comparable to the atomic decay rate. This is a highly non-Markovian system [Sec. 5.4], where the atomic population is revived at a time scale set by the time delay [61, 62].

We consider transmission properties of systems involving giant atoms in paper IV. In paper V, we study an atom in a semi-infinite waveguide, which behaves very similar to a giant atom. The re-absorption of emission is a defining feature of a giant atom with largely separated coupling points — an atom whose emission is reflected against the end of a waveguide experience the same phenomena. As a result, the two systems can be mapped entirely to each other in some parameter regimes.

1.3 Quantum acoustics

A very recent development of superconducting artificial atoms begun in 2014, when a transmon was coupled to propagating surface acoustic waves (SAWs) in solids in a seminal experiment by Gustafsson *et al.* [63]. Soon several experiments demonstrated coupling also to SAW resonators [64–68], and to bulk acoustic wave resonators (BAWs) [69, 70]. The latter system performed so well that Chu *et al.* managed to create phononic Fock states inside a BAW resonator, indicating the great coherent control achievable with acoustic devices. This entire field is now called quantum acoustics.

Paper I is a theoretical study of a SAW coupled atom, and paper II is an experimental study of the same system.

1.4 Electromagnetically induced transparency

EIT is a phenomenon in which electromagnetic absorption in an opaque medium is canceled due to quantum mechanical interference [71–73]. The transparency also comes with a steep dispersion, which can be used to create slow light [74], or

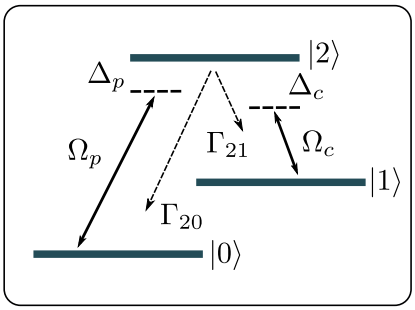

Figure 1.2: *Driving scheme for observing electromagnetically induced transparency in a three-level Λ system.*

even stopping light completely [75, 76]. In quantum optics, it is hard to engineer a strong photon-photon interaction, a problem that does not exist in circuit QED due to the Josephson junction's strong non-linearity. EIT can be used to engineer such interactions, which fueled a lot of the early excitement about EIT in quantum optics [77].

The effect is explained in terms of a three-level Λ system. In a Λ system, only the $|0\rangle - |2\rangle$ and $|1\rangle - |2\rangle$ transitions are allowed. If a strong control field is applied at the $|1\rangle - |2\rangle$ transition, the absorption of photons in a weak probe applied to the $|0\rangle - |2\rangle$ transition can be canceled completely; yielding the system transparent. The driving scheme is illustrated in Fig. 1.2. The cancellation can be understood as destructive interference between two different excitation pathways in the system: the short pathway $|0\rangle \rightarrow |2\rangle$ and the longer pathway $|0\rangle \rightarrow |2\rangle \rightarrow |1\rangle \rightarrow |2\rangle$. In the right parameter regime, the probability amplitudes for these two transitions are equal and interfere destructively.

It has remained hard to observe EIT with superconducting artificial atoms, primarily because its energy levels are formed in a ladder, lacking even a partially stable state. To circumvent this, an atom can be embedded in a resonator, or a cavity [78, 79], to form a Λ system out of dressed states. In paper III, we show that the decay rate of the first excited state in a giant atom can be significantly suppressed, allowing it to form an effective Λ system and showcase EIT. In paper IV, we study how EIT can be constructed in waveguide QED without an external control field, using two closely spaced two-level systems instead.

1.5 Organization of this thesis

This thesis is organized as follows: In chapter 2, we explain the quantization procedure of electrical circuits. As a concrete example, we study two coupled LC-oscillators as a warm-up to the calculation of an artificial atom coupled to an infinite number of oscillators in paper I. In chapter 3, we study the propagation of surface acoustic waves in both non-piezoelectric and piezoelectric materials.

Specifically, we consider gallium arsenide as an example material; it is widely used in cQAD, and its cubic lattice symmetry allows for analytical solutions. We proceed to derive a lumped-element model of interdigital transducers, which is used to transduce an electric to an acoustic signal and vice versa. In chapter 4, we introduce the field of cQAD and review some of the progress that has been made so far in the field. Chapter 5 is an introduction to open quantum systems. In particular, we derive the quantum optical master equation in Lindblad form and discuss the notion of non-Markovianity. The master equation was used to describe the experimental results in paper III and study the inelastic properties of atoms in waveguides in paper IV. Next, chapter 6 explains a single-photon scattering technique used in paper IV. In chapter 7 we introduce the formalism of tensor networks. Within this formalism, highly efficient representations of low-energy states of quantum many-body systems can be formulated. We utilize a numerical technique based on this principle in paper V. Finally, in chapter 8 we summarize the main results of the appended papers I-V. We conclude the thesis in chapter 9 and discuss future research directions.

2 Quantized electrical circuits

In paper I, we build a model of a SAW-coupled artificial atom, based on the quantization of an electrical circuit. In this chapter, we study each component in that model individually. We start by introducing the basic concepts of circuit quantization [80, 81] and move on to study transmission lines and artificial atoms. Finally, we look at the Jaynes-Cummings model, as it can be used to describe many of the experiments performed in the field of circuit QED.

2.1 The LC oscillator

The Harmonic oscillator might be the most well-studied object in the entire field of physics. Not only is it simple to solve mathematically, but it is also applicable, remarkably enough, to a wide range of physical systems. Sometimes the motion of an object is described precisely as a harmonic oscillator, and sometimes it is approximately harmonic, perhaps under certain conditions. The swinging pendulum is one such example, but the relevance of the harmonic oscillator can be found in most fields of physics: from the description of lattice vibrations in solids to the description of quantum fields in quantum field theory. Sidney Coleman said during a lecture at Harvard: "*The career of a young theoretical physicist consists of treating the harmonic oscillator in ever-increasing levels of abstraction*". An artificial atom is a weakly nonlinear system that is often treated as a simple harmonic oscillator to simplify the analysis. We utilize this simplification in paper I to circumvent the problems of treating both ultra-strong coupling and time delays at the same time. As such, we start the scientific part of this thesis with the description of the electronic harmonic oscillator, the LC circuit.

2.1.1 Classical harmonic oscillator

The LC oscillator is formed by coupling an inductor with a capacitor in either series or parallel, see Fig. 2.1. The Lagrangian of the circuit, $\mathcal{L} = T - V$, where T and V is the kinetic and potential energy, respectively, can be written in different ways depending on the choice of position variable. This choice depends on what we associate as the potential energy of the circuit. In the case of the LC circuit, this choice is irrelevant, as we will see shortly. For circuits involving more complicated elements, such as the Josephson junction, a good choice of variables can greatly simplify the calculations.

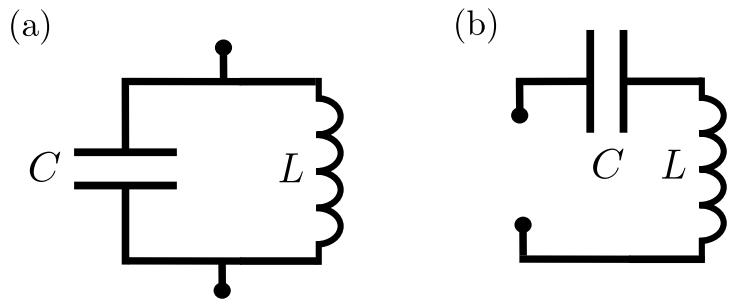

Figure 2.1: *(a) Parallel LC circuit. (b) Series LC circuit.*

The storage of charge on the capacitor is a natural choice of potential energy. With that choice the Lagrangian becomes

$$\mathcal{L} = \frac{LI^2}{2} - \frac{Q^2}{2C}. \tag{2.1}$$

The current in the circuit is defined as the time derivative of the charge $I \equiv \dot{Q}$, and the Lagrangian can then be rewritten as

$$\mathcal{L} = \frac{L\dot{Q}^2}{2} - \frac{Q^2}{2C}. \tag{2.2}$$

It can be instructive to compare the LC circuit to its mechanical counterpart, the mass at the end of a spring (the typical textbook example of a harmonic oscillator). The Lagrangian for such system is: $\mathcal{L} = m\dot{x}^2/2 - kx^2/2$. In the LC circuit, it is thus the charge that plays the role of position, the inductance that plays the role of mass, and the capacitance can be regarded as the inverse of a spring constant.

We write down the Euler-Lagrange equation of motion for the charge,

$$L\ddot{Q} + \frac{Q}{C} = 0 \Leftrightarrow \ddot{Q} = -\omega_0^2 Q, \tag{2.3}$$

where we introduced the resonance frequency $\omega_0 = 1/\sqrt{LC}$. The motion of the charge is thus described by an oscillatory function oscillating with frequency ω_0.

The conjugate momentum to the charge is the flux through the inductor, $\Phi = \partial\mathcal{L}/\partial\dot{Q} = L\dot{Q}$. The Hamiltonian of the system will thus be a function of charge and flux. The Hamiltonian is obtained from the Legendre transformation of the Lagrangian,

$$\begin{aligned} H &= \dot{Q}\phi - \mathcal{L} \\ &= \frac{\Phi^2}{2L} + \frac{Q^2}{2C}. \end{aligned} \tag{2.4}$$

The relationship between flux and charge to the voltage at the capacitor and current through the inductor can be retrieved directly from Hamilton's equations of motions: $\dot{\Phi} = -\partial H/\partial Q$ and $\dot{Q} = \partial H/\partial \Phi$,

$$\begin{aligned} \dot{\Phi} &= -\frac{Q}{C} = V, \\ \dot{Q} &= \frac{\Phi}{L} = I. \end{aligned} \tag{2.5}$$

The "*branch*" flux, Φ, which we introduced earlier, is the flux through the inductor branch of the circuit. In the artificial atom that we introduce later on, the inductor in the LC circuit is replaced by a Josephson junction. In that case, it is easier to work with what is called the "*node*" flux. The node flux is related to the branch flux through the relation $\Phi = \phi_1 - \phi_0$, where ϕ_1 and ϕ_0 are the flux at the two nodes surrounding the inductor in Fig. 2.1(a). Since one of the nodes is grounded, its voltage is zero, and the branch and node flux is equal in this simple case. This is not true in general. We refer to the node flux as ϕ from now on. The node flux can also be defined in terms of the time integral of the node voltage,

$$\phi = \int_{-\infty}^{t} d\tau V(\tau). \tag{2.6}$$

The voltage is thus related to the node flux through the relation: $V = \dot{\phi}$. This means that we can rewrite the capacitive energy in Eq. (2.4) as $C\dot{\phi}^2/2$. Rewritten in terms of the node flux, this energy is more suitably interpreted as kinetic energy than potential energy since it involves the time derivative of the flux. Similarly, what we previously referred to as the kinetic energy, $\phi^2/2L$, gets reinterpreted as potential energy, the energy stored in the inductor. With the node flux as the new position variable, the Lagrangian becomes

$$\mathcal{L} = \frac{C\dot{\phi}^2}{2} - \frac{\phi^2}{2L}. \tag{2.7}$$

The conjugate momentum to the flux has the unit of charge (just as before), $q = \partial\mathcal{L}/\partial\dot{\phi} = C\dot{\phi}$, but it differs from the previously defined charge by a minus sign. That sign difference become important once we quantize the system and impose commutation relations. In terms of ϕ and q, the Hamiltonian now looks like

$$H = \frac{q^2}{2C} + \frac{\phi^2}{2L}, \tag{2.8}$$

with the corresponding equations of motion:

$$\begin{aligned} \dot{\phi} &= \frac{q}{C}, \\ \dot{q} &= -\frac{\phi}{L}. \end{aligned} \tag{2.9}$$

By comparing Eq. (2.9) with Eq. (2.5), it becomes clear that $q = -Q$.

This exercise in shifting variables can be valuable because most of us are used to thinking in terms of voltages and currents, not in magnetic flux and charge. Ultimately, we want to formulate things in terms of node fluxes, the chosen position variable in the appended paper I. These are, however, arbitrary choices, chosen simply for convenience.

In summary, when the charge on the capacitance is chosen as the position variable, the inductance plays the role of mass, whereas the capacitance plays the role of an inverse spring constant. When the node flux is chosen as the position variable, the capacitance plays the role of mass, whereas the inductance plays the role of an inverse spring constant. Additionally, when the flux is taken as the position variable, care has to be taken regarding the sign of the charge. This manifests itself in the classical Poisson bracket relations

$$\{Q, \Phi\} = \{\phi, q\} = 1. \tag{2.10}$$

2.1.2 Quantum harmonic oscillator

We quantize the LC-oscillator of the previous section by imposing canonical commutation relations, and promoting both the flux and the charge to operators,

$$[\hat{\phi}, \hat{q}] = i\hbar. \tag{2.11}$$

The quantum harmonic oscillator is most easily solved by expanding $\hat{\phi}$ and $\hat{q}$ in terms of raising and lowering operators,

$$\hat{\phi} = \sqrt{\frac{\hbar L\omega_0}{2}}\left(\hat{a} + \hat{a}^\dagger\right), \tag{2.12}$$

$$\hat{q} = -i\sqrt{\frac{\hbar C\omega_0}{2}}\left(\hat{a} - \hat{a}^\dagger\right), \tag{2.13}$$

with $\hat{a}$ and $\hat{a}^\dagger$ satisfying the commutation relation $[\hat{a}, \hat{a}^\dagger] = 1$. The prefactors of Eq. (6.30) and Eq. (6.31) can be rewritten in terms of the characteristic impedance of the oscillator $Z_0 = \sqrt{L/C}$, such that

$$\hat{\phi} = \sqrt{\frac{\hbar Z_0}{2}}\left(\hat{a} + \hat{a}^\dagger\right), \tag{2.14}$$

$$\hat{q} = -i\sqrt{\frac{\hbar}{2Z_0}}\left(\hat{a} - \hat{a}^\dagger\right). \tag{2.15}$$

As a consistency check, we note that the flux and charge obey Heisenberg's uncertainty principle (as they must), $\hat{\phi}\hat{q} = \hbar/2$. In terms of the ladder operators, the oscillator Hamiltonian in Eq. (2.8) takes the well-known form,

$$H = \hbar\omega_0\left(\hat{a}^\dagger\hat{a} + \frac{1}{2}\right). \tag{2.16}$$

It is worth mentioning what type of excitations we are dealing with in an electrical circuit, as the LC oscillator. On the one hand, they are excitations of the collective motion of electrons in the circuit. However, they can just as well be regarded as photons. In the lumped-element treatment that we have adopted here, adding charges to the circuit means adding charges to the capacitor, which implies an electric field in between the plates of the capacitor. The magnetic field, on the other hand, resides inside the inductor. For this reason, the excitations are often referred to as photons.

Considering the sheer amount of atoms that physically make up the circuit, it is truly fascinating how simple the quantum description of the oscillator can be made.

2.2 Coupled systems

Most systems studied in the field of cQED consist of several coupled systems. Even in the simplest case of a single circuit, e.g., an artificial atom, it needs to be coupled to some kind of probe and readout device. Dealing with coupled systems is thus essential. This section will derive the Hamiltonian for two coupled LC oscillators, as this perhaps constitutes the simplest non-trivial case of a coupled system. This section also serves as a preparation for the more complicated circuit in paper I.

There are several ways to construct the circuit Lagrangian in terms of node fluxes. We will use a straightforward method where we write down the energy of each component in terms of branch fluxes and then use Kirchhoff's voltage law to reduce the number of variables. As the last step, we express the branch fluxes in terms of the node fluxes surrounding them.

In this example we use two capacitively coupled oscillators, see Fig. 2.2, but both inductive and galvanic couplings are used in practice. We denoted the branch fluxes as ϕ_{C_i} and ϕ_{L_i}, where C_i and L_i is the capacitance and inductance of the two oscillators respectively. The circuit Lagrangian then becomes

$$\mathcal{L} = \frac{1}{2}C_1\dot{\phi}_{C_1}^2 + \frac{1}{2L_1}\phi_{L_1}^2 + \frac{1}{2}C_2\dot{\phi}_{C_2}^2 + \frac{1}{2L_2}\phi_{L_2}^2 + \frac{1}{2}C_c\dot{\phi}_{C_c}^2. \tag{2.17}$$

Kirchhoff's voltage law states that the sum of the voltages in a closed loop is zero. As can be seen in Fig. 2.2, the two oscillators form two closed loops. We choose counterclockwise to be the positive direction of each loop. This gives us the following relations:

$$\dot{\phi}_{C_1} + \dot{\phi}_{L_1} = 0 \;\Rightarrow \dot{\phi}_{L_1} = -\dot{\phi}_{C_1}, \tag{2.18}$$

$$\dot{\phi}_{C_2} + \dot{\phi}_{L_2} = 0 \;\Rightarrow \dot{\phi}_{L_2} = -\dot{\phi}_{C_2}. \tag{2.19}$$

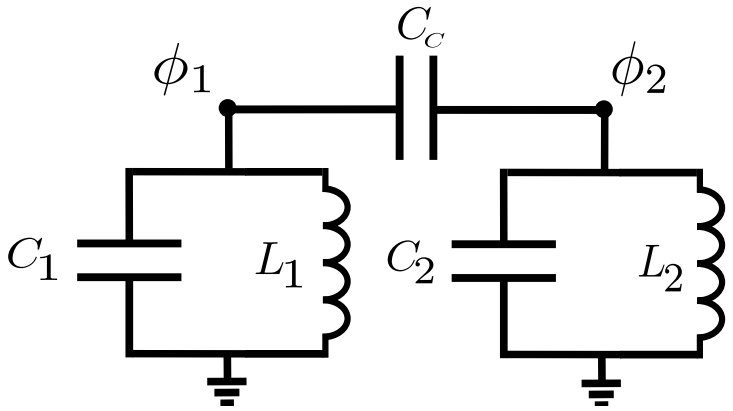

Figure 2.2: *Two capacitively coupled LC oscillators.*

Since both oscillators are connected to ground, the branch fluxes are related to the two node fluxes according to:

$$\dot{\phi}_{C_1} = \dot{\phi}_1 \tag{2.20}$$
$$\dot{\phi}_{C_2} = \dot{\phi}_2 \tag{2.21}$$
$$\dot{\phi}_{C_c} = \dot{\phi}_1 - \dot{\phi}_2. \tag{2.22}$$

Using these relations we can rewrite the circuit Lagrangian in Eq. (2.17) in terms of node fluxes,

$$\mathcal{L} = \frac{1}{2}C_1\dot{\phi}_1^2 - \frac{1}{2L_1}\phi_1^2 + \frac{1}{2}C_2\dot{\phi}_2^2 - \frac{1}{2L_2}\phi_2^2 + \frac{1}{2}C_c\left(\dot{\phi}_1 - \dot{\phi}_2\right)^2. \tag{2.23}$$

For larger systems it is practical to write it in a compact matrix form,

$$\mathcal{L} = \frac{1}{2}\vec{\dot{\phi}}C\vec{\dot{\phi}} - \frac{1}{2}\vec{\phi}L^{-1}\vec{\phi}, \tag{2.24}$$

where the capacitance- and inductance matrices are defined as:

$$C = \begin{pmatrix} C_1 + C_c & -C_c \\ -C_c & C_2 + C_c \end{pmatrix}, \tag{2.25}$$

$$L^{-1} = \begin{pmatrix} 1/L_1 & 0 \\ 0 & 1/L_2 \end{pmatrix}, \tag{2.26}$$

and the flux vector as:

$$\hat{\phi} = (\phi_1, \phi_2). \tag{2.27}$$

The conjugate momenta to the fluxes is then written as

$$\vec{q} = C\vec{\dot{\phi}}, \tag{2.28}$$

which gives us that,

$$\dot{\vec{\phi}} = C^{-1}\vec{q}, \tag{2.29}$$

with,

$$C^{-1} = \frac{1}{C_1C_c + C_2C_c + C_1C_2}\begin{pmatrix} C_2 + C_c & C_c \\ C_c & C_1 + C_c \end{pmatrix} \tag{2.30}$$

Thus, the Hamiltonian, obtained from the Legendre transformation $H = \vec{q}\cdot\dot{\vec{\phi}} - \mathcal{L}$, becomes,

$$\begin{aligned} H &= \frac{1}{2}\vec{q}C^{-1}\vec{q} + \frac{1}{2}\vec{\phi}L^{-1}\vec{\phi} \\ &= \frac{\left(C^{-1}\right)_{11}q_1^2}{2} + \frac{\left(C^{-1}\right)_{22}q_2^2}{2} + \frac{\phi_1^2}{2L_1} + \frac{\phi_2^2}{2L_2} + \left(C^{-1}\right)_{12}q_1q_2, \end{aligned} \tag{2.31}$$

where we used that $C_{12}^{-1} = C_{21}^{-1}$. By introducing the two "bare" oscillator frequencies (which includes the small frequency shift due to the coupling capacitance), $\omega_1^2 = C_{11}^{-1}/L_1$ and $\omega_2^2 = C_{22}^{-1}/L_2$, we can write the Hamiltonian as,

$$H = \frac{1}{2}L_1\omega_1^2q_1^2 + \frac{1}{2L_1}\phi_1^2 + \frac{1}{2}L_2\omega_1^2q_2^2 + \frac{1}{2L_2}\phi_2^2 + C_{12}^{-1}q_1q_2. \tag{2.32}$$

Just as in section 2.1.2, we quantize the Hamiltonian by promoting both ϕ_i and q_i to operators, and imposing canonical commutation relations,

$$[\hat{\phi}_i, \hat{q}_j] = i\hbar\delta_{i,j}. \tag{2.33}$$

By expanding $\hat{\phi}_i$ and $\hat{q}_i$ in terms of creation and annihilation operators according to

$$\hat{\phi}_i = \sqrt{\frac{\hbar L_i\omega_i}{2}}\left(\hat{a}_i + \hat{a}_i^\dagger\right), \tag{2.34}$$

$$\hat{q}_i = i\sqrt{\frac{\hbar\omega_i}{2(C^{-1})_{ii}}}\left(\hat{a}_i - \hat{a}_i^\dagger\right), \tag{2.35}$$

the Hamiltonian can be recast into,

$$H = \sum_{i=1}^{2}\hbar\omega_i\left(\hat{a}_i^\dagger\hat{a}_i + \frac{1}{2}\right) - \hbar g\left(\hat{a}_1 - \hat{a}_1^\dagger\right)\left(\hat{a}_2 - \hat{a}_2^\dagger\right), \tag{2.36}$$

with the coupling constant

$$g = \frac{C_c\sqrt{\omega_1\omega_2}}{2\sqrt{(C_1 + C_c)(C_2 + C_c)}}. \tag{2.37}$$

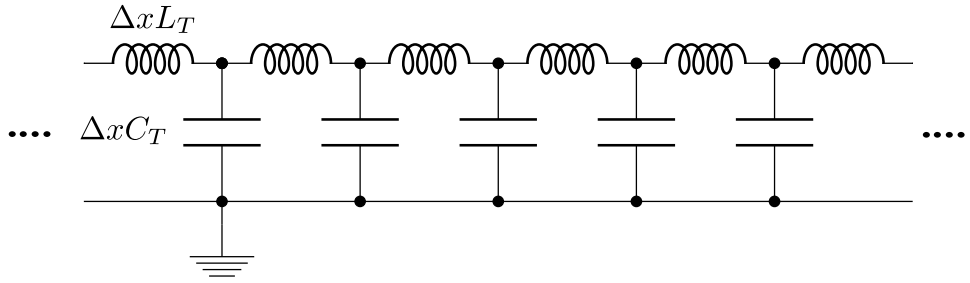

Figure 2.3: *Distributed circuit model of a lossless transmission line. The model consist of an infinite array of harmonic oscillators, with a characteristic inductance L_T and capacitance C_T per unit length.*

2.3 Transmission lines

One-dimensional (1D) microwave transmission lines are one of the basic building blocks of circuit QED. Unlike electromagnetic radiation in free space, the confinement of light to a 1D waveguide only supports field lines normal (i.e., transverse) to the direction of propagation. These modes are referred to as TEM modes, as in Transverse Electro-Magnetic modes. The same type of radiation is found in optical fibers and radio waves. A transmission line can also be terminated at one end, forming a half-cavity, or at both ends and thus forming a microwave resonator. The confinement to 1D has added benefits for light-matter interaction, as was mentioned in chapter 1. Here, the main goal is to introduce the quantization of the distributed circuit diagram describing a transmission line, following the quantization procedure introduced in Sec. 2.1.2.

Dealing with superconducting circuits, the transmission lines we are interested in have zero resistance and are lossless, which is a good approximation for most practical purposes. Hence, they can be described as the distributed circuit in Fig. 2.3 [82, 83], only containing capacitors and inductors. An inductor and capacitor together form an LC oscillator; whether they are coupled in series or parallel does not matter. The transmission line in Fig. 2.3 is thus nothing but an infinite array of oscillators, where each oscillator is inductively coupled to its nearest neighbors. In contrast to the example with the two coupled oscillators from section 2.2, where the capacitive coupling implied a coupling through their momenta, the inductive coupling will couple the oscillators through their position.

The goal of the following section is to show that the field in the transmission line is described by the Klein-Gordon equation for a massless scalar field [84]. Following the same procedure as in section 2.1.1, the transmission line in Fig. 2.3 is described by the following Lagrangian

$$\mathcal{L} = \sum_{i=-\infty}^{\infty} \frac{\Delta x C_T}{2} \dot{\phi}_i^2 + \sum_{i=-\infty}^{\infty} \frac{(\phi_{i+1} - \phi_i)^2}{2\Delta x L_T}, \tag{2.38}$$

where C_T and L_T is the capacitance and inductance per unit length respectively. By introducing the conjugate momentum to the flux $q_i = \partial L/\partial\dot{\phi}_i$, we obtain the Hamiltonian from the Legendre transformation,

$$H = \sum_{i=-\infty}^{\infty} \frac{q_i^2}{2\Delta x C_T} + \sum_{i=-\infty}^{\infty} \frac{(\phi_{i+1} - \phi_i)^2}{2\Delta x L_T} \tag{2.39}$$

As before, we quantize the Hamiltonian by promoting both ϕ_i and q_i to operators and impose canonical quantization relations,

$$[\hat{\phi}_i, \hat{q}_i] = i\hbar\delta_{ij}. \tag{2.40}$$

We next calculate the equations of motion for both the flux and the charge:

$$\begin{aligned} \dot{\hat{\phi}}_i &= \frac{i}{\hbar}[\hat{\phi}_i, H] \\ &= -\frac{\hat{q}_i}{\Delta x C_T}, \end{aligned} \tag{2.41}$$

$$\dot{\hat{q}}_i = -\frac{1}{\Delta x L_T}\left(\hat{\phi}_{i+1} - 2\hat{\phi}_i + \hat{\phi}_{i-1}\right). \tag{2.42}$$

The right hand side of the last equation, is nothing but the second order spatial derivative of $\hat{\phi}$,

$$\begin{aligned} \dot{\hat{q}}_i &= \frac{\Delta x}{L_T}\frac{\left(\hat{\phi}_{i+1} - 2\hat{\phi}_i + \hat{\phi}_{i-1}\right)}{(\Delta x)^2} \\ &= -\frac{\Delta x}{L_T}\hat{\phi}_i'' \end{aligned} \tag{2.43}$$

By combining the time derivative of Eq. (2.41), with Eq. (2.43), while going to the continuum limit, where $\phi_i \to \phi(x_i, t)$, we arrive at the Klein-Gordon equation for a massless scalar field,

$$\ddot{\hat{\phi}}(x,t) - \frac{1}{C_T L_T}\hat{\phi}''(x,t) = 0, \tag{2.44}$$

where the speed of light in the transmission line is given by $c^2 = 1/C_T L_T$.

The Klein Gordon equation is easily solved by expanding the field in terms of Fourier operators,

$$\hat{\phi}(x,t) = \frac{1}{\sqrt{2\pi}}\int_{-\infty}^{\infty} dk\hat{\phi}(k,t)e^{-ikx}, \tag{2.45}$$

and similarly for $\hat{q}(x,t)$. In k space, Eq. (2.44) then becomes,

$$\ddot{\hat{\phi}}(k,t) + c^2|k|^2\hat{\phi}''(k,t) = 0. \tag{2.46}$$

This is nothing but the equation of motion of the simple Harmonic oscillator that we have already seen in section 2.1.1, with the dispersion relation $\omega_k = c|k|$. The Hamiltonian, which is now a field Hamiltonian, reads,

$$H = \frac{1}{2C_T}\int_{-\infty}^{\infty} dk \left(\hat{q}(k,t)\hat{q}(-k,t) + C_T\omega_k^2\hat{\phi}(k,t)\hat{\phi}(-k,t)\right). \tag{2.47}$$

We can expand the operators in terms of creation and annihilation operators. Since we have an infinite number of oscillators we define one operator for each mode,

$$\hat{\phi}(k,t) = \sqrt{\frac{L_T\omega_k\hbar}{2}}\left(\hat{a}_k(t) + \hat{a}^\dagger_{-k}(t)\right), \tag{2.48}$$

$$\hat{q}(k,t) = -i\sqrt{\frac{C_T\omega_k\hbar}{2}}\left(\hat{a}_k(t) - \hat{a}^\dagger_{-k}\right). \tag{2.49}$$

With the annihilation and creation operators fulfilling the commutation relations,

$$[\hat{a}_k, \hat{a}^\dagger_{k'}] = \delta(k-k') \tag{2.50}$$

$$[\hat{a}_k, \hat{a}_{k'}] = [\hat{a}^\dagger_k, \hat{a}^\dagger_{k'}] = 0. \tag{2.51}$$

We can make the operators time independent by transforming to the Schrödinger picture. In the Heisenberg picture, the time evolution of the ladder operators are given by,

$$\hat{a}^H(t) = \hat{a}^S e^{-i\omega t}. \tag{2.52}$$

In terms of the time independent ladder operators, the flux and charge operators are then given by,

$$\hat{\phi}(x,t) = \sqrt{\frac{\hbar L_T}{4\pi}}\int_{-\infty}^{\infty} dk\sqrt{\omega_k}\left(\hat{a}_k e^{-i(kx+\omega t)} + \text{H.c.}\right) \tag{2.53}$$

$$\hat{q}(x,t) = -i\sqrt{\frac{\hbar C_T}{4\pi}}\int_{-\infty}^{\infty} dk\sqrt{\omega_k}\left(\hat{a}_k e^{-i(kx+\omega t)} - \text{H.c.}\right). \tag{2.54}$$

It can be useful to evaluate the fields at one position, e.g., a node to which another circuit is coupled, and separate the field components propagating left and right at that position. The field that propagates into a certain node can then be called an *incoming* field, and the field component that propagates away from that node can be called an *outgoing* field; a notation we adopt in paper I. This is achieved by splitting the integral in Eq. (2.53) into positive and negative wave vectors,

$$\begin{aligned}\hat{\phi}(x,t) = &\sqrt{\frac{\hbar L_T}{4\pi}}\int_0^{\infty} dk\sqrt{\omega_k}\left(\hat{a}_k e^{-i(kx+\omega t)} + \hat{a}^\dagger_k e^{i(kx+\omega t)}\right)\\ &+ \sqrt{\frac{\hbar L_T}{4\pi}}\int_0^{\infty} dk\sqrt{\omega_k}\left(\hat{a}_{-k} e^{-i(-kx+\omega t)} + \hat{a}^\dagger_{-k} e^{i(-kx+\omega t)}\right).\end{aligned} \tag{2.55}$$

As an example, we can define the right going field at the node located at $x = 0$ as incoming, and the left going field at the same position as outgoing. The flux field is then written as,

$$\begin{aligned}\phi_0(t) &= \sqrt{\frac{\hbar L_T}{4\pi}} \int_0^\infty dk \sqrt{\omega_k} \left[a_k^{\text{in}} e^{-i\omega_k t} + \left(a_k^{\text{in}}\right)^\dagger e^{i\omega_k t} + a_k^{\text{out}} e^{-i\omega_k t} + \left(a_k^{\text{out}}\right)^\dagger e^{i\omega_k t} \right] \\ &= \phi_0^{\text{in}}(t) + \phi_0^{\text{out}}(t).\end{aligned} \tag{2.56}$$

2.4 The transmon

Although there are several realizations of qubits based on quantized electrical circuits, such as flux qubits [85, 86], and phase qubits [87], the most common variant used is the charge qubit. The first realization of a charge qubit was called the Cooper-pair box [88], and consisted of a superconducting island connected to a superconducting reservoir by a Josephson junction. The Josephson junction consists of two superconducting leads, separated by a thin non-superconducting layer. The separation is small enough that Cooper-pairs can tunnel from one lead to the other. It turned out that the first realizations of a Cooper-pair box were very sensitive to charge noise. The energy level separation changed dramatically as the charge on the superconducting island fluctuated. A large shunt capacitor was added to the qubit to redeem this problem, which made it insensitive to charge noise. This design was called the transmon [47]. The equivalent circuit of a transmon can be seen in Fig. 2.4, where we have neglected any possible extra charge added to the island by the environment. Some common alterations of the transmon, like the Xmon [89], are identical to the transmon because they operate in the same regime of the same Hamiltonian. The difference is a design choice to make the Xmon, e.g., better suited for a scalable quantum computer architecture.

We do not derive the energy of the Josephson junction here but refer the reader to standard textbooks on the subject, such as [90]. The potential energy of the Josephson junction is given by $\mathcal{L} = -E_J \cos(\delta)$, where δ is the superconducting phase difference across the junction and the Josephson energy $E_J = \Phi_0 I_c / 2\pi$ is set by the magnetic flux quantum Φ_0 and the critical current I_c of the superconductor making up the junction.

We can immediately write down the Lagrangian for the system,

$$\mathcal{L} = \frac{1}{2} C_J \dot{\phi}_1^2 + E_J \cos(\delta), \tag{2.57}$$

which gives us the following Hamiltonian,

$$H = \frac{q_1^2}{2C_J} - E_J \cos(\delta). \tag{2.58}$$

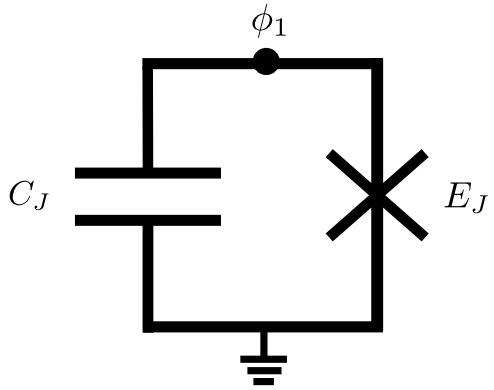

Figure 2.4: *Effective circuit for a simple transmon design, neglecting any offset charge added to the island by an external gate or surrounding.*

The phase difference across the junction can be expressed in terms of the flux $\delta = 2e\phi_1/\hbar = 2\pi\phi_1/\Phi_0$, with e being the electron charge. We can thus quantize the system imposing the usual commutation relations between flux and charge and write the Hamiltonian in terms of the flux instead,

$$H = \frac{\hat{q}_1^2}{2C_J} - E_J \cos\left(\frac{2\pi\hat{\phi}_1}{\Phi_0}\right). \tag{2.59}$$

It is common to rewrite the Cooper pair box Hamiltonian to a slightly different form. By introducing the charging energy $E_C = e^2/2C_J$, the energy it takes to put an electron onto one of the junction islands, and the Cooper-pair number operator $\hat{n} = \hat{q}_1/2e$, the Hamiltonian takes the form,

$$H = 4E_C\hat{n}^2 - E_J \cos(\delta). \tag{2.60}$$

Here we used the phase difference δ again since that is the true conjugate variable to the number operator.

Let us now study the charge qubit's energy spectrum, both the linearized spectrum and the full anharmonic spectrum. The harmonic spectrum is obtained by expanding the Hamiltonian in Eq. (2.59) for small values of $\hat{\phi}_1/\Phi_0$, and throwing away the higher-order terms,

$$H = \frac{\hat{q}_1^2}{2C_J} - E_J\left(\frac{2\pi}{\Phi_0}\right)^2\frac{\hat{\phi}_1^2}{2}. \tag{2.61}$$

The prefactor of the second term defines the so called Josephson inductance $L_J^{-1} = E_J 4\pi^2/\Phi_0^2$. The Hamiltonian is then again a simple harmonic oscillator, with resonance frequency (called the Josephson plasma frequency),

$$\omega_0 = \frac{1}{\sqrt{L_J C_J}} = \frac{1}{\hbar}\sqrt{8E_J E_C}. \tag{2.62}$$

This is, however, only fully valid in a classical sense where we can consider arbitrarily small values of $\hat{\phi}_1$, quantum mechanically the values of $\hat{\phi}_1$ are limited by the zero-point fluctuations. The zero-point fluctuations are only small in the limit of $E_J \gg E_C$, which can be seen by writing the flux operator (which is only correct in the harmonic approximation) as

$$\hat{\phi}_1 = \phi_{\text{ZPF}}(\hat{a} + \hat{a}^\dagger), \tag{2.63}$$

with

$$\phi_{\text{ZPF}} = \sqrt{\frac{\hbar}{2C_J\omega_0}}. \tag{2.64}$$

We write it this way because $\langle 0|\, \hat{\phi}_1^2 \,|0\rangle = \phi_{\text{ZPF}}^2$. We thus have that,

$$\frac{2\pi\phi_{\text{ZPF}}}{\Phi_0} = \sqrt{\frac{2E_C}{E_J}}, \tag{2.65}$$

which shows that the harmonic solution is only approximately true in the limit of $E_J \gg E_C$. This is, however, fulfilled in the transmon regime. Thus, for the transmon, we can use the harmonic solution and add the anharmonicity as a small perturbation. We thus have that $H = H_0 + V$, where H_0 is the linearized Hamiltonian Eq. (2.59), and $V = E_J(2\pi/\Phi_0)^4\phi_{\text{ZPF}}^4(\hat{a} + \hat{a}^\dagger)^4/24$ is the 4th order contribution in the expansion of the Josephson potential. Perturbation theory up to first order then yields that

$$V \approx -\frac{E_C}{2}\left(\hat{a}^\dagger\hat{a}^\dagger\hat{a}\hat{a} + 2\hat{a}^\dagger\hat{a}\right). \tag{2.66}$$

We can understand the two terms in the following way: the second term is a small renormalization to the harmonic oscillator frequency which is now given by $\omega_0' = \sqrt{8E_CE_J} - E_C$. The first term gives rise to an anharmonicity in the energy spectrum, such that $\omega_{21} - \omega_{10} = -E_C$, where $\omega_{ij} = \omega_i - \omega_j$. The energy spectrum of the transmon thus get denser at higher energies.

2.5 The Jaynes-Cummings model and dispersive readout

Although this thesis does not deal with the topic of quantum measurements in general, it can be interesting to see at least one approach to measuring the state of a superconducting qubit. Quantum measurements can be divided into two categories: quantum demolition measurements (QD) and quantum non-demolition measurements (QND). A photon hitting a wall is an example of a QD measurement since the photon is destroyed in the measurement process. The approach we

present here is an example of a QND measurement and is referred to as *dispersive* readout [91].

We start from the Rabi model, which describes the interaction of a two-level system and a single mode of a resonator,

$$H_{\mathrm{R}} = \frac{\omega_0}{2}\sigma_z + \omega_r a^\dagger a + g\sigma_x\left(a + a^\dagger\right), \tag{2.67}$$

where σ_i for $i = x, y, z$ are the Pauli spin operators, ω_0 is the resonance frequency of the two level system, ω_r is the resonator frequency, a ($a^\dagger$) is the bosonic annihilation (creation) operator, and g is a coupling constant. Since σ_x can be rewritten in terms of the raising and lowering operators of the two-level system, $\sigma_x = \sigma_+ + \sigma_-$, the coupling term will exchange excitations between the two-level system and the resonator. By going to the interaction picture, two of the coupling terms, $\sigma_- a$ and $\sigma_+ a^\dagger$, rotate with the frequency $\omega_0 + \omega_r$; these are called counter-rotating terms. The two remaining terms, $\sigma^+ a^\dagger$ and $\sigma^- a$, rotate with the frequency $\omega_0 - \omega_r$. For $\omega_r \approx \omega_0$, the counter-rotating terms thus rotate with frequency $2\omega_0$, and will average out over longer time scales. As long as the coupling constant is much smaller than the other frequencies involved, $g \ll \{\omega_0, \omega_r\}$, the counter-rotating terms can be neglected. This is called the rotating-wave approximation (RWA), and it simplifies the Rabi Hamiltonian to the Jaynes-Cummings Hamiltonian [92],

$$H_{\mathrm{JC}} = \frac{\omega_0}{2}\sigma_z + \omega_r a^\dagger a + g\left(\sigma_+ a + \sigma_- a^\dagger\right), \tag{2.68}$$

where we left the interaction picture after we performed the RWA. In contrast to the Rabi Hamiltonian, the Jaynes-Cummings Hamiltonian preserves the number of excitations in the system.

If the qubit and resonator are far from resonant with each other, this setup can be used to read out the state of the qubit. It becomes clear if we transform the Jaynes-Cummings Hamiltonian into the so-called dispersive regime. If the detuning, $\Delta = |\omega_r - \omega_0|$ is large compared to the coupling constant, $g \ll \Delta$, we can apply the unitary transformation

$$U = e^{\frac{g}{\Delta}(\sigma_- a^\dagger - \sigma_+ a)}, \tag{2.69}$$

and do a perturbation expansion up to first order in g/Δ, which gives the dispersive Hamiltonian,

$$H_{\mathrm{disp}} = \left(\omega_r + \frac{g^2}{\Delta}\sigma_z\right) a^\dagger a + \frac{\omega_0 + g^2/\Delta}{2}\sigma_z. \tag{2.70}$$

From H_{disp}, we see that the resonator and the qubit are no longer exchanging excitations, as they do if they are resonant with each other. However, exciting the qubit will change the resonator frequency. This means that by probing the resonance frequency of the resonator, the state of the qubit can be read out without having to interfere with the qubit itself. The dispersive readout is one of the most common readout schemes of superconducting qubits [3].

3 Surface acoustic waves

This chapter reviews some of the literature on surface acoustic waves (SAWs) and their interaction with electrical circuits, motivated by paper I and II, where the interaction between SAWs and a transmon atom is studied. Parts of this chapter might seem, rightfully so, detailed compared to the other chapters. The detailed introduction is motivated by the very recent introduction of SAWs to the circuit QED community. Before exploring SAWs' quantum properties, we must understand where they come from and what they are.

3.1 Surface waves in non-piezoelectric substrates

It turns out that the motion of surface acoustic waves in piezoelectric materials is primarily determined by the solutions to the wave equations in non-piezoelectric materials. It is a consequence of the small amount of energy residing in the electric field compared to the mechanical energy in the acoustic field. Therefore, we begin the introduction to SAWs by solving the wave equations in non-piezoelectric materials. We follow closely the derivation by Schutz [93], which in turn is based on the results in Refs. [94] and [95].

The elastic wave equation in a solid can be written in terms of the displacement vector u_k,

$$c_{ijkl}\partial_j\partial_k u_l + \rho\ddot{u}_i = 0, \tag{3.1}$$

where ρ is the mass density of the solid, and c_{ijkl} is the elasticity tensor, where we have assumed Einstein's summation convention. This is nothing but three coupled wave equations, one for each direction $i = x, y, z$. The most common material for SAW devices in circuit QAD is gallium arsenide (GaAs), which has a cubic lattice structure. For any cubic lattice, there are only three independent components in the elasticity tensor, denoted c_{11}, c_{12}, and c_{44} (where Voigt notation is used to reduce the number of indices). One can find the values of the elasticity constants in standard references, such as [96].

If we consider a wave that propagates along the surface of the material, with $\hat{z}$ being the direction normal to the surface, we can write the boundary condition that there is no net force acting on the wave at the surface as,

$$c_{\hat{z}jkl}\partial_l u_k = 0. \tag{3.2}$$

Taking the cubic lattice symmetries into account, the wave equation for $i = x$ becomes,

$$c_{11}\partial_x^2 u_x + c_{44}\left(\partial_y^2 u_x + \partial_z^2 u_x\right) + (c_{12} + c_{44})(\partial_x\partial_y u_y + \partial_x\partial_z u_z) + \rho\ddot{u}_x = 0, \quad (3.3)$$

and the other two wave equations can be found by cyclic permutation of the indices. The boundary conditions become,

$$\begin{aligned} c_{44}(\partial_x u_z + \partial_z u_x) &= 0, \\ c_{44}(\partial_y u_z + \partial_z u_y) &= 0, \\ c_{11}\partial_z u_z + c_{12}\left(\partial_x u_x + \partial_y u_y\right) &= 0. \end{aligned} \quad (3.4)$$

Following the reasoning in Ref. [95], the solution we are looking for is a wave propagating in the $x - y$ plane at $z = 0$ (the surface), with wave vector $\vec{k} = k(l\hat{x} + m\hat{y})$, where $l = \cos\theta$, $m = \sin\theta$, and θ denotes the angle between the $\hat{x}$ axis and the wave vector $\vec{k}$. We make the following ansatz,

$$\begin{pmatrix} u_x \\ u_y \\ u_z \end{pmatrix} = \begin{pmatrix} U \\ V \\ W \end{pmatrix} e^{-kqz} e^{ik(lx+my-v_s t)}, \quad (3.5)$$

where q is some decay constant that determines how far into the bulk the wave extends, and v_s is the phase velocity, which we refer to as just the velocity from now on. Inserting this ansatz into the wave equation, Eq. (3.3), and similarly for the two other directions, while writing the wave equation on matrix form $M\vec{A} = 0$, where $\vec{A} = (U, V, W)^T$ and

$$M = \begin{pmatrix} c_{11}l^2 + c_{44}(m^2 - q^2) - \rho v_s^2 & lm(c_{12} + c_{44}) & lq(c_{12} + c_{44}) \\ lm(c_{12} + c_{44}) & c_{11}m^2 + c_{44}(l^2 + q^2) - \rho v_s^2 & mq(c_{12} + c_{44}) \\ lq(c_{12} + c_{44}) & mq(c_{12} + c_{44}) & c_{11}q^2 - c_{44} + \rho v_s^2 \end{pmatrix}, \quad (3.6)$$

we obtain that the only nontrivial solutions are found in the case of a vanishing determinant $\det M = 0$. The equation $\det M = 0$ has in general three roots, q_1^2, q_2^2, and q_3^2, all three depending on the velocity v_s and the angle θ. However, the solutions need to converge as $z \to \infty$, which means that there can not be any surface waves deep into the bulk. Thus, if we only keep the solutions that lead to zero displacements inside the bulk, we can write a general solution as a superposition of surface waves with allowed q_i values,

$$(u_x, u_y, u_z) = \sum_{i=1,2,3} (\xi_i, \eta_i, \chi_i) K_i e^{-kq_i z} e^{ik(lx+my-v_s t)}, \quad (3.7)$$

where the ratios in the amplitudes can be calculated for any $q_i(v_s, \theta)$ according to,

$$K_r = \frac{U_i}{\xi_i} = \frac{V_i}{\eta_i} = \frac{iW_i}{\chi_i}, \quad (3.8)$$

where the quantities ξ_i, η_i and χ_i were introduced as parts of the determinant of M according to,

$$\begin{aligned}
\xi_i &= \begin{vmatrix} c_{11}m^2 + c_{44}(l^2+q^2) - \rho v_s^2 & mq(c_{12}+c_{44}) \\ mq(c_{12}+c_{44}) & c_{11}q^2 - c_{44} + \rho v_s^2 \end{vmatrix}, \\
\eta_i &= \begin{vmatrix} lm(c_{12}+c_{44}) & mq(c_{12}+c_{44}) \\ lq(c_{12}+c_{44}) & c_{11}q^2 - c_{44} + \rho v_s^2 \end{vmatrix}, \\
\chi_i &= \begin{vmatrix} lm(c_{12}+c_{44}) & c_{11}m^2 + c_{44}(l^2+q^2) - \rho v_s^2 \\ lq(c_{12}+c_{44}) & mq(c_{12}+c_{44}) \end{vmatrix}.
\end{aligned} \tag{3.9}$$

Although there is an amplitude for each root q_i and each displacement u_i, the velocity v_s is the same for each q_i and can be determined from the boundary condition at $z = 0$. To do so, we rewrite the boundary condition on matrix form as well: $B\vec{K} = 0$, with $\vec{K} = (K_1, K_2, K_3)$, and where

$$B = \begin{pmatrix} l\chi_1 - q_1\xi_1 & l\chi_2 - q_2\xi_2 & l\chi_3 - q_3\xi_3 \\ m\chi_1 - q_1\eta_1 & m\chi_1 - q_1\eta_1 & m\chi_3 - q_3\eta_3 \\ l\xi_1 + m\eta_1 + aq_1\chi_1 & l\xi_2 + m\eta_2 + aq_2\chi_2 & l\xi_3 + m\eta_3 + aq_3\chi_3 \end{pmatrix}, \tag{3.10}$$

where $a = c_{11}/c_{12}$. This equation also has non-trivial solutions only when $\det B = 0$. In summary, $\det M = 0$ and $\det B = 0$ determines the velocity v_s and decay constant q_i, and Eq. (3.8) determines the amplitudes. The full formal solution can thus be found from these three equations.

Even though a solution could be found for propagation in any direction in principle, one for each value of $l = \cos\theta$ and $m = \sin\theta$, not all solutions are physical or realized in materials. Since q_i can be complex, some solutions may lead to non-vanishing displacements inside the bulk even though reasonable velocities are found. Luckily, we are interested in the [110] direction of GaAs. Since this is a high-symmetry direction for a cubic lattice, a relatively simple analytical solution can be found for this case. For the [110] direction we have that $l = m = 1/\sqrt{2}$. By inserting l and m and subtracting the second row of M in Eq. (3.6) from the first row, we find a common denominator $(c_{12} - c_{12})/\sqrt{2} - \rho v^2$, which leaves the first row as $(1, -1, 0)$. Thus, we have that $U = V$ and the wave equations simplifies to the problem of solving $M' \cdot (U, iW) = 0$, where

$$M' = \begin{pmatrix} c'_{11} - \rho v_s^2 - c_{44}q^2 & \frac{q}{\sqrt{2}}(c_{12}+c_{44}) \\ q\sqrt{2}(c_{12}+c_{44}) & c_{11}q^2 - c_{44} + \rho v_s^2 \end{pmatrix}, \tag{3.11}$$

where we wrote $c'_{11} = (c_{11} - \rho v_s^2 - c_{44}q^2)/2$. The characteristic equation $\det M' = 0$ then gives us the following equation to solve in order to obtain q,

$$(c'_{11} - \rho v_s^2 - c_{44}q^2)(c_{11} - c_{44} + \rho v_s^2) - q^2(c_{12}+c_{44})^2 = 0. \tag{3.12}$$

From this equation it is possible to deduce that vanishing displacements in the bulk are only possible for purely imaginary values of q, or positive and real values

of q. This gives two possible solutions, q_1 and q_2. The velocity we can find from the mechanical boundary condition. First we do a coordinate transformation such that the direction of propagation is aligned with the x-axis, we define the new axis as $x' = x\sqrt{2}$. The boundary condition at $z = 0$ is then written as,

$$\begin{aligned} \partial_{x'} u_z + \partial_z u_{x'} &= 0 \\ c_{12}\partial_{x'} u_{x'} + c_{11}\partial_z u_z &= 0. \end{aligned} \tag{3.13}$$

If we remind ourselves of the ansatz we made earlier, but this time in terms of the new x-axis and the supposed knowledge of q,

$$\begin{pmatrix} u_{x'} \\ u_z \end{pmatrix} = \sum_{i=1,2} \begin{pmatrix} U_i \\ iW_i \end{pmatrix} e^{-kq_i z} e^{-ik(x'-ct)}, \tag{3.14}$$

and by introducing the ratio of the two amplitudes $\gamma_i = iW_i/U_i$, which is found from the kernel of M' to be,

$$\gamma_i = q_i \frac{c_{11} + c_{44}}{c_{11}(X + q_i) + c_{44}}, \tag{3.15}$$

where $X = \rho v_s^2 c_{11}$, we can formulate the boundary condition on a new matrix form as $B' \cdot (U_1', U_2') = 0$, where,

$$B' = \begin{pmatrix} \gamma_1 - q_1 & \gamma_2 - q_2 \\ 1 + \frac{c_{11}}{c_{22}} q_1\gamma_1 & 1 + \frac{c_{11}}{c_{22}} q_2\gamma_2 \end{pmatrix}. \tag{3.16}$$

The characteristic equation for B' then gives,

$$(\gamma_1 - q_1)(1 + \frac{c_{11}}{c_{22}} q_2\gamma_2) - (\gamma_2 - q_2)(1 + \frac{c_{11}}{c_{22}} q_1\gamma_1) = 0. \tag{3.17}$$

Inserting the expressions for γ_1 and γ_2, Eq. (3.15), into this equation, gives after some rearrangement,

$$\begin{aligned} &q_1\Big(c_{12} + \rho v_s^2 + c_{11}q_1^2\Big)\Big(c_{12}(c_{44} - \rho v_s^2) + c_{11}c_{44}q_2^2\Big) - \\ &q_2\Big(c_{12} + \rho v_s^2 + c_{11}q_2^2\Big)\Big(c_{12}(c_{44} - \rho v_s^2) + c_{11}c_{44}q_1^2\Big) = 0. \end{aligned} \tag{3.18}$$

From this equation it is possible to factor out a $q_1 - q_2$, which after some manipulation gives,

$$\begin{aligned} 0 = {} & c_{12}\Big(\frac{c_{12}}{c_{11}} + X\Big)\Big(\frac{c_{44}}{c_{11}} - X\Big) + c_{44}q_1^2 q_2^2 \\ & + c_{12}\Big(\frac{c_{44}}{c_{11}} - X\Big)(q_1^2 + q_2^2 + q_1 q_2) - c_{44}q_1 q_2\Big(\frac{c_{12}}{c_{11}} + X\Big). \end{aligned} \tag{3.19}$$

By plugging in the expressions for q_1^2 and q_2^2 that can be obtained from Eq. (3.17), one arrives at an explicit equation for the velocity v_s,

$$\Big(1 - \frac{c_{11}}{c_{44}}X\Big)\Big(\frac{c_{11}c_{11}' - c_{12}^2}{c_{11}^2} - X\Big)^2 = X^2\Big(\frac{c_{11}'}{c_{11}} - X\Big). \tag{3.20}$$

This equation is cubic in $X = \rho v_s^2$, but we are only interested in the lowest velocity mode, which is the mode referred to as the Rayleigh mode. Finally, we note that we have derived an equation that only depends on material properties: the elasticity constants c_{11}, c_{12}, c_{44} and the mass density ρ.

The ansatz for the displacements in Eq. 3.14 can be simplified. The two roots q_1 and q_2 are related by the relation $q_1 = q_2^*$, from this it follows that also the ratios of the amplitudes satisfies $\gamma_1 = \gamma_2^*$. Hence, we can write $q \equiv q_1 = q_2^*$ and $\gamma \equiv \gamma_1 = \gamma_2^*$, which implies that the original ansatz in Eq. 3.5 can be simplified to,

$$\begin{aligned} u_{x'} &= U\Big(e^{-qkz-i\phi} + e^{-qkz+i\phi}\Big)e^{ik(x'-v_st)}, \\ u_z &= U\Big(\gamma e^{-qkz-i\phi} + \gamma^* e^{-qkz+i\phi}\Big)e^{ik(x'-v_st)}. \end{aligned} \tag{3.21}$$

As an interesting side note, Rayleigh waves are also what we see traveling the earth's surface in an earthquake. SAW beams emitted at a single phonon level, such as in the experiment in paper II, can thus be seen as tiny earthquakes, perhaps the smallest earthquakes ever observed.

3.2 Surface waves in piezoelectric substrates

As we have now seen the case of SAWs in non-piezoelectric materials, we now turn to study how the results obtained above change when we turn on the piezoelectric coupling. We start with a general formulation before turning to the specific case of a cubic lattice and propagation in the [110] direction of a (001) surface.

For an acoustic wave traveling at the surface of a piezoelectric material, the elastic wave and electromagnetic field are coupled. In principle, we want to solve Newton's and Maxwell's equations simultaneously to find the field distributions. Two solutions are then obtained, one describing an elastic wave moving with velocity v_s with an accompanying electric field, and one describing an electromagnetic wave, with velocity $c \approx 10^5 v_s$, traveling with an accompanying mechanical strain. For the elastic wave solution, the magnetic field is negligible, since it is due to an electric field moving with velocity much smaller than the speed of light, so that, $\nabla \times \vec{E} = -\partial_t B \approx 0 \Rightarrow E = -\nabla\phi$. This implies that elastic waves in piezoelectric materials can be described within the quasi-static approximation, i.e., the electric field is static compared to the electromagnetic field.

The wave equations for an acoustic wave in a piezoelectric material connects the mechanical stress tensor T and the electrical displacement D with the mechanical strain u and the electric potential ϕ,

$$\begin{aligned} T_{ij} &= c_{ijkl}\partial_k u_l + e_{ijk}\partial_k\phi, \\ D_i &= -\epsilon_{ij}\partial_j\phi + e_{ijk}\partial_j u_k, \end{aligned} \tag{3.22}$$

where c_{ijkl} is the stress tensor, e_{ijk} is the piezoelectric tensor and ϵ_{ijk} is the permittivity tensor. Compared to the non-piezoelectric case, Hooke's law has now been modified to also take into account an additional stress due to the piezoelectric effect, while the electric displacement field is accounting for the piezoelectricity by an additional polarization induced by the strain. Newton's second law then becomes,

$$\rho\ddot{u}_i = c_{ijkl}\partial_j\partial_k u_l + e_{ijk}\partial_j\partial_k\phi. \tag{3.23}$$

The mechanical boundary condition, that there should be no net force acting on the surface, now becomes,

$$T_{i\hat{z}}\big|_{z=0} = c_{i\hat{z}kl}\partial_k u_l + e_{i\hat{z}k}\partial_k\phi = 0 \tag{3.24}$$

in close analogy to Eq. (3.2), which is the corresponding equation without piezoelectricity. In this case we also have an electrostatic boundary condition,

$$D_z(z = 0^+) = D_z(z = 0^-), \tag{3.25}$$

that is, the dielectric field, normal to the surface, has to be continuous across the surface. Above the surface, at $z > 0$, we assume vacuum. Thus, $D_z = \epsilon_0 E = -\epsilon_0\partial_z\phi_{\text{out}}$ and the electrical potential has to satisfy the Poisson equation $\nabla^2\phi_{\text{out}} = 0$. From this we make the ansatz for the electrical potential above the surface,

$$\phi_{\text{out}} = A_{\text{out}}e^{\Omega kz}e^{ik(x-v_s t)}. \tag{3.26}$$

The Poisson equation then gives us,

$$\nabla^2\phi_{\text{out}} = (-k^2 + \Omega^2 k^2)\phi_{\text{out}} = 0, \tag{3.27}$$

which is only fulfilled if $\Omega = 1$. This means that the electrical potential decays exponentially outside of the medium with an approximate length scale equal to the SAW wavelength $\lambda = 2\pi/k \approx 1\mu$m. We would now like to find the amplitude A_{out}, which is done from the condition that the electric potential, just as the field, has to be continuous across the surface,

$$\phi(z = 0^-) = \phi_{\text{out}}(z = 0^+). \tag{3.28}$$

In summary, the electrical boundary condition reads,

$$e_{\hat{z}jk}\partial_j u_k - \epsilon_{\hat{z}j}\partial_j\phi + \epsilon_0\phi|_{z=0} = 0. \tag{3.29}$$

We now move on and apply what we have formulated above to the specific case of a cubic lattice with propagation in the [110] direction of a (001) surface, relevant for GaAs. In fact, there is only one non-zero independent component in

the piezoelectric tensor for any cubic lattice, denoted e_{14}. The wave equations then simplify to four coupled differential equations,

$$\begin{cases} \rho\ddot{u_x} = c_{11}\partial_x^2 u_x + c_{44}\Big(\partial_y^2 u_x + \partial_z^2 u_x\Big) + (c_{12}+c_{44})\Big(\partial_x\partial_y u_y + \partial_x\partial_z u_z\Big) + 2e_{14}\partial_y\partial_z\phi, \\ \rho\ddot{u_y} = c_{11}\partial_y^2 u_y + c_{44}\Big(\partial_z^2 u_y + \partial_x^2 u_y\Big) + (c_{12}+c_{44})\Big(\partial_y\partial_z u_z + \partial_y\partial_x u_x\Big) + 2e_{14}\partial_z\partial_x\phi, \\ \rho\ddot{u_z} = c_{11}\partial_z^2 u_z + c_{44}\Big(\partial_x^2 u_z + \partial_y^2 u_z\Big) + (c_{12}+c_{44})\Big(\partial_z\partial_x u_x + \partial_z\partial_y u_y\Big) + 2e_{14}\partial_x\partial_y\phi, \\ \epsilon\nabla^2\phi = 2e_{14}\Big(\partial_y\partial_z u_x + \partial_x\partial_z u_y + \partial_x\partial_y u_z\Big), \end{cases} \tag{3.30}$$

with ϵ being the dielectric constant of the material. The mechanical boundary conditions at $z = 0$ become,

$$\begin{aligned} T_{13} &= c_{44}\Big(\partial_x u_z + \partial_z u_x\Big) + e_{14}\partial_y\phi = 0, \\ T_{23} &= c_{44}\Big(\partial_y u_z + \partial_z u\Big) + e_{14}\partial_x\phi = 0, \\ T_{33} &= c_{11}\partial_z u_z + c_{12}\Big(\partial_x u_x + \partial_y u_y\Big) = 0, \end{aligned} \tag{3.31}$$

and the electrical boundary condition becomes,

$$e_{14}\Big(\partial_y u_x + \partial_x u_y\Big) - \epsilon\partial_z\phi + \epsilon_0 k\phi. \tag{3.32}$$

For weak piezoelectric materials, such as GaAs, the piezoelectric constant ϵ_{14} is very small compared to the mechanical amplitude. Because of that, the mechanical wave equations in piezoelectric materials will be solved by the solution obtained in a non-piezoelectric material, with corrections only at the order $e_{14}^2\epsilon$, which is two or three orders of magnitude smaller than a typical mechanical displacement u.

With the expression for the displacements obtained in Eq. (3.21), it is possible to make an ansatz for the electric potential that solves both the wave equation and the boundary condition. We do not prove it here, but it can be shown that it is done by the following expression for ϕ [95],

$$\phi = \begin{cases} i\dfrac{e_{14}}{\epsilon}\mathcal{F}(kz)e^{ik(x-v_s t)}, & \text{in the material} \\ i\dfrac{e_{14}}{\epsilon}\mathcal{F}(0)e^{kz}e^{ik(x-v_s t)}, & \text{outside the material} \end{cases} \tag{3.33}$$

where $\mathcal{F}(kz)$ is a dimensionless function that determines the decay length scale of the wave into the bulk,

$$\mathcal{F}(kz) = 2|A_1|e^{-\alpha kz}\cos(\beta kz + \phi + \epsilon) + A_3 e^{-kz}, \tag{3.34}$$

where,

$$\begin{aligned} A_1 &= \frac{\gamma - 2q}{q^2 - 1}, \\ A_3 &= -\frac{2}{\epsilon + \epsilon_0}\Big(\epsilon \cos\varphi + \epsilon \mathrm{Re}[A_1 q e^{-i\varphi}] + \epsilon_0 \mathrm{Re}[A_1 e^{-i\varphi}]\Big), \end{aligned} \tag{3.35}$$

with q and γ defined in sec 3.1. By plugging in material constants for GaAs, a SAW velocity of $v_s \approx 2900$m/s is obtained, and a SAW decay length of about 1.5λ.

3.3 Lumped-element model of interdigital transducers

Interdigital transducers (IDTs) (see Fig. 3.1) are strips of thin metallic films deposited at the surface of piezoelectric materials in order to transduce an electrical signal to an acoustic signal and vice versa. The transduction is achieved by applying a voltage to the IDT electrodes (often called IDT fingers), and the electric field that is created couples to the substrate via the piezoelectric effect. We denote the width of the IDT fingers in Fig. 3.1 as a, and the distance between a finger of positive voltage and a finger of negative voltage as p, often referred to as the finger pitch. The ratio of a/p is called the metallization ratio and is an important figure of merit for IDTs. In this chapter, we, restrict the discussion to symmetric IDTs with a metallization ratio of 0.5. Such IDTs are bidirectional, and the analysis that follows gets simplified. It is also the most common type of IDTs used for SAW-coupled qubits thus far to maximize transduction. However, exciting work has been done recently [97], in which highly non-symmetric IDTs are used to build unidirectional IDTs in the quantum regime, opening up the possibility to build chiral SAW waveguides [22].

For symmetric IDTs there is a well defined resonance frequency, set by the finger pitch, $\omega_{\mathrm{IDT}} = 2\pi v_s/2p$, where v_s is the speed of SAW. At this frequency, the waves emitted from the IDT interfere constructively, maximizing the transduction. Since the superconducting qubits are operating in the GHz regime, and the SAW speed is around 3000 m/s, a typical finger pitch is around $1 - 10\mu$m. For most circuit QAD devices, the total number of finger pairs N_p (one positive and one negative voltage finger) is usually around 10, which means that an IDT is on the order of 100 μm long.

To discuss the behavior of IDTs in an electrical setting, we derive a lumped-element model of IDTs. We closely follow the description in Ref. [98], with some additions from Ref. [99].

Without the piezoelectric substrate, the IDT is just one large capacitor. By adding the piezoelectric substrate, the IDT radiates SAWs, which can be accounted for in terms of a radiation conductance G_a. Since the emitted SAWs will

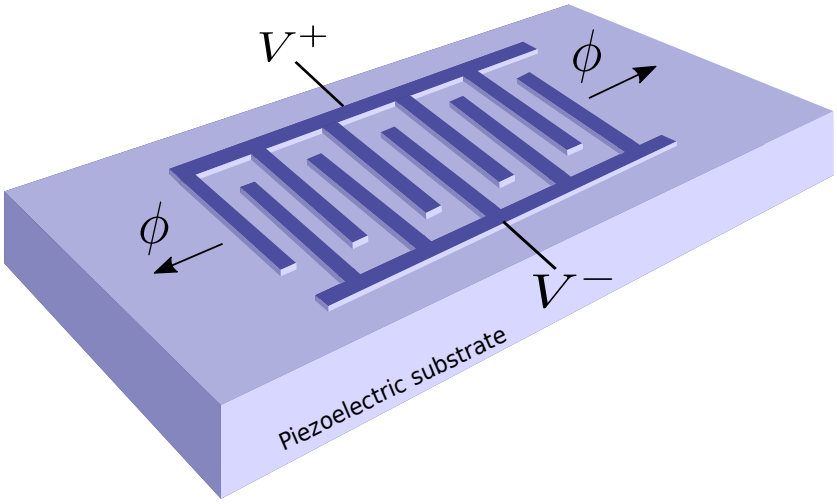

Figure 3.1: *Schematic illustration of an IDT.*

re-interact with the IDT, there will also be a susceptance B_a. Together, these two make up what is called the acoustic admittance $Y_a = G_a + iB_a$. The subscript is there to remind ourselves of its acoustic origin; it would be zero without the piezoelectric substrate. The purely electric capacitance will add to the total admittance of the IDT, $Y = Y_a + i\omega C_{\text{IDT}}$. Let us see how each of these components can be determined.

Since the IDT works both as a receiver and as a transmitter of acoustic waves, it is convenient to define a receiver, and a transmitter response function [98]. An applied voltage, $V_t = V^+ - V^-$, to the transducer, with $V^\pm$ being the voltage of the upper and lower electrodes respectively, produces SAWs with the electric potential $\Phi = \mu_e V_t$, where μ_e is the emitter response function. At the same time, an incoming SAW produces a current in the transducer given by its receiver response function, $I_t = \mu_r \Phi$. We can express the power transmitted to SAWs in terms of the radiation conductance, $P = |V_t|^2 G_a/2$. This power is divided equally between the left and right transmitted SAWs. For a SAW transmission line with characteristic impedance and admittance $Z_0 = 1/Y_0$, the power of the SAWs emitted can be expressed as $P_e = Y_0|\mu_e^L V_t|^2/2 + Y_0|\mu_e^R V_t|^2/2$. For symmetric IDTs, $\mu_e^L = \mu_e^R$, which when equating the electric and the transmitted power, $P = P_e$, gives us a relation for the acoustic conductance,

$$G_a = 2|\mu_e|^2 Y_0. \tag{3.36}$$

Since the imaginary part of any causal response function is related to the real part by the Kramers-Kronig relation, we can find B_a once we know G_a, and thus the emitter response function μ_e determines the acoustic properties of the IDT completely. Our goal in what follows is, therefore, to determine μ_e.

What essentially determines μ_e is the charge density on the IDT electrodes as a voltage is applied. For an arbitrarily shaped IDT, this is a two-dimensional

electrostatic problem that can be solved numerically, often done with commercial software. For periodic IDTs, there is an analytical result [100]. However, this is a rather lengthy derivation and not too relevant to the discussion at hand, so we assume the problem of finding the charge distribution is solved and derive an expression for μ_e in terms of that charge distribution.

If we denote the surface charge per unit area ρ, an alternating voltage on the IDT creates a current per unit length

$$I = i\omega\rho(x)W, \tag{3.37}$$

where W is the width of the electrode. For an infinitesimally small segment dx located at x', this current density produces a SAW with amplitude $\Phi = \frac{1}{2Y_0} i\omega\rho(x')W dx$, in both directions. To obtain the total wave amplitude generated, we have to integrate over the whole length of the IDT. To obtain the amplitude of the wave leaving the IDT at either end, we need to shift the waves generated at different locations to one common reference point. For simplicity, we choose the position $x = 0$, such that the phase shifts become $e^{ikx'}$ for waves propagating to the right. The total SAW amplitude at $x = 0$ is then

$$\begin{aligned} \Phi &= \frac{W}{2Y_0} \int_\infty^\infty I(x') e^{ikx'} dx' \\ &= \frac{i\omega W}{2Y_0} \int_\infty^\infty \rho(x') e^{ikx'} dx' \end{aligned} \tag{3.38}$$

where the factor of 2 comes from the fact that half the current is going in the other direction. However, the last integral in Eq. 3.38 is nothing but the Fourier transform of the charge distribution $\rho(k)$. Since $\Phi = \mu_e V_t$, we have that the emitter function is given by

$$\mu_e(k) = \frac{i\omega W}{2Y_0 V_t} \rho(k). \tag{3.39}$$

Thus, in general, we could solve for the charge distribution numerically for any IDT geometry, take the Fourier transform of that, which in turn gives us the full IDT admittance.

The characteristic admittance of the SAW transmission-line is often expressed in terms of material parameters of the piezoelectric substrate. From Maxwells equations it can be shown that $Y_0 = \omega W \epsilon_{\text{tot}} / K^2$ [98], where K^2 is the piezoelectric coupling constant, and ϵ_{tot} is the sum of the permittivity in the substrate and above the substrate. This gives us the exmitter response in terms of material parameters only,

$$\mu_e(k) = \frac{iK^2}{2\epsilon_{\text{tot}} V_t} \rho(k). \tag{3.40}$$

It can be shown by reciprocity, that the receiver function is related to the emitter function by,

$$\mu_r = 2\mu_e Y_0. \tag{3.41}$$

For periodic IDTs, the emitter response function can be split into two parts. One factor that takes care of the response from one finger pair, which is called the element factor $E(\omega)$, and one factor that sums up the contribution from many such finger pairs, called the array factor $A(\omega)$. This turns the Fourier transform of the full charge distribution into the Fourier transform of a single live electrode's charge distribution, which will define the element factor. This basic charge distribution, ρ_s, only needs to be calculated once since it is the same for all electrodes in symmetric IDTs. The array factor takes this single electrode response, treats each electrode as a single voltage source, and adds them together, taking phase factors into account. In circuit theory, this is called the superposition principle [83]. With this splitting, the SAW amplitude becomes,

$$\Phi^R(\omega) = E(\omega)A(\omega), \tag{3.42}$$

where the superscript R reminds us that it is only the wave leaving the IDT at one side, and where we have defined the element and array factors as

$$E(\omega) = \frac{iK^2}{2\epsilon_{\text{tot}}}\rho_s(\omega), \tag{3.43}$$

$$A(\omega) = \sum_{n=0}^{N_p-1} e^{i\omega\tau n}. \tag{3.44}$$

We rewrote the exponent in the array factor using the relations: $k = \omega/v_s$ and $x'/v_s = n2p/v_s = n\tau$. This is the same array factor we derive in paper I of a SAW-coupled transmon. It turns out that $\rho_s(\omega)$ is a slowly varying function compared to $A(\omega)$ and can as a first approximation be regarded as constant. For a single-finger IDT the element factor is approximately $E \approx 0.8iK^2$. Evaluating the sum in the array factor, which can be approximated as a sinc function centered around the IDT center frequency, gives us the following emitter response

$$\mu_e = 0.8iK^2N_p\frac{\sin(X)}{X},\ X = N_p\pi\frac{\omega-\omega_{\text{IDT}}}{\omega_{\text{IDT}}}. \tag{3.45}$$

Thus, we can finally express the acoustic admittance for periodic IDTs with a metallization ratio of 0.5,

$$G_a = G_0\left(\frac{\sin(X)}{X}\right), \tag{3.46}$$

$$B_a = G_0\left(\frac{\sin(2X)-2X}{2X^2}\right), \tag{3.47}$$

where $G_0 \approx 1.3K^2W\epsilon_{\text{tot}}N_p^2\omega_{\text{IDT}}$, and we obtain B_a from the Hilbert transform of G_a according to the Kramers-Kronig relation. We plot the acoustic conductance and susceptance in Fig. 3.2, for $N_p = 10$, where ω_0 represents the IDT center frequency.

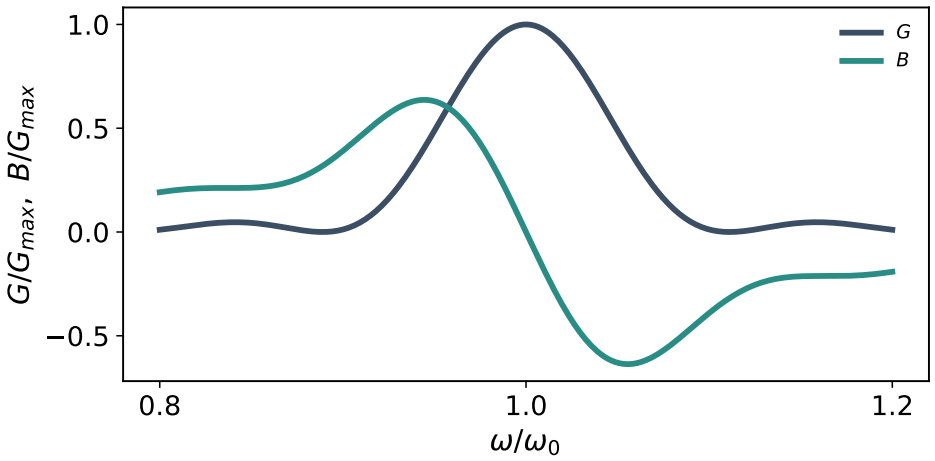

Figure 3.2: *Normalized acoustic conductance G_a and susceptance B_a as a function of frequency.*

The last part of the total IDT admittance is the capacitance. This is a purely electrostatic problem that can be solved analytically for periodic IDTs with a metallization ratio of 0.5. In the limit of large N_p, the capacitance is given by

$$C_{\mathrm{IDT}} = N_p \epsilon_{\mathrm{tot}} W. \tag{3.48}$$

This expression is often taken as approximately correct for IDTs with few fingers as well.

4 Quantum acoustics

In this chapter, we introduce the field of circuit QAD. We review the field's progress over its fairly short life span and highlight some of the main achievements and possible future directions.

Circuit QAD is a hybrid system pioneered and initiated by an experiment at Chalmers in 2014 [63]. It deals with the interaction between superconducting circuits, primarily artificial atoms, and acoustic waves in solids. The idea of using acoustic waves for quantum computation tasks is not new. SAWs have been used, e.g., as propagating potential landscapes, in which electrons or spins, encoded with quantum information, can be trapped [101, 102]. In such a device, the SAWs are used as carriers of another quantum particle to transfer quantum information. This idea has been taken one step further in a recent theoretical proposal to use standing SAWs as a lattice [103], closely resembling the idea of trapping ions in optical lattices [104, 105]. The key difference between these ideas and circuit QAD, is that circuit QAD encodes the quantum information directly into the phonons; it is the quantum properties of SAWs being harvested as a resource. On the other hand, encoding quantum information into phonons is neither something new; this has been done extensively in the field of optomechanics, where small mechanical oscillators can be made to interact with both optical and microwave photons [106]. A limiting factor in the optomechanical systems is that the optomechanical coupling is linear, which means that it is hard to create non-classical states. Nevertheless, one electromechanical system managed to create non-classical states in a pioneering work by O'Connell *et al.* in the year 2010 [107]. However, what is unique for circuit QAD is the ability to couple propagating waves, either at the surface or in the bulk of materials, to superconducting qubits. Thus, utilizing the well-established methods for encoding and reading out information of superconducting qubits while simultaneously utilizing the unique properties of acoustic waves, such as their slow propagation speed and flexible coupling schemes. Additionally, the qubit offers a very strong non-linear element, a major advantage over the optomechanical systems.

4.1 Coupling a transmon to surface acoustic waves

In chapter 2, we learned that a transmon qubit is nothing but a non-linear inductance in parallel with a large capacitance. In chapter 3, we also learned that an electrical circuit could emit SAWs via an interdigital transducer (IDT). Since the

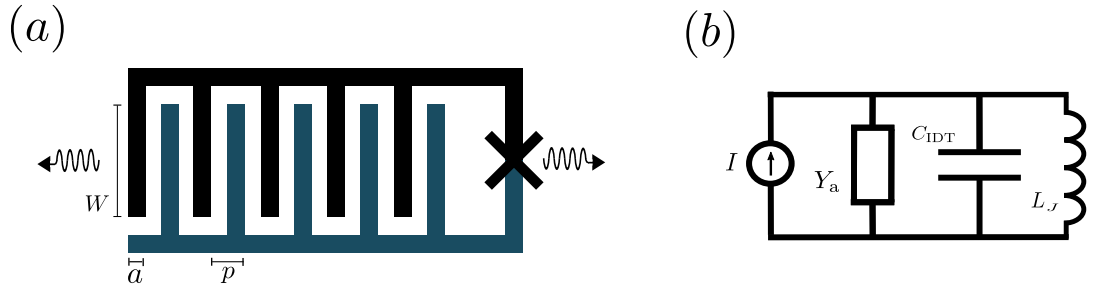

Figure 4.1: *(a) An IDT together with a Josephson junction, forming a SAW-coupled transmon. (b) Effective circuit of the transmon in (a), in the linear regime. The current source represent the conversion from incoming SAWs to a current in the IDT electrodes.*

IDT constitutes a capacitor, in addition to being a phononic antenna, a SAW-coupled atom can be constructed by forming the shunt capacitance of the transmon into an IDT. In Fig. 4.1 we illustrate a Josephson junction together with an IDT, forming a SAW-coupled qubit.

There are several ways to model the interaction between the atom and SAWs. The most straightforward approach is to build on the lumped-element model of the IDT that we presented in chapter 3. The advantage of this approach is that the lumped-element model is a well-tested description of the IDT frequency-response. Some alternative phenomenological models have been presented [58, 61]. They suffer from a couple of drawbacks: (i) they are limited to either the single excitation regime or the weak coupling regime, and (ii) all parameters are fitting parameters. The lumped-element model has been used to interpret several experiments so far [63, 65]. It is also closely related to the model we construct in paper I. For that reason, we will see how the lumped-element model can be used to build a simple model of the SAW-coupled qubit to compare it to the model in paper I later on.

By forming the transmon capacitance into an IDT, as illustrated in Fig. 4.1(a), the Josephson junction is coupled to the positive and negative voltage electrodes of the IDT in parallel. We thus take the lumped-element model of chapter 3.3 and add a Josephson junction. The resulting circuit can be seen in 4.1(b). To proceed, we restrict the discussion to the lowest two energy levels. For such small oscillations, the Josephson inductance is approximately linear. Of course, as we saw in chapter 2, we can not consider arbitrarily small excitations, and the zero-point fluctuations alone imply that we should do a perturbation expansion up to first order, at least. However, for our current purposes, the linear solution is sufficient.

In the linear regime, the Josephson inductance together with the IDT capacitance from Eq. (3.48), gives us the "bare" (uncoupled) approximate resonance

frequency of the qubit,

$$\omega_0 = \sqrt{\frac{1}{L_J C_{\mathrm{IDT}}}}, \tag{4.1}$$

With the acoustic admittance and susceptance from Eq. (3.46) and Eq. (3.47), the admittance of the whole circuit is,

$$\begin{aligned} Y &= Y_{\mathrm{IDT}} + Y_J \\ &= G_a(\omega) + iB_a(\omega) + i\omega C_{\mathrm{IDT}} - \frac{i}{\omega L_J}. \end{aligned} \tag{4.2}$$

Let us now imagine that an external electric gate is coupled to the IDT, which can interact with the qubit by applying a voltage to the IDT. This can then be described as a three-port device, with two acoustic ports and one electric. If we denote the complex amplitude of the in- and outgoing SAWs on the left and right side of the IDT as $\Phi^{\mathrm{L/R}}_{\mathrm{in/out}}$, and likewise the complex amplitude of an incoming/outgoing voltage wave as $V_{\mathrm{in/out}}$, we can describe the system in terms of a scattering matrix

$$\begin{pmatrix} \Phi^{\mathrm{L}}_{\mathrm{out}} \\ \Phi^{\mathrm{R}}_{\mathrm{out}} \\ V_{\mathrm{out}} \end{pmatrix} = \begin{pmatrix} S_{11} & S_{12} & S_{13} \\ S_{21} & S_{22} & S_{23} \\ S_{31} & S_{32} & S_{33} \end{pmatrix} \begin{pmatrix} \Phi^{\mathrm{L}}_{\mathrm{in}} \\ \Phi^{\mathrm{R}}_{\mathrm{in}} \\ V_{\mathrm{in}} \end{pmatrix}. \tag{4.3}$$

To characterize the system dynamics, we are foremost interested in the two diagonal terms S_{11} and S_{33}, which corresponds to the acoustic and electric reflection. For symmetry reasons $S_{11} = S_{22}$. Let us first look at the electric reflection coefficient S_{33}, which we can write down straight away. By taking the gate to correspond to a $Z_0 = 50\ \Omega$ transmission line, the electric reflection coefficient is given by [83],

$$S_{33} = \frac{Z_{\mathrm{IDT}} - Z_0}{Z_{\mathrm{IDT}} + Z_0} = \frac{Y_0 - Y_{\mathrm{IDT}}}{Y_0 + Y_{\mathrm{IDT}}}. \tag{4.4}$$

Let us now consider an incoming acoustic wave from the left of the IDT. In this case, the acoustic reflection coefficient is given by $S_{11} = \Phi^{\mathrm{L}}_{\mathrm{in}}/\Phi^{\mathrm{L}}_{\mathrm{out}}$. An incoming wave will create a current in the IDT equal to $I = YV$, which we can also write in terms of the IDT receiver function in Eq. (3.41), $I = \mu_r \Phi^{\mathrm{L}}_{\mathrm{in}}$. Simultaneously, this will create outgoing SAWs of amplitude $\Phi^{\mathrm{L}}_{\mathrm{out}} = \mu_e V$, where μ_e is the IDT emitter function from Eq. 3.40. This gives us the acoustic reflection coefficient,

$$S_{11} = \frac{G_a(\omega)}{G_a(\omega) + iB_a(\omega) + i\omega C_{\mathrm{IDT}} - \frac{i}{\omega L_J}}. \tag{4.5}$$

For a regular IDT, the capacitive part of the admittance is always dominating over the acoustic susceptance, and can thus often be neglected. For the inductively

shunted IDT the inductive term of the admittance can cancel the capacitive term, making $B_a(\omega)$ important, at least for frequencies close to ω_0.

The denominator in Eq. (4.5) determines the resonant behavior of the system. We refer to it as the qubit susceptibility χ. We can rewrite χ in a more convenient form to analyze its properties,

$$\chi = \frac{1}{\frac{G_a(\omega)}{C_{\mathrm{IDT}}}\omega + i\frac{B_a(\omega)}{C_{\mathrm{IDT}}} + i(\omega^2 - \omega_0^2)}. \tag{4.6}$$

If the real part of the denominator of χ is small, the system is weakly damped. If also G_a and B_a are approximately constant around ω_0, we can make a weak-coupling and close to resonance approximation. Using these approximations we can write $\omega^2 - \omega_0^2 = (\omega - \omega_0)(\omega + \omega_0) \approx 2\omega_0(\omega - \omega_0)$, we also have that $G_a(\omega)\omega \approx G_a(\omega_0)\omega_0$ and that $B_a(\omega)\omega \approx B_a(\omega_0)\omega_0$. By incorporating $B_a(\omega_0)/C_{\mathrm{IDT}}$ as a small shift to the resonance frequency and defining $\omega_0' = \omega_0 + B_a(\omega_0)/2C_{\mathrm{IDT}}$, we can write Eq. (4.6) as

$$\chi = \frac{i}{2\omega_0\left(\omega_0' - \omega + i\gamma/2\right)}, \tag{4.7}$$

where $\gamma = G_a(\omega_0)/C_{\mathrm{IDT}}$. This is nothing but the response of an RLC circuit, with damping factor γ.

The small damping criteria are only fulfilled on weakly piezoelectric substrates, such as GaAs. The approximation done above can thus not be made on strongly piezoelectric materials, such as $LiNbO_3$. Similarly, for strong frequency dependence on G_a and B_a, the approximations also break down, which happens for IDTs with many fingers. The regime of strong damping and many IDT fingers is the regime we study in paper I, whereas the weak coupling regime is studied experimentally in paper II.

For weakly coupled qubits we make the following observation: the only effect of the piezoelectric coupling is to slightly shift the bare resonance frequency of the qubit (unless $\omega_0 = \omega_{\mathrm{IDT}}$ since $B_a(\omega_{\mathrm{IDT}}) = 0$). The damping coefficient is frequency-dependent, but for a fixed qubit frequency it is given by $G_a(\omega_0)/C_{\mathrm{IDT}}$. This implies that standard master equation techniques can be used to model SAW-coupled qubits on weak piezoelectrics.

4.2 Transmons in surface acoustic wave resonators

Several experiments have been performed with transmons inside SAW resonators [64–68]. A SAW mirror is made up of two mechanical reflection gratings. The gratings are made of ripples in the piezoelectric substrate [99], which means the SAW reflection is purely mechanical. There is some obvious motivation for using a SAW resonator instead of a photonic resonator. Since the speed of SAW is five orders of magnitude slower than the speed of light, the resonators can be made

much smaller while operating at the same frequency. Another interesting feature of the SAW resonator is its length. Unlike the mirrors in a photonic resonator, which are negligibly small compared to the photon wavelength, the SAW "mirror" is distributed in space with an effective penetration depth. This means that one can only define an effective length of the resonator, given by the SAWs' average penetration length into the mirror before they are fully reflected. Thus, it is not possible to make a $\lambda/2$ resonator because the mirrors would overlap. At the same time, the coupling-IDT of the qubit would also take up space inside the cavity. Altogether, this means that the SAW resonators are made with mirrors many wavelengths apart, in the 100μm range. Since that is still a pretty small resonator, one can take advantage of the wiggle room available and make the SAW resonator even bigger. By doing that, the free spectral range of the resonator, $\nu_{\mathrm{FSR}} = v_{\mathrm{SAW}}/2L_{\mathrm{eff}}$, becomes very small. This was utilized as a resource in a recent experiment [65], where the qubit coupling strength was larger than the free spectral range, thus realizing the strong multimode coupling regime [108]. A regime that could potentially open up the possibility for analog quantum simulation of many-body physics [109].

The initial challenges for the atoms in SAW resonators have been low qubit coherence times. Most experiments have coherence times around 10 ns, much lower than the 100μs possible in circuit QED [37]. The poor performance is due to a high amount of dielectric losses caused by the piezoelectric material surrounding the qubit [110]. This could be redeemed by etching away parts of the piezoelectric substrates that are not involved in the coupling to the qubit but have remained a major challenge.

4.3 Transmons in bulk acoustic wave resonators

Bulk acoustic waves (BAWs) are propagating in the bulk of materials instead of the surface. One of the major benefits of using BAW resonators is the small amount of piezoelectric material needed. It turns out that the substrate material on which superconducting qubits usually are fabricated, such as sapphire, can act as a BAW resonator. The only adjustment needed to make a qubit-resonator system is to put a small piece of piezoelectric material on top of the surface to make the qubit interact with the substrate. The slab of piezoelectric material acts like a drum hitting on the surface. This produces an acoustic wave that propagates away from the surface towards the bottom, at which point it is reflected. Thus, the BAWs are simply bouncing back and forth between the top and the bottom, forming a cavity. In Fig. 4.2 we illustrate a stripped-down version of a qubit inside a BAW resonator.

BAW resonators have been used for a long time in classical circuits, where they go by the name BAR (bulk acoustic resonators). The quantum version of the BAR have been named $\hbar$BAR, for apparent reasons. This work was pioneered by

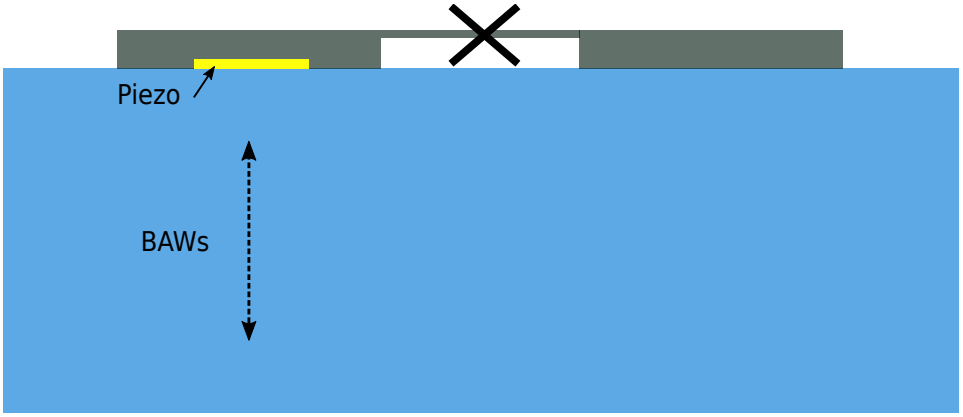

Figure 4.2: *A transmon qubit coupled to a bulk acoustic wave resonator. The small piezoelectric material underneath one of the metals that make up the shunt capacitance of the transmon mediates the coupling.*

Chu *et al.* in 2017 [69]. Shortly after, the same group produced phononic Fock states inside a BAW resonator [111]. Since then, other groups have pursuit similar architectures [70].

5 Open quantum systems

There are no truly closed quantum systems. In one way or another, a system is always in contact with a noisy environment and eventually loses its quantum properties [112]. The loss of information can either be in the form of energy, quantum coherence, or both. This process is called *decoherence*. Decoherence is, in fact, often the main technological limitation in many emerging quantum applications. We do not always have the technology to make quantum systems stay coherent long enough to use them satisfactorily. The quantum computer is perhaps the foremost example, where the computation is in constant fight against the clock set by the qubits' coherence times. In addition to unwanted decoherence induced by the environment, we sometimes want to "open up" a quantum system in order for us to interact with it and to study it. We direct lasers at atoms to induce atomic transitions; we couple readout devices to quantum computers to extract the computation. These are both typical examples of systems that need to be treated partially or entirely within the framework of *open quantum systems*.

This chapter introduces the density matrix formalism and derives the quantum optical master equation for dealing with open quantum systems. Together with input-output theory, the master equation offers a powerful method that can describe a wide range of experiments in quantum optics and related fields. The master equation was used, e.g., in paper III to simulate an experiment where photons in a transmission line are scattered against an artificial atom, and in paper IV it was used to study transmission properties of multiple atoms placed next to each other in a waveguide. Finally, we conclude with a discussion on Markovianity in open quantum systems.

5.1 The density operator

The state ket $|\Psi(t)\rangle$ of an isolated (closed) quantum system, written in the Schrödinger picture, evolves in time according to the Schrödinger equation [113]

$$i\hbar\frac{d}{dt}|\Psi(t)\rangle = H|\Psi(t)\rangle\,, \tag{5.1}$$

where H is the Hamiltonian of the system. The dynamics of open quantum systems is, however, more suitably treated in the *density operator* formalism, for reason that will become clear shortly. In terms of the state ket $|\Psi(t)\rangle$, the density

operator can be written as

$$\rho(t) = |\Psi(t)\rangle \langle\Psi(t)| . \tag{5.2}$$

The mean of an observable O is then

$$\langle O\rangle = \langle\Psi(t)| O |\Psi(t)\rangle = \mathrm{tr}\left(O\rho(t)\right). \tag{5.3}$$

With this definition, the density operator has no clear advantage over the state ket representation. The benefit of the density operator is in its ability to describe *mixed ensembles* (mixed states). Given a collection of quantum systems, e.g., atoms in a gas, the system is a pure ensemble if each subsystem can be described by the same state ket $|\alpha\rangle$. In a mixed ensemble, there is a proportion of subsystems in a state $|\alpha_1\rangle$, with a corresponding weight w_1, and another proportion in state $|\alpha_2\rangle$, with weight w_2, etc. The only constraint is that the weights need to add up to unity, $\sum_i w_i = 1$. These constraints are captured by the following definition of the density operator:

$$\rho \equiv \sum_i w_i |\alpha_i\rangle \langle\alpha_i| . \tag{5.4}$$

In a pure state, all the weights except one is zero, such that $\rho = |\alpha_n\rangle \langle\alpha_n|$. It also has the property $\mathrm{tr}\left(\rho^2\right) = 1$. If $\mathrm{tr}\left(\rho^2\right) < 1$ the ensemble is mixed. This quantity is used to evaluate how mixed an ensemble is, and is referred to as the *purity* P,

$$P \equiv \mathrm{tr}\left(\rho^2\right). \tag{5.5}$$

The power of the density operator is best appreciated with an example. If we consider a beam of spin 1/2-particles, in which 50% are in a spin up state $|\uparrow\rangle$, and 50% in a spin down state $|\downarrow\rangle$; a measurement on any particle would then yield a random outcome of either spin up or spin down. The density operator can then be written as the sum $\rho = \frac{1}{2} |\uparrow\rangle \langle\uparrow| + \frac{1}{2} |\downarrow\rangle \langle\downarrow|$, which can be represented as the matrix

$$\rho = \begin{pmatrix} \frac{1}{2} & 0 \\ 0 & \frac{1}{2} \end{pmatrix}. \tag{5.6}$$

This is a *completely* mixed ensemble with purity $P = \frac{1}{2}$. It does not take long to convince oneself that the density matrix of a mixed state, such as the one in Eq. (5.6), does not have a state ket representation. A first attempt would be the equal superposition state $|\Psi\rangle = \frac{1}{\sqrt{2}}(|\uparrow\rangle + |\downarrow\rangle)$, which is not correct as the density matrix then becomes

$$\rho = \begin{pmatrix} \frac{1}{2} & \frac{1}{2} \\ \frac{1}{2} & \frac{1}{2} \end{pmatrix}. \tag{5.7}$$

The time evolution of the density operator is given by the solution to the von-Neumann equation, [114],

$$\dot{\rho} = -\frac{i}{\hbar}[H, \rho], \tag{5.8}$$

which can be derived directly from the Schrödinger equation, Eq. (5.1), since each ket in the definition of the density matrix must evolve according to the Schrödinger equation. Eq. (5.8) might look like the Heisenberg equation of motion for ρ but with the wrong sign. This is not a problem, because the density operator is not an observable in the Heisenberg picture, but a sum of Schrödinger picture state-kets which evolve according to the Schrödinger equation [113].

5.2 The quantum optical master equation

We now proceed to derive the quantum optical master equation from the von-Neumann equation. There are several approaches to the derivation of the master equation [114–116]. We follow the derivation in [117], which in turn is based on the derivation in [116]. Without loss of generality, we consider a single two-level system, a qubit. The qubit is coupled to an environment with infinitely many degrees of freedom. The environment, or *bath*, is modelled as an infinite number of harmonic oscillators. The Hamiltonian thus has three components: $H = H_q + H_{\text{bath}} + H_{\text{int}}$, with each component written as

$$H_q = \omega_q \sigma^+ \sigma^-, \tag{5.9}$$

$$H_{\text{int}} = \sum_i \omega_i a_i^\dagger a_i, \tag{5.10}$$

$$H_{\text{int}} = \sum_i g_i \left(a_i^\dagger + a_i\right)\left(\sigma^+ + \sigma^-\right), \tag{5.11}$$

where ω_q is the transition frequency of the qubit, σ^+ (σ^-) creates (annihilates) an excitation in the qubit, $a_i^\dagger$ and a_i are the usual ladder operators of a harmonic oscillator with frequency ω_i, and g_i is a coupling constant. Before we go on, we transform each operator O into the interaction picture,

$$O^I(t) = e^{i(H_q + H_{\text{bath}})t} O e^{-i(H_q + H_{\text{bath}})t}. \tag{5.12}$$

This transforms the interaction Hamiltonian into

$$H_{\text{int}}^I = \sum_i (a_i e^{-i\omega_i t} + a_i^\dagger e^{i\omega_i t})(\sigma^- e^{-i\omega_q t} + \sigma^+ e^{i\omega_q t}). \tag{5.13}$$

In the interaction picture, the von-Neumann equation reads

$$\dot{\rho}^I(t) = -i\left[H_{\text{int}}^I(t), \rho^I(t)\right]. \tag{5.14}$$

We note that ρ^I is the density matrix of the combined system and bath at this point. Eq. (5.14) has the solution

$$\rho^I(t) = \rho^I(0) - i\int_0^t d\tau \left[H_{\text{int}}^I(\tau), \rho^I(\tau)\right]. \tag{5.15}$$

By plugging this solution into Eq. (5.14) and tracing out the bath degrees of freedom, we obtain an equation for the density matrix of the qubit,

$$\dot{\rho}_q^I(t) = \mathrm{tr}_{\mathrm{bath}}\left(-i\left[H_{\mathrm{int}}^I(t), \rho^I(0)\right] - \int_0^t d\tau \left[H_{\mathrm{int}}^I(t), \left[H_{\mathrm{int}}^I(\tau), \rho^I(\tau)\right]\right]\right). \tag{5.16}$$

We proceed by making two important approximations:

(i) the *Born approximation* assumes that the bath's degrees of freedoms are many more than the qubit's (a small system in a large environment), and that each coupling constant g_i is small compared to the qubit's transition frequency. With these two assumptions, the bath does not change significantly during the interaction with the qubit;

(ii) the *Markov approximation* assumes that the bath has no memory. That means that there can be no back-action on the qubit based on its own impact on the bath at an earlier time. It can also be interpreted as if no information that is leaked into the bath can come back to the qubit again. What is lost is lost. This, again, relies on a weak coupling between the qubit and the bath. With this assumption, one can replace $\rho_q(\tau)$ with $\rho_q(t)$ in Eq. (5.16) once we have also assumed a separable initial state $\rho(0) = \rho_q \otimes \rho_{\mathrm{bath}}$.

Together, the Born and the Markov approximation allow the quantum optical master equation to be derived from Eq. (5.16). We will outline the most important steps here. First, $\mathrm{tr}\left(H_{\mathrm{int}}^I\right) = 0$, such that Eq. (5.16) simplifies to

$$\dot{\rho}_q^I(t) = \int_0^t d\tau\, \mathrm{tr}_{\mathrm{bath}}\left(-\left[H_{\mathrm{int}}^I(t), \left[H_{\mathrm{int}}^I(\tau), \rho_q^I(t)\rho_{\mathrm{bath}}^I\right]\right]\right). \tag{5.17}$$

The only non-zero terms when taking the trace are terms involving

$$\begin{aligned}\mathrm{tr}_{\mathrm{bath}}\left(\sum_i g_i a_i e^{-i\omega_i t} \sum_j g_j a_j^\dagger e^{i\omega_j \tau} \rho_{\mathrm{bath}}^I\right) &= \sum_{i,j} g_i g_j e^{i\omega_j\tau - \omega_i t}\delta_{ij} \\ &= \sum_i g_i^2 e^{-i\omega(t-\tau)},\end{aligned} \tag{5.18}$$

where we used the commutation relation $[b_i, b_j^\dagger] = \delta_{ij}$, and assumed no thermal excitations from the bath $\langle b^\dagger b\rangle_{\mathrm{bath}} = 0$. Next, we replace the sum over bath modes with an integral and introduce the density of states $J(\omega)$ in the process. Additionally, we extend the time integral to infinity and change the integration variable to $t' = t - \tau$. This is allowed because we assume that bath correlations decay much faster than the qubit evolves in time. All together, Eq. (5.16) can

then be written as

$$\begin{aligned}\dot{\rho}_q^I(t) = \int_0^\infty d\omega J(\omega) g^2(\omega) \int_0^\infty dt' \, [\, & e^{-i(\omega_q-\omega)t'}(\sigma^-\rho_q^I(t)\sigma^+ - \rho_q^I(t)\sigma^+\sigma^-) \\ & + e^{-i(-\omega_q-\omega)}(\sigma^+\rho_q^I(t)\sigma^- - \rho_q^I(t)\sigma^-\sigma^+) \\ & + e^{-i(\omega_q+\omega)}(\sigma^+\rho_q^I(t)\sigma^- - \sigma^-\sigma^+\rho_q^I(t)) \\ & + e^{-i(-\omega_q+\omega)}(\sigma^-\rho_q^I(t)\sigma^+ - \sigma^+\sigma^-\rho_q^I(t))\,]\end{aligned} \tag{5.19}$$

where we also made the the RWA [114] and neglected terms oscillating at 2ω. By using the identity

$$\int_0^\infty dt e^{-i\omega t} = \pi\delta(\omega) - i\mathcal{P}\left(\frac{1}{\omega}\right), \tag{5.20}$$

where $\mathcal{P}$ denotes principal value [118], we arrive at the following equation (after some manipulation)

$$\begin{aligned}\dot{\rho}_q^I(t) = & \, 2\pi J(\omega_q) g^2(\omega_q) \mathcal{D}[\sigma^-]\rho_q^I(t) \\ & + i\mathcal{P}\int_0^\infty d\omega \frac{J(\omega)g^2(\omega)}{\omega-\omega_q}[\sigma^+\sigma^-, \rho_q^I(t)] \\ & + i\mathcal{P}\int_0^\infty d\omega \frac{J(\omega)g^2(\omega)}{\omega+\omega_q}[\sigma^-\sigma^+, \rho_q^I(t)],\end{aligned} \tag{5.21}$$

where we introduced the Lindblad superoperator $\mathcal{D}[X]\rho = X\rho X^\dagger - \frac{1}{2}X^\dagger X\rho - \frac{1}{2}\rho X^\dagger X$. The last two terms in Eq. (5.21) constitutes a small energy shift of the qubit, called a *Lamb shift*. The Lamb shift is often dropped or baked into the transition frequency of the qubit. Finally, we transform out of the interaction picture, while omitting the Lamb shift, and arrive at a master equation on a compact form

$$\dot{\rho}_q = -i[H_q, \rho_q] + \Gamma\mathcal{D}[\sigma^-]\rho_q, \tag{5.22}$$

where we introduced the decay rate $\Gamma = 2\pi J(\omega_q)g^2(\omega_q)$.

This master equation is said to be in Lindblad form [119, 120]. Such master equations have certain properties in common that guarantee that its solution is "physical", as it preserves the identities: $\mathrm{tr}(\rho) = 1$, $\rho > 0$, and $\rho = \rho^\dagger$. The Lindblad master equation describes a completely positive and trace preserving (CPTP) map (a quantum channel or trace preserving operation in the language of quantum information [1]). We discuss this property further in Sec. 5.4.1 regarding Markovianity in open quantum systems.

5.3 Input-output theory

While the master equation, Eq. (5.22), allows us to solve for the system dynamics, it does not give us any information about its output. The output could, e.g., come

from the fluorescence of a coherently driven atom [115], as is studied in paper IV, or the spontaneous emission of an excited atom. The goal of this section is to obtain a relationship between the output and the input.

We start once again from the Hamiltonian of a qubit coupled to a bath of harmonic oscillators, $H = H_q + H_{\text{bath}} + H_{\text{int}}$. This time we start from a continuum description of the bath,

$$H_q = \omega_q \sigma^+ \sigma^-, \tag{5.23}$$

$$H_{\text{bath}} = \int_0^\infty \omega a^\dagger(\omega) a(\omega), \tag{5.24}$$

$$H_{\text{int}} = i \int_0^\infty d\omega \sqrt{\frac{\gamma(\omega)}{2\pi}} \left(a^\dagger(\omega)\sigma^- + a(\omega)\sigma^+ \right), \tag{5.25}$$

where $\gamma(\omega)$ is a frequency dependent coupling strength. Since only energies around the qubit transition energy are important, we can safely extend the lower integration limit to $-\infty$. By doing so we obtain the following Heisenberg equation of motion for the atom and bath operators:

$$\dot{a}(\omega) = -i\omega a(\omega) + \sqrt{\frac{\gamma(\omega)}{2\pi}} \sigma^-, \tag{5.26}$$

$$\dot{\sigma}^- = -i\omega_q \sigma^- + \sigma_z \int_{-\infty}^\infty d\omega \sqrt{\frac{\gamma(\omega)}{2\pi}} a(\omega), \tag{5.27}$$

where we used the commutation relations $[a(\omega), a^\dagger(\omega')] = \delta(\omega - \omega')$, $[\sigma^+, \sigma^-] = \sigma_z$, and $[\sigma^-, \sigma^-] = 0$. If we define the initial bath state at some time $t_0 < t$, as $a_0(\omega) = a(\omega, t = t_0)$, we can write down the solution to Eq. (5.26) as

$$a(\omega) = e^{-i\omega(t-t_0)} a_0(\omega) + \sqrt{\frac{\gamma(\omega)}{2\pi}} \int_{t_0}^t dt' \sigma^-(t') e^{-i\omega(t-t')}. \tag{5.28}$$

We now make the Markov approximation that $\gamma(\omega)$ is a slowly varying function around ω_q, such that we can take it as a constant. This relies on a weak coupling to the bath, $\gamma/\omega_q \ll 1$. We also take the Fourier transform of the first term in Eq. (5.28) and define the incoming field

$$a_{\text{in}}(t) = \frac{1}{\sqrt{2\pi}} \int_{-\infty}^\infty d\omega e^{-i\omega(t-t_0)} a_0(\omega). \tag{5.29}$$

Inserting Eq. (5.28) into Eq. (5.27) together with a_{in} gives the equation

$$\dot{\sigma^-} = -i\omega_q \sigma^- + \sqrt{\gamma}\sigma_z a_{\text{in}} - \frac{\sqrt{\gamma}}{2}\sigma^-. \tag{5.30}$$

We can also solve Eq. (5.26) in terms of an outgoing field. If we define the future state of the bath at time $t_1 > t$ as $a_1(\omega) = a(\omega, t = t_1)$ we can write the solution to Eq. (5.26) as

$$a(\omega) = e^{-i\omega(t-t_1)} a_1(\omega) + \sqrt{\frac{\gamma(\omega)}{2\pi}} \int_t^{t_1} dt' \sigma^-(t') e^{-i\omega(t-t')}. \tag{5.31}$$

By defining the outgoing field as

$$a_{\text{out}}(t) = \frac{1}{\sqrt{2\pi}} \int_{-\infty}^{\infty} d\omega e^{-i\omega(t-t_1)} a_1(\omega), \tag{5.32}$$

we obtain an equation for σ^- in terms of the outgoing field instead,

$$\dot{\sigma^-} = -i\omega_q \sigma^- + \sqrt{\gamma}\sigma_z a_{\text{out}} + \frac{\sqrt{\gamma}}{2}\sigma^-. \tag{5.33}$$

Both Eq. (5.30) and Eq. (5.33) have to give the same result at time t, which gives us the input-output relation

$$a_{\text{out}}(t) = a_{\text{in}}(t) + \sqrt{\gamma}\sigma^-. \tag{5.34}$$

In paper V, we define so called quantum "*noise increments*" [114]. Such noise increments can be expressed in terms of the in-field a_{in}. From the definition of a_{in} in Eq. (5.29), one can show the commutation relation

$$\begin{aligned} [a_{\text{in}}(t), a_{\text{in}}^\dagger(t)] &= \frac{1}{2\pi} \int_{\infty}^{\infty} d\omega \int_{-\infty}^{\infty} d\omega' e^{-i\omega t + i\omega' t'} \left[a_0(\omega), a^\dagger(\omega')\right] \\ &= \frac{1}{2\pi} \int_{-\infty}^{\infty} d\omega e^{-i\omega(t-t')} = \delta(t-t'). \end{aligned} \tag{5.35}$$

The bath is said to be delta-correlated, and can thus be interpreted as white noise from the qubit's perspective. By integrating a_{in} over a time period t, we can define a *quantum Wiener process* [114]

$$B_t = \int_0^t d\tau a_{\text{in}}(\tau), \tag{5.36}$$

from which we get the quantum noise increment $dB_t = a_{\text{in}}(t)dt$, or equivalently

$$dB_t = \int_t^{t+dt} d\tau a_{\text{in}}(\tau). \tag{5.37}$$

5.4 Markovianity vs Non-Markovianity

The notion of a *Markov process* comes from the description of stochastic processes in classical probability theory [121]. Although quantum mechanics can be interpreted as a statistical theory [122], it is a theory of non-commuting operators. This has made it difficult to establish a universal definition of quantum non-Markovianity [123], for reasons we shall soon discuss. Despite that, much work has been done on quantum Markovianity, which can generally be divided into two different categories [124],

(i) The problem of *characterization*. What is the quantum analog of a Markovian process (which subsequently addresses what a quantum non-Markovian process is)?;

(ii) The problem of *quantifying* the degree of non-Markovianity in a process. How much does a system deviate from a Markovian process?

Several measures have been introduced that each focus on a certain aspect of Markovianity, see e.g., [125–130]. Here we look specifically at the measure in Ref. [126] as an example of a widely applied measure. Although the differences between measures could yield different characterization results, they often agree for most realistic physical systems [131].

Non-Markovianity is not only interesting from a fundamental perspective. Small open quantum systems have been proposed to be used as quantum probes of complex environments, such as the critical point of quantum phase transitions [132, 133]. Non-Markovianity has also been experimentally investigated in a number of different systems [132, 134–138].

In Sec. 5.2 we saw how the master equation in Lindblad form could be derived from a microscopic model. Here, we take a more formal approach to the dynamics of open quantum systems. This section is largely based on the two reviews [123] and [124].

5.4.1 Dynamical maps

A composite quantum system consisting of a smaller subsystem and its much larger environment lives in the tensor product space

$$\mathcal{H} = \mathcal{H}_S \otimes \mathcal{H}_E, \tag{5.38}$$

where $\mathcal{H}_S$ and $\mathcal{H}_E$ are the Hilbert spaces of the system and the environment, respectively. The combined system can be considered closed, described by the free Hamiltonian of the system H_S, the environment H_E, and their interaction Hamiltonian H_{int},

$$H = H_S \otimes I_E + I_S \otimes H_E + H_{\text{int}}, \tag{5.39}$$

where I denotes the identity matrix. Although we assume a time independent Hamiltonian here, the following analysis would also hold for a time dependent Hamiltonian. The system then evolves according to the unitary time-evolution operator

$$U(t) = e^{-iHt}, \tag{5.40}$$

where we assume $\hbar = 1$. The von Neumann equation for the density operator of the combined system [Eq. (5.8)] is given by

$$\dot{\rho}_{SE}(t) = -i[H, \rho_{SE}(t)], \tag{5.41}$$

which has the formal solution

$$\rho_{SE}(t) = U(t)\rho_{SE}(0)U^\dagger(t). \tag{5.42}$$

If we assume that the initial state was separable, $\rho_{SE}(0) = \rho_S(0) \otimes \rho_E(0)$, we can write the reduced density operator of the system at time t as

$$\rho_S(t) = \mathrm{tr}_E \left[U(t) \left(\rho_S(0) \otimes \rho_E(0) \right) U^\dagger(t) \right]. \tag{5.43}$$

If we denote the system's state space as $\mathcal{S}(\mathcal{H}_\mathcal{S})$, then, for a fixed initial environment state, $\rho_E(0)$, and any time $t \geq 0$, Eq. (5.43) is said to define a linear map on $\mathcal{S}(\mathcal{H}_\mathcal{S})$,

$$\Phi_t : \mathcal{S}(\mathcal{H}_\mathcal{S}) \to \mathcal{S}(\mathcal{H}_\mathcal{S}), \tag{5.44}$$

which maps any initial system state $\rho_S(0)$ to a final system state $\rho_S(t)$:

$$\rho_S(0) \to \rho_S(t) = \Phi_t \rho_S(0). \tag{5.45}$$

The map Φ_t is referred to as a quantum dynamical map and has the property that it preserves both hermiticity and the trace of operators. It also has the property that positive operators (operators with positive eigenvalues) are mapped to positive operators. This guarantees that states which we associate as "physical" are mapped to other physical states. Φ_t is not only a positive map; it can be shown to be *completely positive*, a much stronger property. We do not prove complete positivity here (for a proof, see [123]), but we can understand its meaning. If the system S is part of a larger system $S + R$, and Φ is a positive map on S, but not completely positive, it could happen that Φ maps physical states on $S + R$ into Hermitian operators describing unphysical states with negative probabilities. This is only possible if S and R are entangled and can thus be considered a genuine quantum feature. If Φ is a completely positive map, it maps not only physical states on S to physical states on S, but also physical states on $S + R$ to physical states on $S + R$. As mentioned before, the master equation in Lindblad form describes a CPTP map, specifically, a dynamical map. Later, we shall see how Markovianity can be defined as a property of the dynamical map describing an open quantum system's evolution.

5.4.2 Markovianity in classical stochastic processes

Given a stochastic process characterized by a family of random variables $\{X(t), t \in I \subset \mathbb{R}\}$, where X is a random variable depending on the parameter t, which for our purposes denotes time. Such a process is said to be Markovian if the random variable X takes the value x_n at time t_n, x_{n-1} at time $t_{n-1} \leq t_n$, is uniquely determined, and does not depend on the value of X at any earlier time than t_{n-1} [124]. We can write this condition in terms of conditional probabilities

$$P(x_n, t_n | x_{n-1}, t_{n-1}, ; \ldots ; x_1, t_1) = P(x_n, t_n; x_{n-1}, t_{n-1}). \tag{5.46}$$

This is very reminiscent of the Markov approximation that we made in the derivation of the quantum optical master equation in Sec. 5.2; that the system dynamics does not depend on the state of the system at an earlier time. This is a good approximation for many open systems. It is not true for the system we study in paper V, an atom in front of a mirror, since the radiation emitted towards the mirror eventually comes back and interacts with the atom again.

Moreover, if we consider the joint probabilities of three consecutive times $t_3 > t_2 > t_1$, one can show that a Markov process must fulfill the Chapman-Kolmogorov equation [123]

$$P(x_3, t_3|x_1, t_1) = \sum_{x_2 \in \mathcal{X}} P(x_3, t_3|x_2, t_2) P(x_2, t_2|x_1, t_1), \tag{5.47}$$

where $\mathcal{X}$ denotes the set of possible values of X.

5.4.3 Problems of quantum Markovianity and measurements

There are immediate problems that arise if the classical definition of a Markov process [Eq. (5.46)] is taken straight to the quantum regime [139]. Let us consider a system observable X with the decomposition $X = \sum_x x\,|\phi_x\rangle\langle\phi_x|$ that we perform projective measurements on at times $t_n \geq t_{n-1} \geq \cdots \geq t_1$. If we write the unitary time-evolution superoperator as $\mathcal{U}_t \rho_{SE}(0) = U(t)\rho_{SE}(0)U^\dagger(t)$, and the measurement outcome x as $\mathcal{M}_x \rho_{SE} = |\phi_x\rangle\,\langle\phi_x|\rho_{SE}|\phi_x\rangle\,\langle\phi_x|$. In analogy to a classical stochastic process, we can form a joint probability distribution on the form

$$P(x_n, t_n; \ldots; x_1, t_1) = \mathrm{tr}\left(\mathcal{M}_{x_n}\mathcal{U}_{t_n - t_{n-1}} \ldots \mathcal{M}_{x_1}\mathcal{U}_{t_1}\rho_{SE}(0)\right). \tag{5.48}$$

Such distribution does indeed describe the probability of measuring x_1 at time t_1, x_2 at time t_2 etc. It is not possible, however, for a quantum process to fulfill the classical Markov condition, $P(x_n, t_n|x_{n-1}, t_{n-1}, ; \ldots; x_1, t_1) = P(x_n, t_n; x_{n-1}, t_{n-1})$, because measurements at intermediate times affect future measurement outcomes by, e.g., destroying quantum interference. A measurement on the system itself can also affect correlations between the system and the environment. If we denote the state before a projective measurement at time t_n as $\rho(t_n)$, then we can write the state after the measurement, conditioned on a certain outcome x, as

$$\rho'_{SE}(t_n)\frac{\mathcal{M}_x \rho_{SE} t_n}{\mathrm{tr}(\mathcal{M}_x \rho_{SE} t_n)} = |\phi_x\rangle\langle\phi_x| \otimes \rho_E^x, \tag{5.49}$$

where the environment state ρ_E^x might depend on x. A projective measurement thus destroys any system-environment correlations, leaving the system in an uncorrelated tensor product state. The future system dynamics are thus heavily influenced by such a measurement. In general, one could consider other measurement schemes, which would lead to other probability distributions. But the definition of Markovianity of a dynamical quantum system cannot depend on the

type of measurement scheme used to verify it [124]. Any attempts to define non-Markovianity in an open quantum system, as we shall soon see, must instead be based on properties of the dynamics of the open system's density matrix ρ_S and the quantum dynamical map Φ_t.

5.4.4 Non-Markovianity in a quantum process

The trace distance between two quantum states ρ_1 and ρ_2 is defined as

$$T(\rho_1, \rho_2) = \frac{1}{2}\sqrt{(\rho_1 - \rho_2)(\rho_1 - \rho_2)^\dagger}, \tag{5.50}$$

and offers a natural distance metric between two quantum states [1]. For two-level systems, the trace distance is nothing but the geometric distance between the two states in the Bloch sphere. It has the bounds $T(\rho_1, \rho_2) = [0, 1]$, where $T(\rho_1, \rho_2) = 1$ if $\rho_1 = \rho_2$, and $T(\rho_1, \rho_2) = 0$ if ρ_1 and ρ_2 are orthogonal. The trace distance has a natural interpretation in terms of *distinguishability* of quantum states [140]. Suppose that Alice and Bob play game in which Alice prepares one out of two possible different states, ρ_1 and ρ_2, with a probability of 1/2 for each state, and sends it to Bob. Bob's task is to distinguish which of the two states Alice sent, using only a single measurement. One can show that the highest success rate Bob can achieve, $P_{\max}$, can be expressed in terms of the trace distance [140],

$$P_{\max} = \frac{1}{2}\left(1 + T(\rho_1, \rho_2)\right). \tag{5.51}$$

Only if the two states are orthogonal can Bob apply a strategy in which he succeeds with 100% probability since the trace distance is then $T_\perp = 1$. Another property of the trace distance between two quantum states ρ_1 and ρ_2 is that it cannot increase as the two states evolve according to some linear map $\rho(t) = \Phi_t\rho(0)$ [141],

$$T(\Phi_t\rho_1, \Phi_t\rho_2) \leq T((\rho_1, \rho_2). \tag{5.52}$$

This is true in general for positive maps, not only for completely positive maps such as the quantum dynamical map in Eq. (5.45). Thus, we can conclude that trace-preserving operations such as the quantum dynamical map Φ_t can never increase the distinguishability of two quantum states.

With this realization, it is possible to define Markovianity in the quantum regime in terms of distinguishability of quantum states, as was done in [126]. If ρ_{S_1} and ρ_{S_2} describe two open quantum systems, and $T(\Phi_t\rho_{S_1}(0), \Phi_t\rho_{S_2}(0))$ is a decreasing function in time, it means that the distinguishability of ρ_{S_1} and ρ_{S_2} decreases too. This can be interpreted as a loss of quantum information as ρ_{S_1/S_2} evolve according to the quantum dynamical map Φ_t. The environment must, in turn, gain the information lost in such a noisy quantum channel. Thus we can define a quantum Markov process as a process in which $T(\rho_{S_1}(t), \rho_{S_2}(t)) =$

$T(\Phi_t\rho_{S_1}(0), \Phi_t\rho_{S_2}(0))$ is a monotonically decreasing function in time, for all pairs of initial states. There is thus a continuous flow of information from the system into the environment in a Markovian system. Conversely, if $T(\rho_{S_1}(t), \rho_{S_2}(t))$ is increasing at some point in time, the system is said to be non-Markovian, characterized by a backflow of information from the environment into the system during this time. To quantify the amount of non-Markovianity, the measure $\mathcal{N}$ was proposed in [126],

$$\mathcal{N} \equiv \max_{\rho(S_1/S_2)} \int_{\sigma>0} dt\ \sigma(t), \tag{5.53}$$

where

$$\sigma(t) = \frac{d}{dt} T(\Phi_t\rho_{S_1}, \Phi_t\rho_{S_1}). \tag{5.54}$$

The maximum in Eq. (5.53) is taken over all pairs of initial states, although it can be shown that orthogonal states yield the maximum [142]. The measure $\mathcal{N}$ thus sums up the regions in which the trace distance is increasing.

We note that the measure in Eq. (5.53) can be used to evaluate non-Markovianity in both undriven and driven systems. It relies, however, on the ability to perform state tomography during all times of the system's evolution. In an initially excited system, radiation will leave the system due to spontaneous emission, and the system will be left in the ground state (or in a thermal equilibrium state). A driven system, however, has a non-trivial steady state. An interesting question is whether there are any traces left of the non-Markovian evolution once the steady state has been reached? If that is the case, a complete state tomography during the transient dynamics to detect non-Markovianity would not be necessary, and a measurement of the steady state alone would be sufficient. This is the topic of the appended paper V.

6 Photon scattering

In paper IV, we used a single photon scattering technique to derive analytical expressions for the scattering coefficients in various systems in waveguide QED. Specifically, we derived a set of equations that can be solved for an arbitrary number of quantum emitters placed in a waveguide in any configuration. The emitters could also have multiple coupling points in the waveguide, forming a giant atom [58]. Since neighboring coupling points in such an array can belong to different atoms, other popular methods such as a transfer matrix approach might not be suitably adopted, at least not in a straightforward matter. The method we used was first developed in Ref. [143], and further illustrated in [144, 145], for studying two-photon scattering. Nevertheless, it works just as well in the single excitation regime and provides an intuitive and flexible method for calculating scattering coefficients.

We first introduce photon scattering by solving the Lippmann-Schwinger equation for a photon scattered against a single two-level system (TLS) by summing over all possible scattering pathways. After that, we introduce another approach in which the summation over scattering pathways can be avoided. This is a considerable simplification that allows for more complicated systems than that of a single TLS to be considered.

6.1 Lippmann-Schwinger equation

We consider the event of a single photon scattered against a single TLS in a waveguide. The goal is to obtain a reflection and transmission coefficient that tells us what happens to the photon after the collision with the TLS. The photon is assumed to have been injected into the waveguide far away from the TLS. For this calculation, we chose a right-going photon. We start the calculation from the Lippmann-Schwinger (LS) equation [113], which reads

$$|\Psi\rangle = |\phi\rangle + G^R(E) H_{\text{int}} |\Psi\rangle \,, \tag{6.1}$$

where $|\Psi\rangle$ is a so called "*out*" state, $|\phi\rangle$ is a non-interacting "*in*" eigenstate of the system Hamiltonian, $H_0 |\phi\rangle = E |\phi\rangle$, H_{int} is an interaction Hamiltonian, and $G^R(E) = 1/(E - H_0 + i\epsilon)$ is the retarded Green's function at energy E. Since the incoming photon is traveling to the right we use the notation $H_0 |\phi\rangle_R = k |\phi\rangle_R$, to denote a "right-going" photon (we set $\hbar = c = 1$). We write the single photon

input state as

$$|\phi(k)\rangle_R = \frac{1}{\sqrt{2\pi}} \int e^{ikx} a_R^\dagger(x) |0\rangle \, dx, \tag{6.2}$$

where $a^\dagger(x)$ [$a(x)$] creates [annihilates] a photon at position x in the waveguide. Here we have considered a plane-wave input-state. Going forward, we define the state with no right or left-going photons in the waveguide and the TLS in its ground state as

$$|0\rangle \equiv |0\rangle_R \otimes |0\rangle_L \otimes |g\rangle \, . \tag{6.3}$$

The interaction Hamiltonian of the TLS and the waveguide is given by

$$H_{\text{int}} = g \int dx \delta(x - x_0) \left[\left(a_R^\dagger(x) + a_L^\dagger(x) \right) \sigma^- + \sigma^+ \left(a_R(x) + a_L(x) \right) \right], \tag{6.4}$$

where x_0 denotes the coupling point, g is a coupling constant, and $\sigma^\pm$ are the creation and annihilation operators for the TLS. By perturbatively expanding the LS-equation in Eq. (6.1),

$$|\Psi\rangle = \overset{\mathcal{O}(0)}{|\phi\rangle} + \overset{\mathcal{O}(1)}{G^R H_{\text{int}} |\phi\rangle} + \overset{\mathcal{O}(2)}{G^R H_{\text{int}} G^R H_{\text{int}} |\phi\rangle} + \ldots, \tag{6.5}$$

it is possible to express the scattering state $|\Psi\rangle$ solely in terms of the unperturbed state $|\phi\rangle$. Plugging in G^R and H_{int} in the expansion above gives, after some calculation, up to fourth order,

$$G^R H_{\text{int}} |\phi\rangle = \frac{g/(2\pi)}{E - \omega_0 + i\epsilon} \sigma^+ |0\rangle \, , \tag{6.6}$$

$$(G^R H_{\text{int}})^2 |\phi\rangle = -i \frac{g^2/(2\pi)}{E - \omega_0 + i\epsilon} \int dx \Big[\theta(x - x_0) e^{iEx} a_R^\dagger(x) + \theta(x_0 - x) e^{-iEx} a_L^\dagger(x) \Big] \sigma^+ |0\rangle \, , \tag{6.7}$$

$$(G^R H_{\text{int}})^3 |\phi\rangle = \frac{g^3/(2\pi)}{(E - \omega_0 + i\epsilon)^2} \sigma^+ |0\rangle \, , \tag{6.8}$$

$$(G^R H_{\text{int}})^4 |\phi\rangle = -i \frac{g^4/(2\pi)}{(E - \omega_0 + i\epsilon)^2} \int dx \Big[\theta(x - x_0) e^{iEx} a_R^\dagger(x) + \theta(x_0 - x) e^{-iEx} a_L^\dagger(x) \Big] \sigma^+ |0\rangle \, . \tag{6.9}$$

The pattern that has already emerged for odd and even terms continue also for higher order terms. In arriving at Eqs. (6.6)-(6.9), the following relation was used

$$\begin{aligned}\frac{1}{E-H_0+i\epsilon}\int dx\delta(x)a_R^\dagger(x)\left|0\right\rangle &= \int dx\frac{1}{E-H_0+i\epsilon}\left(\int dk'\frac{e^{ik'x}}{2\pi}\right)a_R^\dagger(x)\left|0\right\rangle \\ &= \int dx\left(\int dk'\frac{1}{E-k'+i\epsilon}\frac{e^{ik'x}}{2\pi}\right)a_R^\dagger(x)\left|0\right\rangle \\ &= \int dx\left(-ie^{iEx}\theta(x)\right)a_R^\dagger(x)\left|0\right\rangle\end{aligned} \tag{6.10}$$

Collecting the coefficients in front of each of the basis states $a_R^\dagger\left|0\right\rangle, a_L^\dagger\left|0\right\rangle$ and $\sigma^+\left|0\right\rangle$, and equating the Green's function energy with the energy of the incident photon, $G(E=k)$, gives us the following expression for the out-state

$$\left|\Psi(E=k)\right\rangle_R = \int_{-\infty}^{\infty} dx\left[\phi_R(x)a^\dagger + \phi_L(x)a_L^\dagger\right]\left|0\right\rangle + e(k)\sigma^+\left|0\right\rangle, \tag{6.11}$$

with

$$\phi_R = \frac{e^{ikx}}{2\pi}\left[\theta(x_0-x)+t(k)\theta(x-x_0)\right], \tag{6.12}$$

$$\phi_L = \frac{e^{-ikx}}{2\pi}\left[r(k)\theta(x_0-x)\right], \tag{6.13}$$

and where

$$t(k) = 1+\frac{-ig^2}{k-\omega_0+i\epsilon}+\frac{-g^4}{(k-\omega_0+i\epsilon)^2}+\ldots \overset{\lim\epsilon\to 0}{=} \frac{k-\omega_0}{k-\omega_0+ig^2}, \tag{6.14}$$

$$r(k) = \frac{-ig^2}{k-\omega_0+i\epsilon}+\frac{-g^4}{(k-\omega_0+i\epsilon)^2}+\ldots \overset{\lim\epsilon\to 0}{=} \frac{-ig^2}{k-\omega_0+ig^2}, \tag{6.15}$$

$$e(k) = \frac{g/(2\pi)}{k-\omega_0+i\epsilon}+\frac{ig^2/(2\pi)}{(k-\omega_0+i\epsilon)^2}+\ldots \overset{\lim\epsilon\to 0}{=} \frac{g/(2\pi)}{k-\omega_0+ig^2}. \tag{6.16}$$

Here, we see that the scattering coefficients r and t emerge as summations over all possible scattering pathways. This can become a tedious calculation for more complicated systems. Next, we shall see how these summations can be avoided.

6.2 Schrödinger-equation scattering

Given what we already know about scattering from solving the LS equation, we keep the same notation as before, but starting this time from the Schrödinger equation

$$H\left|\Psi(k)\right\rangle_R = k\left|\Psi(k)\right\rangle_R, \tag{6.17}$$

with the Hamiltonian $H = H_{\rm TLS} + H_{\rm 1ph} + H_{\rm int}$, of the TLS, the propagating single photon, and their interaction:

$$H_{\rm TLS} = \omega_0 \sigma^+ \sigma^-, \tag{6.18}$$

$$H_{\rm 1Ph} = -i \int dx \left[a_R^\dagger(x) \frac{d}{dx} a_R(x) - a_L^\dagger(x) \frac{d}{dx} a_L(x) \right], \tag{6.19}$$

$$H_{\rm int} = g \int \delta(x - x_0) \left[\left(a_R^\dagger(x) + a_L^\dagger(x) \right) \sigma^- + \sigma^+ \left(a_R(x) + a_L(x) \right) \right], \tag{6.20}$$

and where

$$|\Psi\rangle_R = \int dx \left(\phi_R a_R^\dagger(x) + \phi_L a_L^\dagger(x) \right) |0\rangle + e(k) \sigma^+ |0\rangle . \tag{6.21}$$

where $\phi_{R/L} = \phi_{R/L}(k, x)$. We then make a plane-wave ansatz

$$\phi_R = \frac{e^{ikx}}{2\pi} \left[\theta(x_0 - x) + t(k) \theta(x - x_0) \right], \tag{6.22}$$

$$\phi_L = \frac{e^{-ikx}}{2\pi} r(k) \theta(x_0 - x). \tag{6.23}$$

From the left hand side of the Schrödinger equation we get

$$H_q |\Psi\rangle_R = \omega_0 e(k) \sigma^+ |0\rangle , \tag{6.24}$$

$$H_{\rm 1ph} |\Psi\rangle_R = -i \int dx \left[a_R^\dagger(x) \frac{d\phi_R}{dx} - a_L^\dagger(x) \frac{d\phi_L}{dx}, \right] |0\rangle , \tag{6.25}$$

$$\begin{aligned} H_{\rm int} |\Psi\rangle_R = {} & g \int dx \delta(x - x_0) \left(a_R^\dagger(x) + a_L^\dagger(x) \right) e(k) |0\rangle \\ & + g \int dx \delta(x - x_0) \left(\phi_R + \phi_L \right) \sigma^+ |0\rangle . \end{aligned} \tag{6.26}$$

By collecting terms in front of the three basis states $a_R^\dagger |0\rangle , a_L^\dagger |0\rangle$ and $\sigma^+ |0\rangle$, we obtain the following three equations from the Schrödinger equation

$$0 = -i \frac{d\phi_R}{dx} + g \delta(x - x_0) e(k) - k \phi_R, \tag{6.27}$$

$$0 = i \frac{d\phi_L}{dx} + g \delta(x - x_0) e(k) - k \phi_L, \tag{6.28}$$

$$0 = \omega_0 e(k) + g \left(\phi_R(x_0) + \phi_L(x_0) \right) - k e(k). \tag{6.29}$$

Using the explicit expressions for $\phi_{R/L}$, gives after some manipulation the following three equations,

$$0 = \left(-i \frac{e^{ikx}}{\sqrt{2\pi}} \left[-1 + t(k) \right] + g e(k) \right) \delta(x - x_0), \tag{6.30}$$

$$0 = \left(-i \frac{e^{-ikx}}{\sqrt{2\pi}} r(k) + g e(k) \right) \delta(x - x_0), \tag{6.31}$$

$$0 = (\omega_0 - k) e(k) + g \frac{e^{ikx_0}}{2\sqrt{2\pi}} \left[1 + t(k) \right] + g \frac{e^{-ikx_0}}{2\sqrt{2\pi}} r(k), \tag{6.32}$$

where we used the relations $d\theta(x_0-x)/dx = -\delta(x-x_0)$, $d\theta(x-x_0)/dx = \delta(x-x_0)$, and that $\theta(0) = 1/2$. Evaluating the integral over x in Eq. (6.30) and Eq. (6.31) gives the following system of equations to solve for the scattering amplitudes,

$$e(k) = \frac{ie^{ikx_0}[t(k)-1]}{g\sqrt{2\pi}}, \tag{6.33}$$

$$e(k) = \frac{ie^{-ikx_0}r(k)}{g\sqrt{2\pi}}, \tag{6.34}$$

$$e(k) = \frac{g}{2\sqrt{2}(k-\omega_0)}\left[e^{ikx_0}(1+t(k)) + e^{-ikx_0}r(k)\right]. \tag{6.35}$$

For $x_0 = 0$ we obtain the following solutions,

$$e(k) = \frac{g}{\sqrt{2\pi}(k-\omega_0+ig^2)}, \tag{6.36}$$

$$r(k) = \frac{-ig^2}{k-\omega_0+ig^2}, \tag{6.37}$$

$$t(k) = \frac{k-\omega_0}{k-\omega_0+ig^2}. \tag{6.38}$$

If we compare with the solution to the LS equation, Eqs. (6.14)-(6.16), we see that the two approaches agree.

It is straight forward to generalize this method to the case of N two-level systems by simple adding terms to the original Hamiltonians

$$H_{\text{TLS}} = \sum_{i=1}^{N}\omega_i\sigma_i^+\sigma_i^-, \tag{6.39}$$

$$H_{\text{int}} = \sum_{i=1}^{N} g_i\int dx\delta(x-x_i)\left[\left(a_R^\dagger(x)+a_L^\dagger(x)\right)\sigma_i^- + \text{H.c}\right], \tag{6.40}$$

where x_i and g_i denotes the position and the coupling strength of emitter i, respectively. The free photon Hamiltonian stays the same as in Eq. (6.19). In the case of 2 TLS, with the first TLS positioned at $x_1 = 0$ and the second at $x_2 = \Delta x$, with equal coupling strength, g, to the waveguide, we obtain the following set of equations by repeating the derivation above:

$$e_1(k) = \frac{i[t_1(k)-1]}{g\sqrt{2\pi}}, \tag{6.41}$$

$$e_2(k) = \frac{ie^{ik\Delta x}[t_2(k)-t_1(k)]}{g\sqrt{2\pi}}, \tag{6.42}$$

$$e_1(k) = \frac{i[r_1(k)-r_2(k)]}{g\sqrt{2\pi}}, \tag{6.43}$$

$$e_2(k) = \frac{ie^{-ik\Delta x}r_2(k)}{g\sqrt{2\pi}}, \tag{6.44}$$

$$e_1(k) = \frac{g}{2\sqrt{2}(k-\omega_1)}\left[1 + t_1(k) + r_1(k) + r_2(k)\right]. \tag{6.45}$$

$$e_2(k) = \frac{g}{2\sqrt{2}(k-\omega_2)}\left[e^{ik\Delta x}\left(t_1(k) + t_2(k)\right) + e^{-ik\Delta x} r_2(k)\right], \tag{6.46}$$

where $r_i(t_i)$ denotes the reflection (transmission) coefficient at the position of the ith TLS. From these equations we obtain the total transmission through the entire system,

$$t_2(k) = \frac{(k-\omega_1)(k-\omega_2)}{g^4 e^{2ikx} + \left(ig^2 + k - \omega_1\right)\left(ig^2 + k - \omega_2\right)}. \tag{6.47}$$

The transmission is thus characterized by two coupled Lorentzian resonances, with a coupling strength that depends on the separation of the two TLS in the waveguide and their energy detuning. This type of coupling is referred to as being waveguide mediated.

As mentioned before, this method was used in paper IV, where the atoms also could be giant.

7 Matrix Product States

Dimensionality is perhaps the largest hurdle to overcome in the study of quantum many-body physics. Even for relatively small systems, the Hilbert space is an enormous place, and searching for specific states in there, like low-energy states of a Hamiltonian, can seem like looking for a needle in a haystack. Take a simple spin chain of N spin 1/2 particles; we would need 2^N number of parameters to represent every possible state. The problem at hand thus grows exponentially in the system size, and we run out of computational power rather quickly. Since only a limited number of states are physically relevant in most systems, it would be practical to have methods that could target those relevant states directly, allowing us to forget about those other unnecessary states. Remarkably, it turns out that physically relevant states are not just any state in the full Hilbert space; they often have specific properties in common that allow them to be singled out. For one-dimensional gapped Hamiltonians with local interactions, there is even something called an area law for the entanglement entropy [146] that guarantees an efficient representation of low energy states in the form of a class of quantum states called *Matrix Product States* (MPS) [147].

MPS is a family of quantum states described by a formalism called tensor networks (TNs) [148], a formalism that entails several classes of quantum states, numerical techniques to manipulate them, and a diagrammatic language to describe them with and to study their analytical properties [149]. Initially, the ideas of TNs come from condensed matter physics, but TNs have proved themselves as a natural language for quantum physics in general and have therefore found usage in a wide variety of fields of physics [150]. In fact, the numerical techniques coming from the TN community have been so successful that they have reached beyond the physics community and are currently being investigated by computer scientists for applications in machine learning [151–153].

When we derived the quantum optical master equation in Sec. 5.2, we used the Markov approximation (that the environment has no memory). This approximation is not valid in paper V, where we study a driven two-level system in a semi-infinite waveguide. Instead, we use a recently proposed method based on MPS [154, 155]. Specifically, it is a method for describing coherent quantum feedback, in which the system depends on past versions of itself. This chapter introduce the necessary ingredients to be able to understand the method described in detail in Ref. [154].

7.1 Tensor network notation: tensor diagrams

In tensor network notation (TNN), a tensor $A_{\alpha\beta}$ is represented by a geometric shape with one leg for each index,

$$A_{\alpha\beta} = \boxed{A}\!\!\begin{array}{l}\alpha\\ \beta\end{array}. \tag{7.1}$$

The index on the right hand side is included here for clarity but is often omitted. The number of indices denotes the rank of the tensor. The tensor in Eq. (7.1) thus represents a rank 2 tensor, and a zero-legged object would represent a scalar. The most important tensor operation is the *contraction*, which is performed by simply connecting two legs,

$$\sum_{\alpha,\beta} A_{\alpha\beta} B^{\alpha\beta} = \boxed{A}\!\!-\!\!\boxed{B}. \tag{7.2}$$

The direction of the legs does not have a meaning in general, but can, e.g., be used to denote if the corresponding vector lives in the Hilbert space ("kets") or its dual ("bras"). We list some common vector and matrix operations in what follows:

$$\vec{x} \cdot \vec{y} = \boxed{x}\!-\!\boxed{y}, \tag{7.3}$$

$$A\vec{x} = -\boxed{A}\!-\!\boxed{x}, \tag{7.4}$$

$$AB = -\boxed{A}\!-\!\boxed{B}\!-, \tag{7.5}$$

$$\mathrm{tr}\,(A) = \boxed{A}. \tag{7.6}$$

As we can see in the equations above, the scalar product correctly produces a scalar since no unconnected legs are left after the contraction. The matrix multiplication has left two legs open, forming a new matrix. The beauty of any good notation, such as Einstein notation, or Feynman diagrams, is that it makes calculations simpler while minimizing mistakes; TNN does both. To illustrate how intuitive TNN can be, consider the cyclic property of the trace operation, $\mathrm{tr}(ABCDE) = \mathrm{tr}(EABCD)$. In TNN the proof of this property is inherent in the formalism itself,

$$\boxed{D}\,\boxed{C}\,\boxed{E}\,\boxed{B}\,\boxed{A} = \boxed{C}\,\boxed{B}\,\boxed{D}\,\boxed{A}\,\boxed{E}. \tag{7.7}$$

The tensor product has a particularly easy representation, in which tensors are simply positioned next to each other,

$$\boxed{A}\;\boxed{B} = \boxed{A \otimes B}\;. \tag{7.8}$$

An actual *tensor network* is formed when several tensors are connected, as in

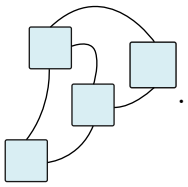

. (7.9)

A contraction of this network would yield a scalar, as it has no open legs. A network describing a quantum state thus must have some unconnected legs. The structure of the network, how the individual tensors are connected, contain information about the entanglement structure of the underlying quantum state, as we shall see an example of later. Much of the success of TNs comes from the fact that they are formulated around entanglement, one of the defining features of quantum mechanics.

7.2 Singular value decomposition and Schmidt decomposition

The singular value decomposition (SVD) is at the heart of most MPS calculations, for reasons that will become clear soon. The SVD states that for every matrix M of dimension $N_a \times N_b$ there exists a decomposition

$$M = USV^\dagger, \tag{7.10}$$

where U is of dimension $N_a \times \min(N_a, N_b)$, fulfilling $UU^\dagger = I$, V is of dimension $\min(N_a, N_b) \times N_b$, fulfilling $VV^\dagger = I$, and S is a diagonal matrix of dimension $\min(N_a, N_b) \times \min(N_a, N_b)$. There is a nice mnemonic to remember the shapes of the matrices involved in the SVD illustrated in Fig. 7.1. One applications of the SVD is in the approximation of a matrix M of rank r by a new matrix M' of rank r', where $r' < r$. Suppose that the diagonal elements of $S = \mathrm{diag}(s_1, s_2, \ldots, s_r)$ are ordered from largest to smallest value (this is allowed because the SVD is not unique). An optimal approximation of M according to the Fröbenius norm, $\|M\|_F^2 = \sum_{ij} |M_{ij}|^2$, is performed by setting all but the r' largest singular values in S to zero, $M' = US'V^\dagger$, where $S = \mathrm{diag}(s_1, s_2, \ldots, s_{r'}, 0, \ldots, 0)$. In practice, this means that we can reduce the number of columns in U and the number of rows in V, and we end up with a lower-rank approximation of M. This is the mathematical operation that allows MPS to represent quantum states that would otherwise be too large. The question is how to write a quantum state in such a way that we can take advantage of this approximation, and at the same time give a meaning to the singular values that we throw away. This is where the Schmidt decomposition comes in.

Consider a pure state $|\Psi\rangle$, written as

$$|\Psi\rangle = \sum_{ij} \Psi_{ij} |i\rangle_a |j\rangle_b , \tag{7.11}$$

Figure 7.1: *Illustration of the two different "shapes" involved in a singular value decomposition, $M = USV^\dagger$.*

where $\{|i\rangle_a\}$ and $\{|j\rangle_b\}$ are orthonormal bases of dimension N_a and N_b, respectively. The coefficients Ψ_{ij} can be interpreted as a matrix, on which we can perform the SVD, which we write in index notation as

$$|\Psi\rangle = \sum_{ij} \sum_{\lambda=1}^{\min(N_a,N_b)} U_{i\lambda} S_{\lambda\lambda} V^*_{j\lambda} |i\rangle_a |j\rangle_b . \tag{7.12}$$

With U and V we can define a new set of orthonormal bases by defining $|\lambda\rangle_a \equiv \sum_i U_{i\lambda} |i\rangle_a$ and $|\lambda\rangle_b \equiv \sum_j V^*_{j\lambda} |j\rangle_b$. Let us denote the singular values of S as s_λ, and rewrite Eq. (7.12) in terms of $|\lambda\rangle_a$ and $|\lambda\rangle_b$, we then obtain the Schmidt decomposition

$$|\Psi\rangle = \sum_{\lambda=1}^{r} s_\lambda |\lambda\rangle_a |\lambda\rangle_b , \tag{7.13}$$

where $r \leq \min(N_a, N_b)$. s_λ is referred to as the Schmidt weights in this context, and the number of Schmidt weights is called the Schmidt rank. An entangled state thus has a Schmidt rank of $r > 1$, and $r = 1$ describes a product state. The reduced density matrices for a and b can now be written as

$$\rho_a = \sum_{\lambda=1}^{r} s_\lambda^2 |\lambda\rangle_{a\,a}\langle\lambda|, \tag{7.14}$$

$$\rho_b = \sum_{\lambda=1}^{r} s_\lambda^2 |\lambda\rangle_{b\,b}\langle\lambda|. \tag{7.15}$$

From the reduced density matrices, we can calculate the von-Neumann entropy of entanglement, $S_{a|b}$, between the two parts a and b,

$$S_{a|b} = -\operatorname{tr}(\rho_a \log \rho_a) = -\operatorname{tr}(\rho_b \log \rho_b) = \sum_{\lambda=1}^{r} -s_\lambda^2 \log\left(s_\lambda^2\right). \tag{7.16}$$

Using the low-rank matrix-approximation method described earlier, we now have a procedure to approximate $|\Psi\rangle$ by a state $|\Psi'\rangle$ that takes fewer parameters to represent. By restricting the number of non-zero Schmidt weights in the Schmidt decomposition to the r' largest values, we obtain the approximate state,

$$|\Psi'\rangle = \sum_{\lambda=1}^{r'} s_\lambda |\lambda\rangle_a |\lambda\rangle_b . \tag{7.17}$$

We note that the weights s_λ need to be rescaled for the state to be normalized. The prize we have to pay for doing this approximation is that we put a restriction on the possible amount of entanglement in the system (as is clear from Eq. (7.16)).

7.3 Decomposition into an MPS

Although MPS is mostly used in the study of 1D systems, any state can be written in the form of an MPS. Let us show that by decomposing an arbitrary quantum state into an MPS. However, this decomposition is not efficient as the original state we start from might take exponentially many parameters in the system size to describe. We discuss how and in what way MPS is efficient later on.

We start by considering a general pure state on a lattice of length N,

$$|\Psi\rangle = \sum_{i_1,\ldots,i_N} C_{i_1\ldots i_N} |i_1 \ldots i_N\rangle \,, \tag{7.18}$$

where the sites have d dimensional local state spaces $\{i_j\}$, for sites $j = 1, \ldots, N$, and C is a rank N coefficient tensor. The coefficient tensor thus has d^N number of parameters. We are free to reshape this tensor into a matrix of dimension $(d \times d^{N-1})$. We denote this new matrix as $\Psi_{i_1(i_2\ldots i_N)} = C_{i_1\ldots i_N}$. In TNN this is called *grouping* and is often represented by thickening of a leg

(7.19)

This particular example reshaped a matrix into a vector. We now perform a SVD on the matrix Ψ and obtain

$$\begin{aligned} C_{i_1\ldots i_N} = \Psi_{i_1(i_2\ldots i_N)} &= \sum_{a_1}^{r_1} U_{i_1 a_1} S_{a_1 a_1} V^\dagger_{a_1(i_2\ldots i_N)} \\ &= \sum_{a_1}^{r_1} U_{i_1 a_1} C_{a_1 i_2\ldots i_N}, \end{aligned} \tag{7.20}$$

where S and $V^\dagger$ was multiplied in the last step, C was shaped back into a tensor, and $r_1 \leq d$ denotes the number of non-zero Schmidt weights. Next, we write $U_{i_1 a_1}$ in terms of d row vectors A^{i_1} with entries $A^{i_1}_{a_1} = U_{i_1 a_1}$, and reshape $C_{a_1 i_2\ldots i_N}$ into a matrix $\Psi_{(a_1 i_2)(i_3\ldots i_N)}$ of dimension $r_1 d \times d^{N-2}$ which gives us

$$C_{i_1\ldots i_N} = \sum_{a_1}^{r_1} A^{i_1}_{a_1} \Psi_{(a_1 i_2)(i_3\ldots i_N)}. \tag{7.21}$$

Performing a SVD on Ψ gives

$$C_{i_1\ldots i_N} = \sum_{a_1}^{d_1} \sum_{a_2}^{d_2} A^{i_1}_{a_1} U_{a_1(i_2 a_2)} S_{a_2 a_2} V^\dagger_{a_2(i_3\ldots i_N)}. \tag{7.22}$$

After this step we introduce d matrices A^{i_2} with entries $A^{i_2}_{a_1 a_2} = U_{a_1(i_2 a_2)}$, which gives us

$$C_{i_1 \ldots i_N} = \sum_{a_1}^{d_1} \sum_{a_2}^{d_2} A^{i_1}_{a_1} A^{i_2}_{a_1 a_2} \Psi_{(a_2 i_3)(i_4 \ldots i_N)}, \tag{7.23}$$

where we again multiplied S and $V^\dagger$ and reshaped the result into a matrix $\Psi_{(a_2 i_3)(i_4 \ldots i_N)}$. If this process is iterated until the end of the chain, we end up with a sum over products of matrices,

$$C_{i_1 \ldots i_N} = \sum_{a_1 \ldots a_N} A^{i_1}_{a_1} A^{i_2}_{a_1 a_2} \ldots A^{i_N}_{a_{N-1}}. \tag{7.24}$$

The indices a_i are called *virtual* or *bond* indices, and the number of values in a_i gives the so called *bond dimension*. The indices i_j are called *physical* indices since they correspond to the physical site i_j in the lattice. If the summation sign in Eq. (7.24) is omitted we can write the original quantum state $|\Psi\rangle$ compactly in a way that explains the name *matrix product states*,

$$|\Psi\rangle = \sum_{i_1, \ldots, i_N} A^{i_1} A^{i_2} \ldots A^{i_N} |i_1 \ldots i_N\rangle . \tag{7.25}$$

It is important to remember that the objects A^{i_j} are not matrices but rank 3 tensors, they carry one physical index and two virtual indices. The first and last As are exceptions as they carry one virtual index each and are thus only vectors.

Although it can be an instructive exercise to perform the decomposition of a quantum state into an MPS like we just did, the whole procedure could have been illustrated much more conveniently in TNN. For a 4-site lattice, the decomposition in terms of repeated SVDs can be written as

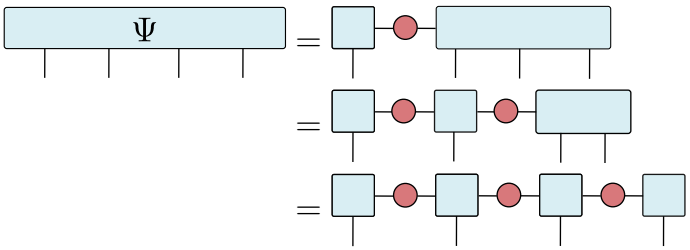

(7.26)

At this point, the singular S-matrices (pink circles) have not been absorbed yet. Whether the S matrices are absorbed to the left or to the right is arbitrary, and is related to gauge fixing, but it does affect the normalization of the matrices involved. If we again carry out the contraction of the S matrices with the tensors to their right side, we obtain a MPS written in TNN as,

$$|\Psi\rangle = \quad , \tag{7.27}$$

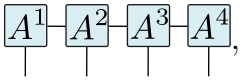

where the involved matrices can be shown to be left normalized $\sum_j (A^{i_j})^\dagger A^{i_j} = I$. A MPS that only contains left normalized matrices is said to be in *left canonical* form.

7.4 Comments on MPS algorithms

In the previous section we decomposed an arbitrary quantum state on a lattice into a MPS. It might not be obvious at first sight that we have done anything useful. In the worst case scenario, there where no non-zero singular values during the decomposition in Eq. (7.26). If we count the dimensions of the matrices: $(1 \times d)(d \times d^2) \dots (d^{N/2-1} \times d^{N/2})(d^{N/2} \times d^{N/2-1}) \dots (d^2 \times d)(d \times 1)$, assuming N is even, we still have an exponential number of parameters in the system size, just as as we started out with. However, if the entanglement along a bipartite cut is restricted, we could use the MPS form to truncate the matrices involved and obtain a more efficient representation. In fact, there is an area law stating that: for a 1D spin chain of length N of d-dimensional spins with a gap Δ between the ground and first excited state, and only local interactions, the entanglement entropy along any bipartite cut in the chain is bounded by $\mathcal{O}((\log d)^3/\Delta)$ [146, 156]. For such systems, the ground state can be approximated to arbitrary good precision only using poly(N) bond dimension [157]. MPS algorithms are constructed to take advantage of this fact; that the entanglement in quantum systems often has a structure to it, and TNs, and MPS in particular, is a formalism that allows us to explore that.

We do not go through the details of the various algorithms that exist for MPS, as that goes beyond the scope of this thesis, but refer to one of the many reviews on the topic [147, 148, 150]. Instead, let us make some general comments.

Before MPS, the most efficient algorithm for ground-state calculations was the *density matrix renormalization group* (DMRG) algorithm [158]. When the algorithm was put forward, there were no other methods known to be efficient. It allowed the low energy physics of some 1D systems to be extracted to a much higher accuracy than before. It was not until later that the success of DMRG was understood in terms of MPS [147], as DMRG produces quantum states on MPS form [159, 160]. In its essence, the DMRG algorithm can thus be viewed as an MPS algorithm. Once the DMRG algorithm was reformulated in the MPS language, other efficient algorithms for quantum spin chains were discovered, such as: *time evolving block decimation* (TEBD) for calculating time evolutions [161, 162], which could also be extended to finite temperatures [163, 164]; infinite system algorithms [165]; continous MPS for continous variable systems [166]; and extensions to higher dimensions [166]. It is worth noting that the higher dimensional TNs are not numerically efficient but are nevertheless interesting from an analytical perspective. Interestingly, some higher dimensional TNs have even been used to construct toy models of the AdS/CFT correspondence in string theory [167, 168], showcasing the, nowadays, widespread application of TNs as a general framework.

Let us take a ground-state search as a typical example of a MPS algorithm. The ground state can be obtained, e.g., from the TEBD algorithm using imaginary

time. The algorithm can broadly be divided into the following steps: (i) a random initial state is generated as an MPS ansatz with a low bond-dimension. (ii) The state is evolved according to the Hamiltonian using TEBD, but with $t \to it$, in which the state is continuously truncated in each time step to make sure the bond dimension does not grow beyond a predefined maximally allowed value, $D_{\max}$. This projects the state onto the ground state for $t \to \infty$. (iii) The calculation is repeated until the calculation has converged, using a larger bond dimension for each iteration. With this approach, it is not necessary to know beforehand if a certain Hamiltonian fulfills the area law and has an efficient representation. This is a common theme in many algorithms; they start with some MPS ansatz, and then the state is truncated, using SVDs, throughout the calculation to ensure numerical feasibility.

8 Overview of papers

In this final chapter, we give a summary and explanation of the main results in each of the five appended papers.

8.1 Paper I: Cavity-free vacuum-Rabi splitting in circuit quantum acoustodynamics

Cavity QED and waveguide QED are often thought of as two distinctly different regimes of light-matter interaction. The ingredients are similar; an atom, artificial or real, interacts with either a single electromagnetic mode (cavity QED) or a continuum of modes in a waveguide (waveguide QED). The hallmark of strong coupling in cavity QED is the observation of Rabi-oscillation, in which an excitation is repeatedly exchanged between the atom and the cavity until it eventually leaks out. An atom in a waveguide behaves, of course, very differently. Without the confinement of the cavity, the system is characterized by a continuous loss of energy into the waveguide at a rate given by the atom's coupling strength. Despite their fundamental differences, these two systems can be thought of as two regimes of the same system, which, if we restrict the discussion to a two-level atom, is captured by the same interaction Hamiltonian [169]

$$H_{\text{int}} = \sqrt{\frac{\gamma}{\pi}} \int d\omega \left(g(\omega) a(\omega) \sigma^{+} + \text{H.c.} \right), \tag{8.1}$$

where $g(\omega)$ is a frequency-dependent coupling amplitude that takes the local density of states of the electromagnetic field at the atom's position into account. For an open transmission line, g is constant, whereas it is not in the case of a cavity. Any type of electromagnetic environment can thus be captured by Eq. (8.1) by simply inserting the correct $g(\omega)$. From this perspective, the cavity shapes the electromagnetic environment around the atom, which may, or may not, alter the system dynamics from that of an atom in a continuum. In the case of an excited atom in a cavity, three different regimes can be identified, depending on the dipole coupling strength, γ, in relation to the cavity lifetime [169]: (i) Overdamped decay of the atom. The decay rate is enhanced due to the localization of the electromagnetic field in the cavity; this is called the Purcell effect. The cavity can be understood as an antenna for the atom. (ii) Underdamped decay, giving rise to oscillations at a frequency given by the vacuum-Rabi frequency. This is

the strong coupling regime of cavity QED mentioned above. (iii) A revival of the atomic inversion at a time scale given by the cavity round-trip time. This regime is also referred to as the multimode coupling regime [65, 170–173], in which the coupling strength exceeds the free spectral range of the cavity and couples to several modes at the same time.

It is in the light of this discussion that paper I should be viewed. In paper I, we studied the interaction between a transmon atom and SAWs in various parameter regimes. The piezoelectric substrate in which the SAWs are propagating can be seen as an acoustic waveguide. The interaction between the atom and SAWs is mediated by an IDT [Sec. 3.3], which has a spatial extension on the order of several wavelengths. In the simplest of models, the IDT can be viewed as coupling the atom to the waveguide at multiple points. As was mentioned in the introduction of this thesis, Kockum et al. [58] first investigated this system and named it a giant atom.

The extended nature of the interdigitated coupling allows the system to behave in a very similar manner to an atom in a cavity, operating in one of the three regimes discussed above, determined by the piezoelectric coupling constant. Motivated by ongoing experimental efforts at the time, we considered two of the most commonly used piezoelectric substrates, gallium arsenide, which is weakly piezoelectric, and lithium niobate, which is strongly piezoelectric. We found that a phonon emitted at one coupling point could be reabsorbed by the atom at another coupling point on lithium niobate. This process is possible because the atom couples strongly at each coupling point, making the interaction process fast enough for this to occur. Similar behavior occurs for an atom in a cavity, where an emitted phonon has time to be reabsorbed several times before it leaves the cavity. One could say that the IDT forms the cavity, but since the IDT also constitutes the transmon's capacitance, the atom forms its own cavity. However, on gallium arsenide, the interaction is weak, and the atom does not have time to reabsorb an emitted photon. In this case, the IDT only behaves like an acoustic antenna and an acoustic analogy to the Purcell effect occurs. A caveat is if the IDT is made very long, then the cavity behavior would also be observed on weakly piezoelectric substrates.

The main message of paper I is that a SAW-coupled atom is fundamentally different from an atom coupled to a microwave transmission line. The differences come from the IDT, a necessary ingredient that cannot be avoided, and its sizeable spatial extension needs to be accounted for in strongly coupled systems.

8.2 Paper II: Towards phonon routing: controlling propagating acoustic waves in the quantum regime

In this experimental work, a low power coherent SAW beam was scattered against an artificial atom and routed in either the forward or backward direction. The routing was performed by tuning the atom in and out of resonance with the incoming SAWs by two different means: (i) by varying the magnetic flux through the squid loop of the transmon, or (ii) by splitting the $|0\rangle - |1\rangle$ transition through the Stark effect; the resulting states are called an Autler-Townes doublet [55]. The first method is a relatively slow process compared to the second method performed by sending a short pulse through an external drive port.

An important figure of merit in this experiment is the level of extinction obtained in the forward direction. In quantum optics, the extinction of a laser impinging on a trapped ion [41], or a dye molecule [40] could not exceed 12% due to the mode mismatch between the incoming and reflected field in 3D space. With the advent of waveguide QED, the confinement to 1D enabled more than 90% extinction with flux qubits [**extinctionflux**, 174] and more than 99% extinction later on with a transmon [39]. In paper II, an extinction of 80% was observed, indicating the relatively good level of control achievable also with acoustic devices.

8.3 Paper III: Engineering the Level Structure of a Giant Artificial Atom in Waveguide Quantum Electrodynamics

In an ordinary transmon [47] (Sec. 2.4), the energy levels are formed as a ladder. If Γ_{10} denotes the decay rate of the first excited state, the decay rate of energy level n to $(n-1)$ is given by $\Gamma_n = n\Gamma_{10}$. As mentioned in Sec. 1.2, additional coupling points to the waveguide can change this property of the transmon by making it giant. The giant atom's coupling points each correspond to a relaxation pathway to the waveguide. The different pathways interfere either constructively or destructively and thus enhance or suppress the decay rate. Whether the interference is constructive or destructive depends on the separation of the coupling points in relation to the wavelength or equivalently the energy of the involved transition. Since the energy-level spacing is non-equidistant in a transmon, some transition rates can be enhanced while others are suppressed.

In paper III, a giant atom was used to suppress the decay rate of the $|0\rangle - |1\rangle$ transition while at the same time enhancing the decay rate of the $|1\rangle - |2\rangle$ transition. The modulation range was greater than a factor of 200. Within the manifold of these first three states, a so-called Λ system is formed, in which the

$|1\rangle$ state is a stable or metastable state. To verify that a Λ system was successfully formed, electromagnetically induced transparency (EIT) [73] was demonstrated as a typical Λ system application. In EIT, an atom is made transparent by applying a strong coherent field at one of the two allowed atomic transitions in the Λ system. There have not been many demonstrations of EIT with superconducting artificial atoms before since it naturally lacks an appropriate level structure. Previously, this has been circumvented by embedding the atom in a cavity or resonator, which can form an effective Λ system in terms of dressed states [78, 79]. The giant atom can be considered a simpler approach.

One of the benefits of using artificial atoms over natural atoms in quantum applications is the extra level of control that artificial atoms offer. The ability to engineer the properties of the atom, or even alter their properties *in situ*, is a great advantage. With the physics demonstrated in paper III, giant atoms can now be considered an addition to the waveguide QED toolbox that allows for additional control of the atomic properties.

8.4 Paper IV: Synthesizing electromagnetically induced transparency without a control field in waveguide QED using small and giant atoms

Electromagnetically induced transparency is considered a "classic" quantum optics phenomenon in which an opaque medium is turned transparent by applying a strong coherent field at one of the atomic transitions in a three-level atom [73]. In Fig. 1.2, a typical driving scheme to achieve EIT in a Λ system is shown, where only the $|0\rangle - |2\rangle$ and $|1\rangle - |2\rangle$ transitions are allowed. The strong *control* field, Ω_c, mediates a coherent coupling between the two upper states. In the right parameter regime, the absorption of incoming photons in the much weaker *probe* field, Ω_p, can be canceled completely. The canceled absorption is often explained in terms of destructive interference between the $|0\rangle \to |2\rangle$ and $|0\rangle \to |2\rangle \to |1\rangle \to |2\rangle$ pathways.

In paper IV, we show that transparencies in waveguide QED can be synthesized with two closely spaced two-level systems, without a control field present. The coherent coupling between energy levels is mediated by the waveguide instead of the control field, and since effective two-level systems are easier to construct than three-level Λ systems, e.g., with superconducting circuits, the resulting system is a simpler setup to deal with.

8.5 Paper V: Non-Markovian steady states of a driven two-level system

Much work has gone into characterizing and defining non-Markovianity in open quantum systems over the last decade [123], yet there exists no universal definition of Markovianity, and consequently for non-Markovianity, for open quantum systems. The notion of Markovianity comes from the theory of classical stochastic processes, but the definition of a Markov process in that theory cannot be translated directly to the quantum regime [139]. The problem comes from the fact that a quantum theory is a theory of non-commuting operators, a significant difference from any classical theory, and measurements affect quantum systems in ways we cannot avoid. As a solution, or perhaps as a compromise until a universal definition can be agreed upon, an appropriate definition and measure has to be chosen depending on the context [175].

No matter which definition one adheres to, it would be interesting to understand if traces of the interaction with a non-Markovian environment can remain to be seen in the steady state. For this to be possible, the environment's impact needs to be of such nature that one can distinguish the final state from states the system could reach in a Markovian environment. This is the question we address in paper V, where we show that there are indeed states that fulfill this criterion.

Since the environment's memory makes the system dynamics hard to calculate both analytically and numerically, one often has to resort to substantial approximations, such as restricting the discussion to the single excitation regime or, in the case of driven systems, to short time scales. In paper V, we use a recently proposed MPS method [154] (for an introduction to MPS see Sec. 7.3) to account for both long-time memory effects and the many excitations that can be involved in a driven system. This is a regime in the study of non-Markovian systems that, to our knowledge, has not been explored previously but are crucial for detecting traces of non-Markovianity in the steady state of a driven system.

We model a non-Markovian environment by considering an atom in a semi-infinite waveguide (an atom in front of a mirror) [176–180]. The distance to the mirror gives the environment a characteristic memory-time from the atom's perspective. By varying the atom's distance to the mirror, we can compare Markovian and non-Markovian dynamics.

9 Conclusions

9.1 Summary

We have studied artificial atoms made from superconducting circuits and their interaction with quantum fields in one-dimensional waveguides. These systems can, e.g., explore new regimes of quantum optics, create, store, or retrieve quantum information, or form nodes in a quantum network [181]. A large part of the thesis was devoted to introducing the main theoretical frameworks used to model and study the systems described in the appended papers I-V. Specifically, we reviewed: quantization of electrical circuits, SAW propagation in piezoelectric substrates, master equations, input-output formalism, dynamics of open quantum systems, quantum Markov processes, a scattering technique, and matrix product states. Together, they form a powerful toolbox that can be used to understand a wide range of quantum mechanical phenomena involving artificial atoms coupled to either microwave photons or acoustic phonons.

9.2 Outlook

In paper I, we predicted a regime where SAW-coupled atoms could form their own cavity, depending on their coupling strength to the substrate. This idea is closely connected to the concept of *bound states in the continuum* (BICs) [182]. A bound state in an open system is typically found if its frequency lies outside of the spectral range spanned by propagating waves in the waveguide. In BICs, the frequency of the system lies inside this range. A SAW-coupled atom has been studied from this perspective, and BICs are predicted to exist [183]. An atom in a semi-infinite waveguide is another system that exhibits BICs; the excitation of such a BIC via two-photon scattering was discussed in Ref. [184]. Given the long history of BICs in both quantum and classical systems [182], it will be interesting to see if BICs can be utilized for practical purposes in quantum acoustic devices.

As was studied experimentally in paper II and III, giant atoms constitutes an exciting new regime of quantum optics [185]. Their individually tunable coupling to the waveguide [186], and their tunable collective decay [59] could potentially be used for quantum simulations [187], and generation of non-classical photonic states [188]. There is also a proposal to realize giant atoms in 3D geometries in cold atoms [189]. Generally, there are many quantum optical phenomena that could

be revisited with giant atoms, just as we did in paper IV, where we studied EIT. There, we did not find any new effects coming from the giant atom configurations, however.

The non-Markovian regime of a giant atom [22], which was realized experimentally with a SAW coupled atom [62], could be used to explore the non-Markovian steady states that we introduced in paper V. The coherence times of SAW-coupled atoms might be a limiting factor, however. Their relatively short coherence times are limited by additional dielectric losses introduced by the piezoelectric substrate [110]. A better-suited approach might be to use an atom in front of a mirror as we proposed to use in paper V. This system has already been realized in several systems in the Markovian regime [177–180]. It should, however, be realizable in the non-Markovian regime using a long meandering transmission line, which was used in Ref. [171] to form a multimode cavity.

References

[1] M. A. Nielsen and I. L. Chuang, *Quantum Computation and Quantum Information: 10th Anniversary Edition*, 10th (Cambridge University Press, New York, NY, USA, 2011) (cit. on pp. 1, 45, 51).

[2] A. Montanaro, "Quantum algorithms: an overview", npj Quantum Information **2**, 15023 (2016) (cit. on p. 1).

[3] M. Kjaergaard, M. E. Schwartz, J. BraumÃ¼ller, P. Krantz, J. I.-J. Wang, S. Gustavsson, and W. D. Oliver, "Superconducting Qubits: Current State of Play", Annual Review of Condensed Matter Physics **11**, 369–395 (2020) (cit. on pp. 1, 22).

[4] B. M. Terhal, "Quantum error correction for quantum memories", Rev. Mod. Phys. **87**, 307–346 (2015) (cit. on p. 1).

[5] M. Mirrahimi, Z. Leghtas, V. V. Albert, S. Touzard, R. J. Schoelkopf, L. Jiang, and M. H. Devoret, "Dynamically protected cat-qubits: a new paradigm for universal quantum computation", New Journal of Physics **16**, 045014 (2014) (cit. on p. 1).

[6] F. Arute et al., "Quantum supremacy using a programmable superconducting processor", Nature **574**, 505–510 (2019) (cit. on p. 1).

[7] G. J. Mooney, G. A. L. White, C. D. Hill, and L. C. L. Hollenberg, "Whole-device entanglement in a 65-qubit superconducting quantum computer", (2021), arXiv:2102.11521 (cit. on p. 1).

[8] M. Gong et al., "Quantum walks on a programmable two-dimensional 62-qubit superconducting processor", (2021), arXiv:2102.02573 (cit. on p. 1).

[9] K. Bharti, A. Cervera-Lierta, T. H. Kyaw, T. Haug, S. Alperin-Lea, A. Anand, M. Degroote, H. Heimonen, J. S. Kottmann, T. Menke, W.-K. Mok, S. Sim, L.-C. Kwek, and A. Aspuru-Guzik, "Noisy intermediate-scale quantum (NISQ) algorithms", (2021), arXiv:2101.08448 (cit. on p. 1).

[10] A. Peruzzo, J. McClean, P. Shadbolt, M.-H. Yung, X.-Q. Zhou, P. J. Love, A. Aspuru-Guzik, and J. L. O'Brien, "A variational eigenvalue solver on a photonic quantum processor", Nature Communications **5**, 4213 (2014) (cit. on p. 1).

[11] J. R. McClean, J. Romero, R. Babbush, and A. Aspuru-Guzik, "The theory of variational hybrid quantum-classical algorithms", New Journal of Physics **18**, 023023 (2016) (cit. on p. 1).

[12] N. Moll, P. Barkoutsos, L. S. Bishop, J. M. Chow, A. Cross, D. J. Egger, S. Filipp, A. Fuhrer, J. M. Gambetta, M. Ganzhorn, A. Kandala, A. Mezzacapo, P. Müller, W. Riess, G. Salis, J. Smolin, I. Tavernelli, and K. Temme, "Quantum optimization using variational algorithms on near-term quantum devices", Quantum Science and Technology **3**, 030503 (2018) (cit. on p. 1).

[13] E. Farhi, J. Goldstone, and S. Gutmann, "A Quantum Approximate Optimization Algorithm", (2014), arXiv:1411.4028 (cit. on p. 1).

[14] E. Farhi and A. W. Harrow, "Quantum Supremacy through the Quantum Approximate Optimization Algorithm", (2019), arXiv:1602.07674 (cit. on p. 1).

[15] A. Smith, M. S. Kim, F. Pollmann, and J. Knolle, "Simulating quantum many-body dynamics on a current digital quantum computer", npj Quantum Information **5**, 106 (2019) (cit. on p. 1).

[16] N. P. D. Sawaya, T. Menke, T. H. Kyaw, S. Johri, A. Aspuru-Guzik, and G. G. Guerreschi, "Resource-efficient digital quantum simulation of d-level systems for photonic, vibrational, and spin-s Hamiltonians", npj Quantum Information **6**, 49 (2020) (cit. on p. 1).

[17] M. H. devoret and J. M. Martinis, "Implementing Qubits with Superconducting Integrated Circuits", Quantum Information Processing **3**, 163–203 (2004) (cit. on p. 1).

[18] G. Wendin and V. S. Shumeiko, "Quantum bits with Josephson junctions (Review Article)", Low Temperature Physics **33**, 724–744 (2007) (cit. on p. 1).

[19] J. Clarke and F. K. Wilhelm, "Superconducting quantum bits", Nature **453**, 1031–1042 (2008) (cit. on p. 1).

[20] S. M. Girvin, M. H. Devoret, and R. J. Schoelkopf, "Circuit QED and engineering charge-based superconducting qubits", Physica Scripta **T137**, 014012 (2009) (cit. on p. 1).

[21] J. M. Martinis, "Superconducting phase qubits", Quantum Information Processing **8**, 81–103 (2009) (cit. on p. 1).

[22] X. Gu, A. F. Kockum, A. Miranowicz, Y.-x. Liu, and F. Nori, "Microwave photonics with superconducting quantum circuits", Physics Reports **718**, 1–102 (2017) (cit. on pp. 1, 30, 74).

[23] J. Q. You and F. Nori, "Atomic physics and quantum optics using superconducting circuits", Nature **474**, 589–597 (2011) (cit. on p. 1).

[24] P. Goy, J. M. Raimond, M. Gross, and S. Haroche, "Observation of Cavity-Enhanced Single-Atom Spontaneous Emission", Phys. Rev. Lett. **50**, 1903–1906 (1983) (cit. on p. 1).

[25] W. Jhe, A. Anderson, E. A. Hinds, D. Meschede, L. Moi, and S. Haroche, "Suppression of spontaneous decay at optical frequencies: Test of vacuum-field anisotropy in confined space", Phys. Rev. Lett. **58**, 666–669 (1987) (cit. on p. 1).

[26] M. Brune, J. M. Raimond, P. Goy, L. Davidovich, and S. Haroche, "Realization of a two-photon maser oscillator", Phys. Rev. Lett. **59**, 1899–1902 (1987) (cit. on p. 1).

[27] C. Guerlin, J. Bernu, S. Deléglise, C. Sayrin, S. Gleyzes, S. Kuhr, M. Brune, J.-M. Raimond, and S. Haroche, "Progressive field-state collapse and quantum non-demolition photon counting", Nature **448**, 889–893 (2007) (cit. on p. 1).

[28] D. J. Wineland, R. E. Drullinger, and F. L. Walls, "Radiation-Pressure Cooling of Bound Resonant Absorbers", Phys. Rev. Lett. **40**, 1639–1642 (1978) (cit. on p. 1).

[29] D. Wineland and W. M. Itano, "Spectroscopy of a single Mg+ ion", Physics Letters A **82**, 75–78 (1981) (cit. on p. 1).

[30] J. C. Bergquist, R. G. Hulet, W. M. Itano, and D. J. Wineland, "Observation of Quantum Jumps in a Single Atom", Phys. Rev. Lett. **57**, 1699–1702 (1986) (cit. on p. 1).

[31] C. Monroe, D. M. Meekhof, B. E. King, S. R. Jefferts, W. M. Itano, D. J. Wineland, and P. Gould, "Resolved-Sideband Raman Cooling of a Bound Atom to the 3D Zero-Point Energy", Phys. Rev. Lett. **75**, 4011–4014 (1995) (cit. on p. 1).

[32] C. Monroe, D. M. Meekhof, B. E. King, W. M. Itano, and D. J. Wineland, "Demonstration of a Fundamental Quantum Logic Gate", Phys. Rev. Lett. **75**, 4714–4717 (1995) (cit. on p. 1).

[33] A. Wallraff, D. I. Schuster, A. Blais, L. Frunzio, R.-S. Huang, J. Majer, S. Kumar, S. M. Girvin, and R. J. Schoelkopf, "Strong coupling of a single photon to a superconducting qubit using circuit quantum electrodynamics", Nature **431**, 162–167 (2004) (cit. on pp. 1, 3).

[34] A. Blais, R.-S. Huang, A. Wallraff, S. M. Girvin, and R. J. Schoelkopf, "Cavity quantum electrodynamics for superconducting electrical circuits: An architecture for quantum computation", Phys. Rev. A **69**, 062320 (2004) (cit. on p. 1).

[35] P. Wang, C.-Y. Luan, M. Qiao, M. Um, J. Zhang, Y. Wang, X. Yuan, M. Gu, J. Zhang, and K. Kim, "Single ion qubit with estimated coherence time exceeding one hour", Nature Communications **12**, 233 (2021) (cit. on p. 2).

[36] T. P. Harty, D. T. C. Allcock, C. J. Ballance, L. Guidoni, H. A. Janacek, N. M. Linke, D. N. Stacey, and D. M. Lucas, "High-Fidelity Preparation, Gates, Memory, and Readout of a Trapped-Ion Quantum Bit", Phys. Rev. Lett. **113**, 220501 (2014) (cit. on p. 2).

[37] J. J. Burnett, A. Bengtsson, M. Scigliuzzo, D. Niepce, M. Kudra, P. Delsing, and J. Bylander, "Decoherence benchmarking of superconducting qubits", npj Quantum Information **5**, 54 (2019) (cit. on pp. 2, 39).

[38] C. Monroe and J. Kim, "Scaling the Ion Trap Quantum Processor", Science **339**, 1164–1169 (2013) (cit. on p. 2).

[39] I.-C. Hoi, C. M. Wilson, G. Johansson, T. Palomaki, B. Peropadre, and P. Delsing, "Demonstration of a Single-Photon Router in the Microwave Regime", Phys. Rev. Lett. **107**, 073601 (2011) (cit. on pp. 2, 3, 69).

[40] G. Wrigge, I. Gerhardt, J. Hwang, G. Zumofen, and V. Sandoghdar, "Efficient coupling of photons to a single molecule and the observation of its resonance fluorescence", Nature Physics **4**, 60–66 (2008) (cit. on pp. 2, 69).

[41] M. K. Tey, Z. Chen, S. A. Aljunid, B. Chng, F. Huber, G. Maslennikov, and C. Kurtsiefer, "Strong interaction between light and a single trapped atom without the need for a cavity", Nature Physics **4**, 924–927 (2008) (cit. on pp. 2, 69).

[42] J. J. Burnett, A. Bengtsson, M. Scigliuzzo, D. Niepce, M. Kudra, P. Delsing, and J. Bylander, "Decoherence benchmarking of superconducting qubits", npj Quantum Information **5**, 54 (2019) (cit. on p. 3).

[43] R. F. Voss and R. A. Webb, "Macroscopic Quantum Tunneling in 1-μm Nb Josephson Junctions", Phys. Rev. Lett. **47**, 265–268 (1981) (cit. on p. 3).

[44] M. H. Devoret, J. M. Martinis, and J. Clarke, "Measurements of Macroscopic Quantum Tunneling out of the Zero-Voltage State of a Current-Biased Josephson Junction", Phys. Rev. Lett. **55**, 1908–1911 (1985) (cit. on p. 3).

[45] J. M. Martinis, M. H. Devoret, and J. Clarke, "Energy-Level Quantization in the Zero-Voltage State of a Current-Biased Josephson Junction", Phys. Rev. Lett. **55**, 1543–1546 (1985) (cit. on p. 3).

[46] Y. Nakamura, Y. A. Pashkin, and J. S. Tsai, "Coherent control of macroscopic quantum states in a single-Cooper-pair box", Nature **398**, 786–788 (1999) (cit. on p. 3).

[47] J. Koch, T. M. Yu, J. Gambetta, A. A. Houck, D. I. Schuster, J. Majer, A. Blais, M. H. Devoret, S. M. Girvin, and R. J. Schoelkopf, "Charge-insensitive qubit design derived from the Cooper pair box", Phys. Rev. A **76**, 042319 (2007) (cit. on pp. 3, 19, 69).

[48] D. I. Schuster, A. A. Houck, J. A. Schreier, A. Wallraff, J. M. Gambetta, A. Blais, L. Frunzio, J. Majer, B. Johnson, M. H. Devoret, S. M. Girvin, and R. J. Schoelkopf, "Resolving photon number states in a superconducting circuit", Nature **445**, 515–518 (2007) (cit. on p. 3).

[49] M. Hofheinz, E. M. Weig, M. Ansmann, R. C. Bialczak, E. Lucero, M. Neeley, A. D. O'Connell, H. Wang, J. M. Martinis, and A. N. Cleland, "Generation of Fock states in a superconducting quantum circuit", Nature **454**, 310–314 (2008) (cit. on p. 3).

[50] M. A. Sillanpää, J. I. Park, and R. W. Simmonds, "Coherent quantum state storage and transfer between two phase qubits via a resonant cavity", Nature **449**, 438–442 (2007) (cit. on p. 3).

[51] O. Astafiev, K. Inomata, A. O. Niskanen, T. Yamamoto, Y. A. Pashkin, Y. Nakamura, and J. S. Tsai, "Single artificial-atom lasing", Nature **449**, 588–590 (2007) (cit. on p. 3).

[52] L. DiCarlo, J. M. Chow, J. M. Gambetta, L. S. Bishop, B. R. Johnson, D. I. Schuster, J. Majer, A. Blais, L. Frunzio, S. M. Girvin, and R. J. Schoelkopf, "Demonstration of two-qubit algorithms with a superconducting quantum processor", Nature **460**, 240–244 (2009) (cit. on p. 3).

[53] O. Astafiev, A. M. Zagoskin, A. A. Abdumalikov, Y. A. Pashkin, T. Yamamoto, K. Inomata, Y. Nakamura, and J. S. Tsai, "Resonance Fluorescence of a Single Artificial Atom", Science **327**, 840–843 (2010) (cit. on p. 3).

[54] I.-C. Hoi, T. Palomaki, J. Lindkvist, G. Johansson, P. Delsing, and C. M. Wilson, "Generation of Nonclassical Microwave States Using an Artificial Atom in 1D Open Space", Phys. Rev. Lett. **108**, 263601 (2012) (cit. on p. 3).

[55] S. H. Autler and C. H. Townes, "Stark Effect in Rapidly Varying Fields", Phys. Rev. **100**, 703–722 (1955) (cit. on pp. 3, 69).

[56] R. H. Dicke, "Coherence in Spontaneous Radiation Processes", Phys. Rev. **93**, 99–110 (1954) (cit. on p. 4).

[57] A. F. van Loo, A. Fedorov, K. Lalumière, B. C. Sanders, A. Blais, and A. Wallraff, "Photon-Mediated Interactions Between Distant Artificial Atoms", Science **342**, 1494–1496 (2013) (cit. on p. 4).

[58] A. Frisk Kockum, P. Delsing, and G. Johansson, "Designing frequency-dependent relaxation rates and Lamb shifts for a giant artificial atom", Phys. Rev. A **90**, 013837 (2014) (cit. on pp. 5, 36, 53, 68).

[59] B. Kannan, M. J. Ruckriegel, D. L. Campbell, A. Frisk Kockum, J. Braumüller, D. K. Kim, M. Kjaergaard, P. Krantz, A. Melville, B. M. Niedzielski, A. Vepsäläinen, R. Winik, J. L. Yoder, F. Nori, T. P. Orlando, S. Gustavsson, and W. D. Oliver, "Waveguide quantum electrodynamics with superconducting artificial giant atoms", Nature **583**, 775–779 (2020) (cit. on pp. 5, 73).

[60] A. F. Kockum, G. Johansson, and F. Nori, "Decoherence-Free Interaction between Giant Atoms in Waveguide Quantum Electrodynamics", Physical Review Letters **120**, 140404 (2018), arXiv:1711.08863 (cit. on p. 5).

[61] L. Guo, A. Grimsmo, A. F. Kockum, M. Pletyukhov, and G. Johansson, "Giant acoustic atom: A single quantum system with a deterministic time delay", Phys. Rev. A **95**, 053821 (2017) (cit. on pp. 5, 36).

[62] G. Andersson, B. Suri, L. Guo, T. Aref, and P. Delsing, "Non-exponential decay of a giant artificial atom", Nature Physics **15**, 1123–1127 (2019) (cit. on pp. 5, 74).

[63] M. V. Gustafsson, T. Aref, A. F. Kockum, M. K. Ekström, G. Johansson, and P. Delsing, "Propagating phonons coupled to an artificial atom.", Science **346**, 207–11 (2014) (cit. on pp. 5, 35, 36).

[64] R. Manenti, A. F. Kockum, A. Patterson, T. Behrle, J. Rahamim, G. Tancredi, F. Nori, and P. J. Leek, "Circuit quantum acoustodynamics with surface acoustic waves", Nature Communications **8**, 975 (2017) (cit. on pp. 5, 38).

[65] B. A. Moores, L. R. Sletten, J. J. Viennot, and K. W. Lehnert, "Cavity Quantum Acoustic Device in the Multimode Strong Coupling Regime", Phys. Rev. Lett. **120**, 227701 (2018) (cit. on pp. 5, 36, 38, 39, 68).

[66] A. Noguchi, R. Yamazaki, Y. Tabuchi, and Y. Nakamura, "Qubit-Assisted Transduction for a Detection of Surface Acoustic Waves near the Quantum Limit", Phys. Rev. Lett. **119**, 180505 (2017) (cit. on pp. 5, 38).

[67] A. N. Bolgar, J. I. Zotova, D. D. Kirichenko, I. S. Besedin, A. V. Semenov, R. S. Shaikhaidarov, and O. V. Astafiev, "Quantum Regime of a Two-Dimensional Phonon Cavity", Phys. Rev. Lett. **120**, 223603 (2018) (cit. on pp. 5, 38).

[68] K. J. Satzinger, Y. P. Zhong, H. S. Chang, G. A. Peairs, A. Bienfait, M.-H. Chou, A. Y. Cleland, C. R. Conner, É. Dumur, J. Grebel, I. Gutierrez, B. H. November, R. G. Povey, S. J. Whiteley, D. D. Awschalom, D. I. Schuster, and A. N. Cleland, "Quantum control of surface acoustic-wave phonons", Nature **563**, 661–665 (2018) (cit. on pp. 5, 38).

[69] Y. Chu, P. Kharel, W. H. Renninger, L. D. Burkhart, L. Frunzio, P. T. Rakich, and R. J. Schoelkopf, "Quantum acoustics with superconducting qubits.", Science **358**, 199–202 (2017) (cit. on pp. 5, 40).

[70] M. Kervinen, I. Rissanen, and M. Sillanpää, "Interfacing planar superconducting qubits with high overtone bulk acoustic phonons", Phys. Rev. B **97**, 205443 (2018) (cit. on pp. 5, 40).

[71] K.-J. Boller, A. Imamoğlu, and S. E. Harris, "Observation of electromagnetically induced transparency", Phys. Rev. Lett. **66**, 2593–2596 (1991) (cit. on p. 5).

[72] S. E. Harris, J. E. Field, and A. Imamoğlu, "Nonlinear optical processes using electromagnetically induced transparency", Phys. Rev. Lett. **64**, 1107–1110 (1990) (cit. on p. 5).

[73] M. Fleischhauer, A. Imamoglu, and J. P. Marangos, "Electromagnetically induced transparency: Optics in coherent media", English, Reviews of Modern Physics **77**, 633–673 (2005) (cit. on pp. 5, 70).

[74] L. V. Hau, S. E. Harris, Z. Dutton, and C. H. Behroozi, "Light speed reduction to 17 metres per second in an ultracold atomic gas", Nature **397**, 594–598 (1999) (cit. on p. 5).

[75] C. Liu, Z. Dutton, C. H. Behroozi, and L. V. Hau, "Observation of coherent optical information storage in an atomic medium using halted light pulses", Nature **409**, 490–493 (2001) (cit. on p. 6).

[76] I. Novikova, A. V. Gorshkov, D. F. Phillips, A. S. Sørensen, M. D. Lukin, and R. L. Walsworth, "Optimal Control of Light Pulse Storage and Retrieval", Phys. Rev. Lett. **98**, 243602 (2007) (cit. on p. 6).

[77] M. D. Lukin and A. Imamoğlu, "Controlling photons using electromagnetically induced transparency", Nature **413**, 273–276 (2001) (cit. on p. 6).

[78] S. Novikov, T. Sweeney, J. E. Robinson, S. P. Premaratne, B. Suri, F. C. Wellstood, and B. S. Palmer, "Raman coherence in a circuit quantum electrodynamics lambda system", Nature Physics **12**, 75–79 (2016) (cit. on pp. 6, 70).

[79] J. Long, H. S. Ku, X. Wu, X. Gu, R. E. Lake, M. Bal, Y.-x. Liu, and D. P. Pappas, "Electromagnetically Induced Transparency in Circuit Quantum Electrodynamics with Nested Polariton States", Phys. Rev. Lett. **120**, 083602 (2018) (cit. on pp. 6, 70).

[80] S. M. Girvin, "Circuit qed: Superconducting qubits coupled to microwave photons", Proceedings of the 2011 Les Houches Summer School (2011) (cit. on p. 9).

[81] M. H. Devoret, "Quantum fluctuations in electrical circuits", Les Houches, Session LXIII **7** (1995) (cit. on p. 9).

[82] B. Yurke and J. S. Denker, "Quantum network theory", Physical Review A **29**, 1419–1437 (1984) (cit. on p. 16).

[83] D. M. Pozar, *Microwave engineering* (Wiley, 2012), p. 732 (cit. on pp. 16, 33, 37).

[84] M. E. Peskin and D. V. Schroeder, *An Introduction To Quantum Field Theory.* (Westview Press, 1995), p. 864 (cit. on p. 16).

[85] C. H. Van der Wal, A. C. Ter Haar, F. K. Wilhelm, R. N. Schouten, C. J. Harmans, T. P. Orlando, S Lloyd, and J. E. Mooij, "Quantum superposition of macroscopic persistent-current states", Science **290**, 773–777 (2000) (cit. on p. 19).

[86] J. R. Friedman, V. Patel, W. Chen, S. K. Tolpygo, and J. E. Lukens, "Quantum superposition of distinct macroscopic states", Nature **406**, 43–46 (2000) (cit. on p. 19).

[87] J. M. Martinis, S. Nam, J. Aumentado, and C. Urbina, "Rabi Oscillations in a Large Josephson-Junction Qubit", Phys. Rev. Lett. **89**, 117901 (2002) (cit. on p. 19).

[88] V. Bouchiat, D. Vion, P. Joyez, D. Esteve, and M. H. Devoret, "Quantum Coherence with a Single Cooper Pair", Physica Scripta **T76**, 165 (1998) (cit. on p. 19).

[89] R. Barends, J. Kelly, A. Megrant, D. Sank, E. Jeffrey, Y. Chen, Y. Yin, B. Chiaro, J. Mutus, C. Neill, P. O'Malley, P. Roushan, J. Wenner, T. C. White, A. N. Cleland, and J. M. Martinis, "Coherent Josephson Qubit Suitable for Scalable Quantum Integrated Circuits", Phys. Rev. Lett. **111**, 080502 (2013) (cit. on p. 19).

[90] M. Tinkham, *Introduction to superconductivity* (Dover Publications, 2004), p. 454 (cit. on p. 19).

[91] A. Lupaşcu, S. Saito, T. Picot, P. C. de Groot, C. J. P. M. Harmans, and J. E. Mooij, "Quantum non-demolition measurement of a superconducting two-level system", Nature Physics **3**, 119–123 (2007) (cit. on p. 22).

[92] E. T. Jaynes and F. W. Cummings, "Comparison of quantum and semiclassical radiation theories with application to the beam maser", Proceedings of the IEEE **51**, 89–109 (1963) (cit. on p. 22).

[93] M. J. A. Schütz, *Quantum Dots for Quantum Information Processing: Controlling and Using their Environment*, tech. rep. (2015) (cit. on p. 23).

[94] S. H. Simon, "Coupling of surface acoustic waves to a two-dimensional electron gas", Phys. Rev. B **54**, 13878–13884 (1996) (cit. on p. 23).

[95] R. Stoneley, "The Propagation of Surface Elastic Waves in a Cubic Crystal", Proceedings of the Royal Society A: Mathematical, Physical and Engineering Sciences **232**, 447–458 (1955) (cit. on pp. 23, 24, 29).

[96] M Grundmann, O Stier, and D Bimberg, *InAs/GaAs pyramidal quantum dots: Strain distribution, optical phonons, and electronic structure*, tech. rep. (1995), pp. 15–1995 (cit. on p. 23).

[97] M. K. Ekström, T Aref, A Ask, G Andersson, B Suri, H Sanada, G Johansson, and P Delsing, "Towards phonon routing: controlling propagating acoustic waves in the quantum regime", New Journal of Physics **21**, 123013 (2019) (cit. on p. 30).

[98] S. Datta, *Surface Acoustic Wave Devices* (Prentice-Hall, 1986), p. 208 (cit. on pp. 30–32).

[99] D. P. Morgan, *Surface acoustic wave filters : with applications to electronic communications and signal processing* (Academic Press, 2007), p. 429 (cit. on pp. 30, 38).

[100] S. Datta and B. Hunsinger, "Element Factor for Periodic Transducers", IEEE Transactions on Sonics and Ultrasonics **27**, 42–44 (1980) (cit. on p. 32).

[101] C. H. W. Barnes, J. M. Shilton, and A. M. Robinson, "Quantum computation using electrons trapped by surface acoustic waves", Physical Review B **62**, 8410–8419 (2000) (cit. on p. 35).

[102] H. Flentje, P.-A. Mortemousque, R. Thalineau, A. Ludwig, A. D. Wieck, C. Bäuerle, and T. Meunier, "Coherent long-distance displacement of individual electron spins", Nature Communications **8**, 501 (2017) (cit. on p. 35).

[103] M. Schuetz, J. Knörzer, G. Giedke, L. Vandersypen, M. Lukin, and J. Cirac, "Acoustic Traps and Lattices for Electrons in Semiconductors", Phys. Rev. X **7**, 041019 (2017) (cit. on p. 35).

[104] J. I. Cirac and P. Zoller, "Quantum Computations with Cold Trapped Ions", Phys. Rev. Lett. **74**, 4091–4094 (1995) (cit. on p. 35).

[105] R. Blatt and C. F. Roos, "Quantum simulations with trapped ions", Nature Physics **8**, 277–284 (2012) (cit. on p. 35).

[106] M. Aspelmeyer, T. J. Kippenberg, and F. Marquardt, "Cavity optomechanics", Reviews of Modern Physics **86**, 1391–1452 (2014) (cit. on p. 35).

[107] A. D. O'Connell, M. Hofheinz, M. Ansmann, R. C. Bialczak, M. Lenander, E. Lucero, M. Neeley, D. Sank, H. Wang, M. Weides, J. Wenner, J. M. Martinis, and A. N. Cleland, "Quantum ground state and single-phonon control of a mechanical resonator", Nature **464**, 697–703 (2010) (cit. on p. 35).

[108] N. M. Sundaresan, Y. Liu, D. Sadri, L. J. Szs, D. L. Underwood, M. Malekakhlagh, H. E. Türeci, and A. A. Houck, "Beyond Strong Coupling in a Multimode Cavity", Phys. Rev. X **5**, 021035 (2015) (cit. on p. 39).

[109] I. M. Georgescu, S. Ashhab, and F. Nori, "Quantum simulation", Reviews of Modern Physics **86**, 153–185 (2014), arXiv:1308.6253 (cit. on p. 39).

[110] M. Scigliuzzo, L. E. Bruhat, A. Bengtsson, J. J. Burnett, A. F. Roudsari, and P. Delsing, "Phononic loss in superconducting resonators on piezoelectric substrates", New Journal of Physics **22**, 053027 (2020) (cit. on pp. 39, 74).

[111] Y. Chu, P. Kharel, T. Yoon, L. Frunzio, P. T. Rakich, and R. J. Schoelkopf, "Creation and control of multi-phonon Fock states in a bulk acoustic-wave resonator", Nature **563**, 666–670 (2018) (cit. on p. 40).

[112] H. P. Breuer and F Petruccione, *The Theory of Open Quantum Systems* (OUP Oxford, 2007) (cit. on p. 41).

[113] J. J. Sakurai and J. Napolitano, *Modern quantum mechanics; 2nd ed.* (Addison-Wesley, San Francisco, CA, 2011) (cit. on pp. 41, 43, 53).

[114] G. Crispin and P. Zoller, *Quantum Noise, A Handbook of Markovian and Non-Markovian Quantum Stochastic Methods with Applications to Quantum Optics*, 3rd ed. (Springer, 2004), p. 450 (cit. on pp. 42, 43, 45, 47).

[115] C. Cohen-Tannoudji, J. Dupont-Roc, and G. Grynberg, *Atom-Photon Interactions* (Wiley-VCH Verlag GmbH, Weinheim, Germany, 1998) (cit. on pp. 43, 46).

[116] H. J. Carmichael, *Statistical Methods in Quantum Optics 1, Master Equations and Fokker-Planck Equations*, 1st ed. (Springer-Verlag Berlin Heidelberg, 1999), p. 361 (cit. on p. 43).

[117] A. Frisk Kockum, "Quantum optics with artificial atoms", PhD thesis (Dec. 2014) (cit. on p. 43).

[118] A. G. Brown, H.-J. Weber, and F. E. Harris, *No Title* (Elsevier, 2005), p. 1182 (cit. on p. 45).

[119] G Lindblad, "On the generators of quantum dynamical semigroups", Communications in Mathematical Physics **48**, 119–130 (1976) (cit. on p. 45).

[120] V. Gorini, A. Kossakowski, and E. C. G. Sudarshan, "Completely positive dynamical semigroups of Nâ€level systems", Journal of Mathematical Physics **17**, 821–825 (1976) (cit. on p. 45).

[121] C. Gardiner, *Stochastic Methods, A Handbook for the Natural and Social Sciences*, 4th ed. (Springer-Verlag Berlin Heidelberg, 2009) (cit. on p. 47).

[122] J. E. Moyal, "Quantum mechanics as a statistical theory", Mathematical Proceedings of the Cambridge Philosophical Society **45**, 99–124 (1949) (cit. on p. 47).

[123] H. P. Breuer, E. M. Laine, J. Piilo, and B. Vacchini, "Colloquium: Non-Markovian dynamics in open quantum systems", Reviews of Modern Physics **88** (2016) 10.1103/RevModPhys.88.021002 (cit. on pp. 47–50, 71).

[124] Á. Rivas, S. F. Huelga, and M. B. Plenio, "Quantum non-Markovianity: characterization, quantification and detection", Reports on Progress in Physics **77**, 094001 (2014) (cit. on pp. 47–49, 51).

[125] M. M. Wolf, J. Eisert, T. S. Cubitt, and J. I. Cirac, "Assessing Non-Markovian Quantum Dynamics", Phys. Rev. Lett. **101**, 150402 (2008) (cit. on p. 48).

[126] H.-P. Breuer, E.-M. Laine, and J. Piilo, "Measure for the Degree of Non-Markovian Behavior of Quantum Processes in Open Systems", Phys. Rev. Lett. **103**, 210401 (2009) (cit. on pp. 48, 51, 52).

[127] A. Rivas, S. F. Huelga, and M. B. Plenio, "Entanglement and Non-Markovianity of Quantum Evolutions", Phys. Rev. Lett. **105**, 050403 (2010) (cit. on p. 48).

[128] S. C. Hou, X. X. Yi, S. X. Yu, and C. H. Oh, "Alternative non-Markovianity measure by divisibility of dynamical maps", Phys. Rev. A **83**, 62115 (2011), eprint: 1102.4659 (cit. on p. 48).

[129] S. Luo, S. Fu, and H. Song, "Quantifying non-Markovianity via correlations", Phys. Rev. A **86**, 44101 (2012) (cit. on p. 48).

[130] R. Vasile, S. Maniscalco, M. G. A. Paris, H.-P. Breuer, and J. Piilo, "Quantifying non-Markovianity of continuous-variable Gaussian dynamical maps", Phys. Rev. A **84**, 052118 (2011) (cit. on p. 48).

[131] P Haikka, J. D. Cresser, and S Maniscalco, "Comparing different non-Markovianity measures in a driven qubit system", Phys. Rev. A **83**, 12112 (2011) (cit. on p. 48).

[132] S. Cialdi, A. Smirne, M. G. A. Paris, S. Olivares, and B. Vacchini, "Two-step procedure to discriminate discordant from classical correlated or factorized states", Phys. Rev. A **90**, 050301 (2014) (cit. on p. 48).

[133] M. Gessner, M. Ramm, H. HÃ¤ffner, A. Buchleitner, and H.-P. Breuer, "Observing a quantum phase transition by measuring a single spin", EPL (Europhysics Letters) **107**, 40005 (2014) (cit. on p. 48).

[134] C.-F. Li, J.-S. Tang, Y.-L. Li, and G.-C. Guo, "Experimentally witnessing the initial correlation between an open quantum system and its environment", Phys. Rev. A **83**, 064102 (2011) (cit. on p. 48).

[135] B.-H. Liu, L. Li, Y.-F. Huang, C.-F. Li, G.-C. Guo, E.-M. Laine, H.-P. Breuer, and J. Piilo, "Experimental control of the transition from Markovian to non-Markovian dynamics of open quantum systems", Nature Physics **7**, 931–934 (2011) (cit. on p. 48).

[136] A. Smirne, D. Brivio, S. Cialdi, B. Vacchini, and M. G. A. Paris, "Experimental investigation of initial system-environment correlations via trace-distance evolution", Phys. Rev. A **84**, 032112 (2011) (cit. on p. 48).

[137] M. Gessner, M. Ramm, T. Pruttivarasin, A. Buchleitner, H.-P. Breuer, and H. Häffner, "Local detection of quantum correlations with a single trapped ion", Nature Physics **10**, 105–109 (2014) (cit. on p. 48).

[138] J.-S. Tang, Y.-T. Wang, G. Chen, Y. Zou, C.-F. Li, G.-C. Guo, Y. Yu, M.-F. Li, G.-W. Zha, H.-Q. Ni, Z.-C. Niu, M. Gessner, and H.-P. Breuer, "Experimental detection of polarization-frequency quantum correlations in a photonic quantum channel by local operations", Optica **2**, 1014–1018 (2015) (cit. on p. 48).

[139] B. Vacchini, A. Smirne, E.-M. Laine, J. Piilo, and H.-P. Breuer, "Markovianity and non-Markovianity in quantum and classical systems", New Journal of Physics **13**, 093004 (2011) (cit. on pp. 50, 71).

[140] C. A. Fuchs and J. van de Graaf, "Cryptographic distinguishability measures for quantum-mechanical states", IEEE Transactions on Information Theory **45**, 1216–1227 (1999) (cit. on p. 51).

[141] M. B. Ruskai, "Beyond subadditivity? Importev bounds on the contraction of generalized relative entropy", Reviews in Mathematical Physics **06**, 1147–1161 (1994) (cit. on p. 51).

[142] S. Wißmann, A. Karlsson, E.-M. Laine, J. Piilo, and H.-P. Breuer, "Optimal state pairs for non-Markovian quantum dynamics", Phys. Rev. A **86**, 062108 (2012) (cit. on p. 52).

[143] H. Zheng and H. U. Baranger, "Persistent Quantum Beats and Long-Distance Entanglement from Waveguide-Mediated Interactions", Phys. Rev. Lett. **110**, 113601 (2013) (cit. on p. 53).

[144] Y. L. L. Fang, H. Zheng, and H. U. Baranger, "One-dimensional waveguide coupled to multiple qubits: Photon-photon correlations", EPJ Quantum Technology **1**, 3 (2014) (cit. on p. 53).

[145] Y.-L. L. Fang and H. U. Baranger, "Waveguide QED: Power spectra and correlations of two photons scattered off multiple distant qubits and a mirror", Phys. Rev. A **91**, 053845 (2015) (cit. on p. 53).

[146] M. B. Hastings, "An area law for one-dimensional quantum systems", Journal of Statistical Mechanics: Theory and Experiment **2007**, P08024–P08024 (2007) (cit. on pp. 59, 65).

[147] U. Schollwöck, "The density-matrix renormalization group in the age of matrix product states", Annals of Physics **326**, 96–192 (2011), arXiv:1008.3477 (cit. on pp. 59, 65).

[148] R. Orús, "A practical introduction to tensor networks: Matrix product states and projected entangled pair states", Annals of Physics **349**, 117–158 (2014) (cit. on pp. 59, 65).

[149] J. C. Bridgeman and C. T. Chubb, "Hand-waving and interpretive dance: an introductory course on tensor networks", Journal of Physics A: Mathematical and Theoretical **50**, 223001 (2017) (cit. on p. 59).

[150] I. Cirac, D. Perez-Garcia, N. Schuch, and F. Verstraete, "Matrix Product States and Projected Entangled Pair States: Concepts, Symmetries, and Theorems", (2020), arXiv:2011.12127 (cit. on pp. 59, 65).

[151] C. Roberts, A. Milsted, M. Ganahl, A. Zalcman, B. Fontaine, Y. Zou, J. Hidary, G. Vidal, and S. Leichenauer, "TensorNetwork: A Library for Physics and Machine Learning", (2019), arXiv:1905.01330 (cit. on p. 59).

[152] S. Efthymiou, J. Hidary, and S. Leichenauer, "TensorNetwork for Machine Learning", (2019), arXiv:1906.06329 (cit. on p. 59).

[153] F. Kong, X. yang Liu, and R. Henao, "Quantum Tensor Network in Machine Learning: An Application to Tiny Object Classification", (2021), arXiv:2101.03154 (cit. on p. 59).

[154] H. Pichler and P. Zoller, "Photonic Circuits with Time Delays and Quantum Feedback", Phys. Rev. Lett. **116**, 093601 (2016) (cit. on pp. 59, 71).

[155] P.-O. Guimond, M Pletyukhov, H Pichler, and P Zoller, "Delayed coherent quantum feedback from a scattering theory and a matrix product state perspective", Quantum Science and Technology **2**, 044012 (2017) (cit. on p. 59).

[156] I. Arad, A. Kitaev, Z. Landau, and U. Vazirani, "An area law and sub-exponential algorithm for 1D systems", (2013), arXiv:1301.1162 (cit. on p. 65).

[157] F. Verstraete and J. I. Cirac, "Matrix product states represent ground states faithfully", Phys. Rev. B **73**, 094423 (2006) (cit. on p. 65).

[158] S. R. White, "Density matrix formulation for quantum renormalization groups", Phys. Rev. Lett. **69**, 2863–2866 (1992) (cit. on p. 65).

[159] S. Östlund and S. Rommer, "Thermodynamic Limit of Density Matrix Renormalization", Phys. Rev. Lett. **75**, 3537–3540 (1995) (cit. on p. 65).

[160] J. Dukelsky, M. MartÃn-Delgado, T. Nishino, and G. Sierra, "Equivalence of the variational matrix product method and the density matrix renormalization group applied to spin chains", Europhysics Letters **43**, cited By 107, 457–462 (1998) (cit. on p. 65).

[161] G. Vidal, "Efficient Classical Simulation of Slightly Entangled Quantum Computations", Phys. Rev. Lett. **91**, 147902 (2003) (cit. on p. 65).

[162] G. Vidal, "Efficient Simulation of One-Dimensional Quantum Many-Body Systems", Phys. Rev. Lett. **93**, 040502 (2004) (cit. on p. 65).

[163] F. Verstraete, J. J. García-Ripoll, and J. I. Cirac, "Matrix Product Density Operators: Simulation of Finite-Temperature and Dissipative Systems", Phys. Rev. Lett. **93**, 207204 (2004) (cit. on p. 65).

[164] A. E. Feiguin and S. R. White, "Finite-temperature density matrix renormalization using an enlarged Hilbert space", Phys. Rev. B **72**, 220401 (2005) (cit. on p. 65).

[165] G. Vidal, "Classical Simulation of Infinite-Size Quantum Lattice Systems in One Spatial Dimension", Phys. Rev. Lett. **98**, 070201 (2007) (cit. on p. 65).

[166] F. Verstraete and J. I. Cirac, "Renormalization algorithms for Quantum-Many Body Systems in two and higher dimensions", (2004), arXiv:`cond-mat/0407066` (cit. on p. 65).

[167] B. Swingle, "Entanglement renormalization and holography", Phys. Rev. D **86**, 065007 (2012) (cit. on p. 65).

[168] G. Evenbly and G. Vidal, "Tensor Network States and Geometry", Journal of Statistical Physics **145**, 891–918 (2011) (cit. on p. 65).

[169] D. O. Krimer, M. Liertzer, S. Rotter, and H. E. Türeci, "Route from spontaneous decay to complex multimode dynamics in cavity QED", Phys. Rev. A **89**, 033820 (2014) (cit. on p. 67).

[170] N. M. Sundaresan, Y. Liu, D. Sadri, L. J. Szőcs, D. L. Underwood, M. Malekakhlagh, H. E. Türeci, and A. A. Houck, "Beyond Strong Coupling in a Multimode Cavity", Phys. Rev. X **5**, 021035 (2015) (cit. on p. 68).

[171] F. Massel, S. U. Cho, J.-M. Pirkkalainen, P. J. Hakonen, T. T. Heikkilä, and M. A. Sillanpää, "Multimode circuit optomechanics near the quantum limit", Nature Communications **3**, 987 (2012) (cit. on pp. 68, 74).

[172] X. Han, C.-L. Zou, and H. X. Tang, "Multimode Strong Coupling in Superconducting Cavity Piezoelectromechanics", Phys. Rev. Lett. **117**, 123603 (2016) (cit. on p. 68).

[173] A. Wickenbrock, M. Hemmerling, G. R. M. Robb, C. Emary, and F. Renzoni, "Collective strong coupling in multimode cavity QED", Phys. Rev. A **87**, 043817 (2013) (cit. on p. 68).

[174] A. A. Abdumalikov, O. Astafiev, A. M. Zagoskin, Y. A. Pashkin, Y. Nakamura, and J. S. Tsai, "Electromagnetically Induced Transparency on a Single Artificial Atom", Phys. Rev. Lett. **104**, 193601 (2010) (cit. on p. 69).

[175] L. Li, M. J. Hall, and H. M. Wiseman, "Concepts of quantum non-Markovianity: A hierarchy", Physics Reports **759**, Concepts of quantum non-Markovianity: A hierarchy, 1–51 (2018) (cit. on p. 71).

[176] U. Dorner and P. Zoller, "Laser-driven atoms in half-cavities", Phys. Rev. A **66**, 023816 (2002) (cit. on p. 71).

[177] J. Eschner, C. Raab, F. Schmidt-Kaler, and R. Blatt, "Light interference from single atoms and their mirror images", Nature **413**, 495–498 (2001) (cit. on pp. 71, 74).

[178] M. A. Wilson, P. Bushev, J. Eschner, F. Schmidt-Kaler, C. Becher, R. Blatt, and U. Dorner, "Vacuum-Field Level Shifts in a Single Trapped Ion Mediated by a Single Distant Mirror", Phys. Rev. Lett. **91**, 213602 (2003) (cit. on pp. 71, 74).

[179] F. Dubin, D. Rotter, M. Mukherjee, C. Russo, J. Eschner, and R. Blatt, "Photon Correlation versus Interference of Single-Atom Fluorescence in a Half-Cavity", Phys. Rev. Lett. **98**, 183003 (2007) (cit. on pp. 71, 74).

[180] I. C. Hoi, A. F. Kockum, L. Tornberg, A. Pourkabirian, G. Johansson, P. Delsing, and C. M. Wilson, "Probing the quantum vacuum with an artificial atom in front of a mirror", Nature Physics **11**, 1045–1049 (2015), arXiv:1410.8840 (cit. on pp. 71, 74).

[181] H. J. Kimble, "The quantum internet", Nature **453**, 1023–1030 (2008) (cit. on p. 73).

[182] C. W. Hsu, B. Zhen, A. D. Stone, J. D. Joannopoulos, and M. Soljačić, "Bound states in the continuum", Nature Reviews Materials **1**, 16048 (2016) (cit. on p. 73).

[183] S. Guo, Y. Wang, T. Purdy, and J. Taylor, "Beyond spontaneous emission: Giant atom bounded in the continuum", Phys. Rev. A **102**, 033706 (2020) (cit. on p. 73).

[184] G. Calajó, Y.-L. L. Fang, H. U. Baranger, and F. Ciccarello, "Exciting a Bound State in the Continuum through Multiphoton Scattering Plus Delayed Quantum Feedback", Phys. Rev. Lett. **122**, 073601 (2019) (cit. on p. 73).

[185] A. Frisk Kockum, "Quantum Optics with Giant Atoms—the First Five Years", in International Symposium on Mathematics, Quantum Theory, and Cryptography, edited by T. Takagi, M. Wakayama, K. Tanaka, N. Kunihiro, K. Kimoto, and Y. Ikematsu (2021), pp. 125–146 (cit. on p. 73).

[186] A. M. Vadiraj, A. Ask, T. G. McConkey, I. Nsanzineza, C. W. S. Chang, A. F. Kockum, and C. M. Wilson, "Engineering the level structure of a giant artificial atom in waveguide quantum electrodynamics", Phys. Rev. A **103**, 023710 (2021) (cit. on p. 73).

[187] L. García-Álvarez, J. Casanova, A. Mezzacapo, I. L. Egusquiza, L. Lamata, G. Romero, and E. Solano, "Fermion-Fermion Scattering in Quantum Field Theory with Superconducting Circuits", Phys. Rev. Lett. **114**, 070502 (2015) (cit. on p. 73).

[188] A. González-Tudela, V. Paulisch, D. E. Chang, H. J. Kimble, and J. I. Cirac, "Deterministic Generation of Arbitrary Photonic States Assisted by Dissipation", Phys. Rev. Lett. **115**, 163603 (2015) (cit. on p. 73).

[189] A. González-Tudela, C. S. Muñoz, and J. I. Cirac, "Engineering and Harnessing Giant Atoms in High-Dimensional Baths: A Proposal for Implementation with Cold Atoms", Phys. Rev. Lett. **122**, 203603 (2019) (cit. on p. 73).